AD-A124 703 WIND TUNNEL INVESTIGATION OF VARYING HINGED FLAPS(U) 1/2
AIR FORCE INST OF TECH WRIGHT-PATTERSON AFB OH SCHOOL
OF ENGINEERING H J PRICE DEC 82 AFIT/GAE/AA/82D-23

UNCLASSIFIED F/G 14/2 NL

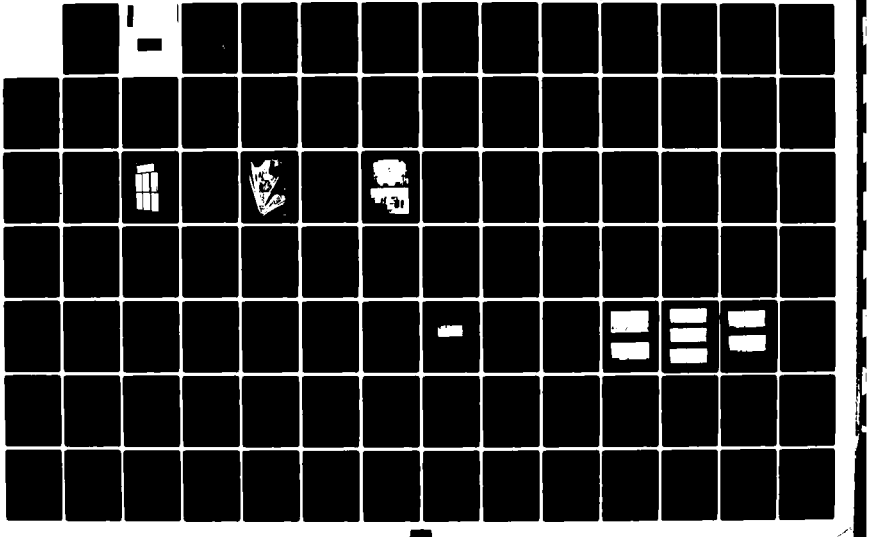

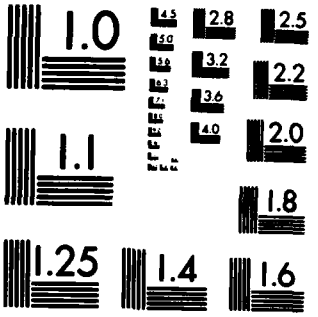

MICROCOPY RESOLUTION TEST CHART
NATIONAL BUREAU OF STANDARDS-1963-A

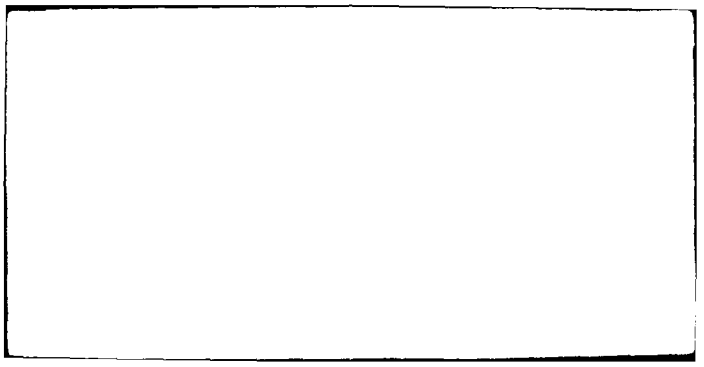

AFIT/GAE/AA/82D-23

WIND TUNNEL INVESTIGATION OF VARYING HINGED FLAPS

DTIC
ELECTE
FEB 2 2 1983
A

THESIS

AFIT/GAE/AA/82D-23

Howard J. Price, Jr.
Capt USAF

Approved for public release; distribution unlimited

AFIT/GAE/AA/82D-23

WIND TUNNEL INVESTIGATION OF VARYING HINGED FLAPS

THESIS

Presented to the Faculty of the School of Engineering
of the Air Force Institute of Technology
Air University
in Partial Fulfillment of the
Requirements for the Degree of
Master of Science

by

Howard J. Price, Jr., B.S.A.E.
Capt USAF
Graduate Aeronautical Engineering

December 1982

Approved for public release; distribution unlimited.

Preface

During the fall quarter of 1981, I took a basic course in low-speed aerodynamics, AE 5.35 Aerodynamics. Major Eric J. Jumper was the instructor for the course. While covering thin-airfoil theory, he suggested a possible thesis project to verify theoretical predictions concerning the flapped airfoil by collecting experimental data in the 5 Foot Wind Tunnel. I became interested and decided to tackle the project because it combined theory with experiment. This thesis is the end result of that decision.

I would like to thank my thesis advisor, Major Jumper, for his guidance and assistance throughout the project; Professor Harold C. Larsen for sharing some of his vast knowledge and experience with me; Mr. Jack Tiffany and Mr. Russell Murray for their model construction and timely responses to modifications; and Mr. Wales S. Whitt and Mr. Nicholas Yardich for their tunnel operation. Special thanks to my wife, Linda, who is now a bona fide number cruncher and frustrated typist.

Howard J. Price, Jr.

Accession For
NTIS GRA&I
DTIC TAB
Unannounced
Justification
By
Distribution/
Availability Codes
Dist | Avail and/or Special
A

Contents

Preface ii

List of Figures v

List of Tables vii

List of Symbols ix

Abstract xi

I. Introduction 1

Objective 1
Background 1

II. Numerical Solution for Thin-Airfoil 5

Cambered Airfoils 5
Flapped Airfoils 6

III. Wind Tunnel Investigation 12

Models 12
Wind Tunnel 17
Installation 17
Investigation Procedure 19
Data 23

IV. Results 25

Data Reduction 25
Comparison of Experimental Data to Theoretical Predictions 27

V. Conclusions and Recommendations 30

Conclusions 30
Recommendations 31

Bibliography 34

Appendix A: Analytical Solution for α_{LO} and C_{mac} 35

Appendix B: Computer Program 38

Appendix C: Model Geometry 44

Appendix D: Flap Deflection Settings 48

Appendix E: Tuft Studies 51

Appendix F: Raw Tunnel Data..... 55
Appendix G: Data Reduction Calculations..... 77
Appendix H: Experimental Data Plots..... 81
Vita..... 96

List of Figures

Figure		Page
1a	Coordinate system for an arbitrary airfoil and angle of attack.....	7
1b	Flap arbitrarily chosen and deflected.....	7
1c	New coordinate system (x',z') to find new α_{LO} and C_{mac}.....	7
2	Effect of flap-chord ratio, E, on $\Delta\alpha_{LO}/\eta$.....	9
3	Effect of flap-chord ratio on $\Delta C_{mac}/\eta$.....	10
4	Effect of camber on $\Delta C_{mac}/\eta$ versus E.....	11
5	Basic components of a fully assembled model.....	12
6	Brass flap deflection plate.....	13
7	Cross section of lift bar.....	15
8	Investigation airfoils showing the different sizes of the flap section.....	16
9	AFIT Five-Foot Wind Tunnel setup.....	18
10a	Rear view of installed model.....	20
10b	Side view of installed model.....	20
11	Experiment versus theory for $\Delta\alpha_{LO}/\eta$ versus E....	26
12	Experiment versus theory for $\Delta C_{mac}/\eta$ versus E...	28
13	Balance angle and associated measurements.....	46
14	Side view of flap deflection mechanism in operation.....	49
15	Tufts being applied to model with E = .8.....	52
16	8° angle of attack and 0° flap deflection.....	52
17	8° angle of attack and 8° flap deflection.....	53
18	10° angle of attack and 0° flap deflection.....	53
19	8° angle of attack and 4° flap deflection.....	53

Figure		Page
20	6° angle of attack and 8° flap deflection.....	54
21	0° angle of attack and 15° flap deflection.....	54
22a	Experimental C_ℓ versus α plots used to find $\Delta\alpha_{LO}/\eta$ for E = .2.....	82
22b	Experimental C_{mac} versus η plots used to find $\Delta C_{mac}/\eta$ for E = .2.....	83
23a	Experimental C_ℓ versus α plots used to find $\Delta\alpha_{LO}/\eta$ for E = .3.....	84
23b	Experimental C_{mac} versus η plots used to find $\Delta C_{mac}/\eta$ for E = .3.....	85
24a	Experimental C_ℓ versus α plots used to find $\Delta\alpha_{LO}/\eta$ for E = .4.....	86
24b	Experimental C_{mac} versus η plots used to find $\Delta C_{mac}/\eta$ for E = .4.....	87
25a	Experimental C_ℓ versus α plots used to find $\Delta\alpha_{LO}/\eta$ for E = .5.....	88
25b	Experimental C_{mac} versus η plots used to find $\Delta C_{mac}/\eta$ for E = .5.....	89
26a	Experimental C_ℓ versus α plots used to find $\Delta\alpha_{LO}/\eta$ for E = .6.....	90
26b	Experimental C_{mac} versus η plots used to find $\Delta C_{mac}/\eta$ for E = .6.....	91
27a	Experimental C_ℓ versus α plots used to find $\Delta\alpha_{LO}/\eta$ for E = .7.....	92
27b	Experimental C_{mac} versus η plots used to find $\Delta C_{mac}/\eta$ for E = .7.....	93
28a	Experimental C_ℓ versus η plots used to find $\Delta\alpha_{LO}/\eta$ for E = .8.....	94
28b	Experimental C_{mac} versus η plots used to find $\Delta C_{mac}/\eta$ for E = .8.....	95

List of Tables

Table		Page
I	Typical event sequence and data gathered.....	22
II	Airfoil measurements.....	44
III	Balance angles and associated measurements.....	45
IV	Rear lift wire movement.....	47
V	Hole alignments for flap deflection.....	50
VI	Angles of separation from tuft studies.....	51
VIIa	Raw Front Lift Data for Model with E = .2.....	56
VIIb	Raw Rear Lift Data for Model with E = .2.....	57
VIIc	Raw Drag Data for Model with E = .2.....	58
VIIIa	Raw Front Lift Data for Model with E = .3.....	59
VIIIb	Raw Rear Lift Data for Model with E = .3.....	60
VIIIc	Raw Drag Data for Model with E = .3.....	61
IXa	Raw Front Lift Data for Model with E = .4.....	62
IXb	Raw Rear Lift Data for Model with E = .4.....	63
IXc	Raw Drag Data for Model with E = .4.....	64
Xa	Raw Front Lift Data for Model with E = .5.....	65
Xb	Raw Rear Lift Data for Model with E = .5.....	66
Xc	Raw Drag Data for Model with E = .5.....	67
XIa	Raw Front Lift Data for Model with E = .6.....	68
XIb	Raw Rear Lift Data for Model with E = .6.....	69
XIc	Raw Drag Data for Model with E = .6.....	70
XIIa	Raw Front Lift Data for Model with E = .7.....	71
XIIb	Raw Rear Lift Data for Model with E = .7.....	72
XIIc	Raw Drag Data for Model with E = .7.....	73

Table		Page
XIIIa	Raw Front Lift Data for Model with E = .8.....	74
XIIIb	Raw Rear Lift Data for Model with E = .8.....	75
XIIIc	Raw Drag Data for Model with E = .8.....	76
XIV	Calculations for Model with E = .7.....	79

List of Symbols

A_o, A_1, A_n	coefficients in thin-airfoil theory
A-G	designations for a model part
b	wing span
c	airfoil chord length
C_ℓ	section lift coefficient
C_m	section moment coefficient
E	flap-chord ratio which implies a flap-hinge location
e,f,g,	model measurements
ℓ	section lift
L	wing lift
m	maximum ordinate of mean camber line
M	moment
NACA	National Advisory Committee of Aeronautics
p	chord wise position of the maximum ordinate
q	dynamic pressure
V	velocity
x	abscissae of the mean camber line
z	ordinate of the mean camber line
dz/dx	slope of the mean camber line
α	angle of attack
α_{LO}	angle of zero lift
β	transformation angle corresponding to p
γ	strength per unit length of vortices on mean camber line
η	flap deflection angle
θ	transformation angle

π	3.1415927
ρ	density
4412	an NACA four digit airfoil with maximum thickness of .12c and maximum camber of .04c above the .4c location on the chord line from the leading edge

prefix

Δ	change in
Σ	summation process

superscript

'	prime symbol, used to show a different coordinate system and associated quantities
°	degrees

subscript

ac	aerodynamic center
i	indicates values at the beginning of a segment
in	quantity induced by vortices along mean camber line
o	designates a specific point or value
∞	free stream

Abstract

This investigation compared thin-airfoil theory predictions of change in zero-lift angle of attack divided by flap deflection ($\Delta\alpha_{LO}/\eta$) versus flap-hinge location (E) and change in moment coefficient about the aerodynamic center divided by flap deflection ($\Delta C_{mac}/\eta$) versus E to wind tunnel studies of the same effect for a cambered airfoil. This comparison for cambered airfoils has not been previously reported. The NACA 4412 airfoil was chosen for this study. Results of this study show that thin-airfoil theory does predict the trend of the data. The $\Delta\alpha_{LO}/\eta$ versus E prediction favorably matched the data. The $\Delta C_{mac}/\eta$ versus E data differed from the predictions in a similar way to that reported for uncambered airfoils; however, the data in this investigation showed less favorable agreement to thin-airfoil theory than the previously reported results. This difference might be explained in part by the experimental setup used in this study.

WIND TUNNEL INVESTIGATION OF VARYING HINGED FLAPS

I Introduction

Objective

The objective of this thesis was to compare thin-airfoil theoretical predictions of the change in zero-lift angle of attack divided by flap deflection ($\Delta\alpha_{LO}/\eta$) versus flap-hinge location (E) and the change in moment coefficient about the aerodynamic center divided by flap deflection ($\Delta C_{mac}/\eta$) versus E to wind-tunnel studies of the same effects for the moderately cambered NACA 4412 airfoil.

Background

In thin-airfoil theory, the airfoil is replaced with its mean camber line. Point vortices with a differential strength of γdx are then distributed continuously along the mean camber line to induce velocities which, when added vectorially to the free-stream velocity, produce velocities tangential to the mean camber line. Because the maximum camber is usually small in comparison to the chord, the boundary conditions for the flow can be satisfied on the chord instead of at the mean camber line. This produces an induced velocity (V_{in}) at x_o such that

$$V_{in}(x_o) = \frac{1}{2\pi}\int_0^c \frac{\gamma(x)dx}{x - x_o} \qquad (1)$$

at each point on the chord line. With the assumption of small angles, the free-stream velocity's normal component to the mean camber line ($V_{\infty n}$) is such that

$$V_{\infty n} = V_\infty \left[\alpha - \frac{dz}{dx}\right] \tag{2}$$

The induced velocity must also be equal to the negative of $V_{\infty n}$ at x_o if there is to be no flow through the airfoil, i.e. $V_{in} = -V_{\infty n}$. So, from equations 1 and 2

$$\frac{1}{2\pi}\int_0^c \frac{\gamma(x)dx}{x - x_o} = V_\infty\left[\frac{dz}{dx}(x_o) - \alpha\right] \tag{3}$$

By specifying a $\gamma(x)$-distribution, the shape of the mean camber line and α to produce such a distribution can be found or vice versa. The only restriction on the $\gamma(x)$-distribution is the Kutta condition, $\gamma(c) = 0$, which must be applied to determine the circulation and keep $V_{in}(c)$ finite so that the flow can leave smoothly and tangentially from the trailing edge as in a real viscous flow.

By using the transformation $x = \frac{c}{2}(1 - \cos\theta)$, the relationship $[\cos(n-1)\theta - \cos(n+1)\theta]/2 = \sin n\theta \sin\theta$, the definite integral $\int_0^\pi \frac{\cos n\theta}{\cos\theta - \cos\theta_o} d\theta = \pi\left[\frac{\sin n\theta_o}{\sin\theta_o}\right]$, and expanding γ into a fourier series of the form

$$\gamma = 2V_\infty\left[A_o\frac{(1+\cos\theta)}{\sin\theta} + \sum_{n=1}^{\infty} A_n \sin n\theta\right] \tag{4}$$

the induced velocity or left hand side of equation 3 now becomes

$$V_{in}(\theta) = V_\infty\left[-A_o + \sum_{n=1}^{\infty} A_n \cos n\theta\right] \tag{5}$$

Equations 3 and 5 imply that

$$\frac{dz}{dx} = (\alpha - A_o) + \sum_{n=1}^{\infty} A_n \cos n\theta \tag{6}$$

Equation 6 has the form of the cosine series expansion of $\frac{dz}{dx}$. For a given mean camber line $\frac{dz}{dx}$ is a known function of θ, and therefore the values of A_o and A_n may be written directly as

$$A_o = \alpha - \frac{1}{\pi}\int_0^{\pi} \frac{dz}{dx}\, d\theta \tag{7}$$

and

$$A_n = \frac{2}{\pi}\int_0^{\pi} \frac{dz}{dx} \cos n\theta d\theta \tag{8}$$

Since the section lift(ℓ) equals the density times the free-stream velocity times the circulation ($\rho V_\infty \Gamma$) where Γ equals the integral of differential γ distribution over the chord $\left[\int_0^c \gamma dx\right]$, the aerodynamic coefficient, C_ℓ, *defined as* $\ell/\frac{1}{2}\rho V_\infty^2 c$, can now be rewritten as

$$C_\ell = \frac{2}{V_\infty c}\int_0^c \gamma dx \tag{9}$$

By using equation 4 for γ, and carrying out the integral in equation 9, C_ℓ can be found in terms of A_o and A_1 as

$$C_\ell = 2\pi A_o + \pi A_1 \tag{10}$$

Replacing A_o and A_1 with their integral forms from equations 7 and 8

$$C_\ell = 2\pi\left[\alpha + \frac{1}{\pi}\int_0^{\pi} \frac{dz}{dx}(\cos\theta - 1)d\theta\right] \tag{11}$$

The angle of attack which makes the lift or the lift coefficient in equation 11 equal to zero is called the angle of zero lift, α_{LO}. Applying the definition of α_{LO} to equation 11 gives

$$\alpha_{LO} = \frac{-1}{\pi}\int_0^{\pi} \frac{dz}{dx} (\cos\theta - 1)\, d\theta \qquad (12)$$

A similar development for C_{mac} will give

$$C_{mac} = \frac{1}{2}\int_0^{\pi} \frac{dz}{dx} (\cos 2\theta - \cos\theta)\, d\theta \qquad (13)$$

(Refs 1:44-47 and 2:116-132)

Equations 12 and 13 are used in Section II to predict influences from varying sizes of simple hinged flaps.

II Numerical Solution for Thin-Airfoil

Cambered Airfoils

As we saw in Section I, thin-airfoil theory produces integral equations for C_{mac} and α_{LO}. By assuming that the camber line is made up of straight line segments, these equations can be rewritten as follows (Ref 3:34)

$$\alpha_{LO} = \frac{-1}{\pi}\int_0^{\pi} \frac{dz}{dx}(\cos\theta - 1)\,d\theta = \frac{-1}{\pi}\sum_{i=1}^{n}\left[\frac{dz}{dx}\right]_i \int_{\theta_i}^{\theta_{i+1}} (\cos\theta - 1)\,d\theta \tag{14}$$

and

$$C_{mac} = \frac{1}{2}\int_0^{\pi} \frac{dz}{dx}(\cos 2\theta - \cos\theta)\,d\theta = \frac{1}{2}\sum_{i=1}^{n}\left[\frac{dz}{dx}\right]_i \int_{\theta_i}^{\theta_{i+1}} (\cos 2\theta - \cos\theta)\,d\theta \tag{15}$$

or, after evaluating the straight line segment integrals

$$\alpha_{LO} = \frac{-1}{\pi}\sum_{i=1}^{n}\left[\left[\frac{dz}{dx}\right]_i \left[(\sin\theta_{i+1} - \theta_{i+1}) - (\sin\theta_i - \theta_i)\right]\right] \tag{16}$$

and

$$C_{mac} = \frac{1}{2}\sum_{i=1}^{n}\left[\left[\frac{dz}{dx}\right]_i \left[\left[\frac{\sin 2\theta_{i+1}}{2} - \sin\theta_{i+1}\right] - \left[\frac{\sin 2\theta_i}{2} - \sin\theta_i\right]\right]\right] \tag{17}$$

These equations can be numerically integrated through the summation sign by using a digital computer as long as $\frac{dz}{dx}$, θ_i, and θ_{i+1} can be determined for each straight line segment.

The correctness and accuracy of the above equations can be checked by evaluating α_{LO} and C_{mac} analytically and then numerically with the computer for the same airfoil. Since this investigation used the NACA 4412 airfoil which has its

camber line in functional form, both methods can be accomplished for the zero flap deflection case. The analytic solutions as given in Appendix A yield $\alpha_{L0} = -4.1544826°$ and $C_{mac} = -.1062391$. The numerical computer solution using 400 straight line segments yields $\alpha_{L0} = -4.1540554°$ and $C_{mac} = -.1062276$. While the computer solution is a crude, brute force method, it gives extremely accurate results. Appendix B contains the program from which α_{L0} and C_{mac} for the 4412 were computed.

Flapped Airfoils

The influence of small flap deflections on α_{L0} and C_{mac} can also be found through computer numerical integration. Figure 1a shows the coordinate system arrangement for an arbitrarily cambered thin airfoil at an arbitrary angle of attack under which the α_{L0} and C_{mac} numerical equations hold. By choosing any point along the cambered line as a hinge point for a flap deflected by an amount η, the thin airfoil in Fig. 1a changes to that in Fig. 1b. α_{L0} and C_{mac} may be computed for the flap deflected airfoil by defining a new coordinate system (z' and x') as shown in Fig. 1c. Before the α_{L0} and C_{mac}s of the flapped and unflapped airfoils can be compared to arrive at $\Delta\alpha_{L0}/\eta$ and $\Delta C_{mac}/\eta$ for particular flap-chord ratios, corrections, if they exist, for using the z' and x' coordinates as the computational axes must be applied to the new α_{L0} and C_{mac}. Because α_{L0} is an angle dependent upon the coordinate system for its value, the angle $(\alpha' - \alpha)$ between the coordinate systems in Fig. 1c must be subtracted from the new or flapped airfoil α_{L0}. No correction is necessary for

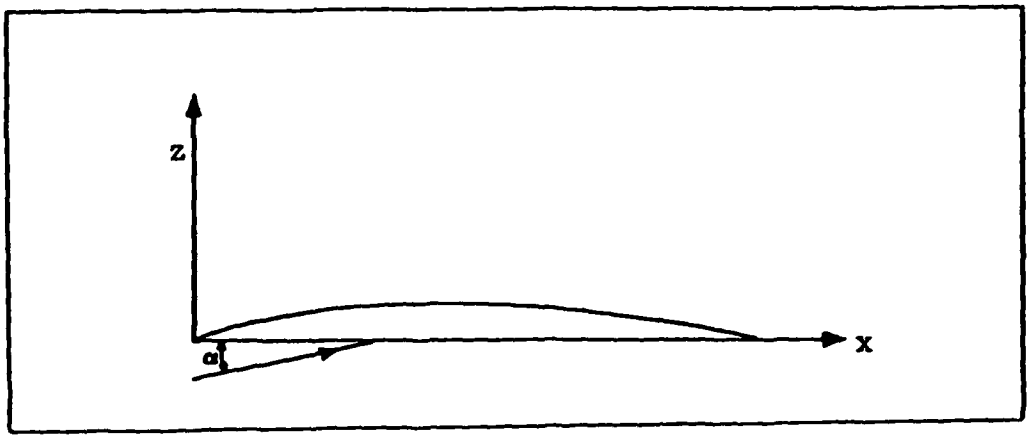

Fig. 1a Coordinate system for an arbitrary airfoil and angle of attack.

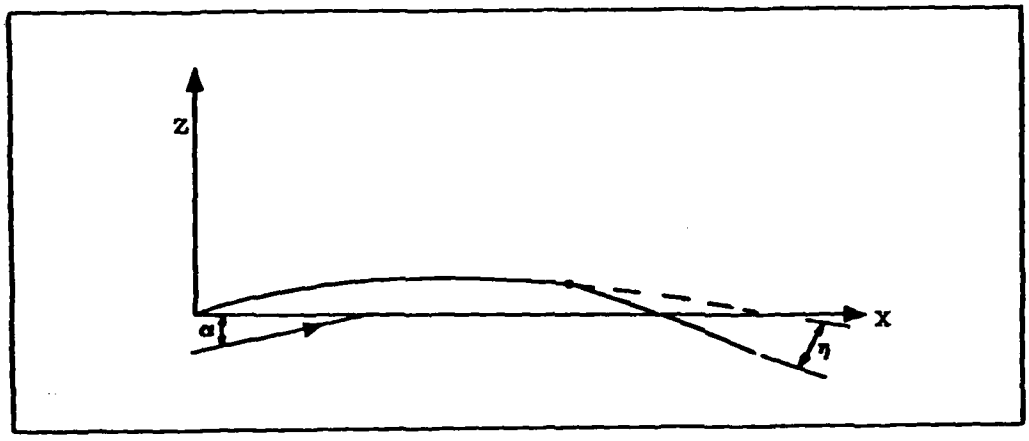

Fig. 1b Flap arbitrarily chosen and deflected.

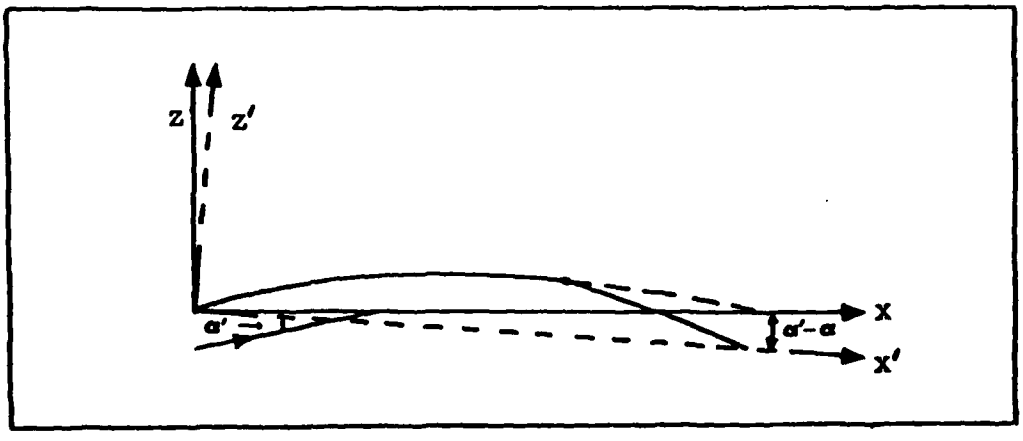

Fig. 1c New coordinate system (x',z') to find new α_{LO} and C_{mac}.

the new C_{mac} since it is related to the airfoil and not the coordinate system. By doing this for many points along the camber line of an NACA 4412 airfoil one can obtain the curves in Figs. 2 and 3 depicting the influence of small flap deflections on α_{LO} and C_{mac}. Reference Appendix B for the program used to find the data points for Figs. 2 and 3.

Figures 2 and 3 show flap influences for a 4% cambered airfoil. If the camber is different, then slightly different curves will result for $\Delta C_{mac}/\eta$ versus E with the differences for $\Delta\alpha_{LO}/\eta$ versus E due to camber being negligible. This effect of camber on the $\Delta C_{mac}/\eta$ can be shown by comparing 4%, 2%, and uncambered airfoils as in Fig. 4. In general, even the largest difference among the cambered airfoils and uncambered airfoil is small. The above results can be checked by comparing them to predictions which have not been derived in a numerical manner. Chow's (Ref 2:133-137) analytic derivation of $\Delta\alpha_{LO}/\eta$ versus E and $\Delta C_{mac}/\eta$ versus E for uncambered airfoils results in exactly the same curves derived through numerical integration for uncambered airfoils, as they should be in order for the numerical integration approach to be valid. Chow goes on to state that because all angles are small, it is sufficient to find the properties of an uncambered airfoil at zero angle of attack with flap deflected and add them directly to the properties of the cambered airfoil at any angle of attack. That statement agrees with the small differences noted between the uncambered and cambered airfoils for $\Delta C_{mac}/\eta$ versus E and also serves to validate the numerical approach as explained here.

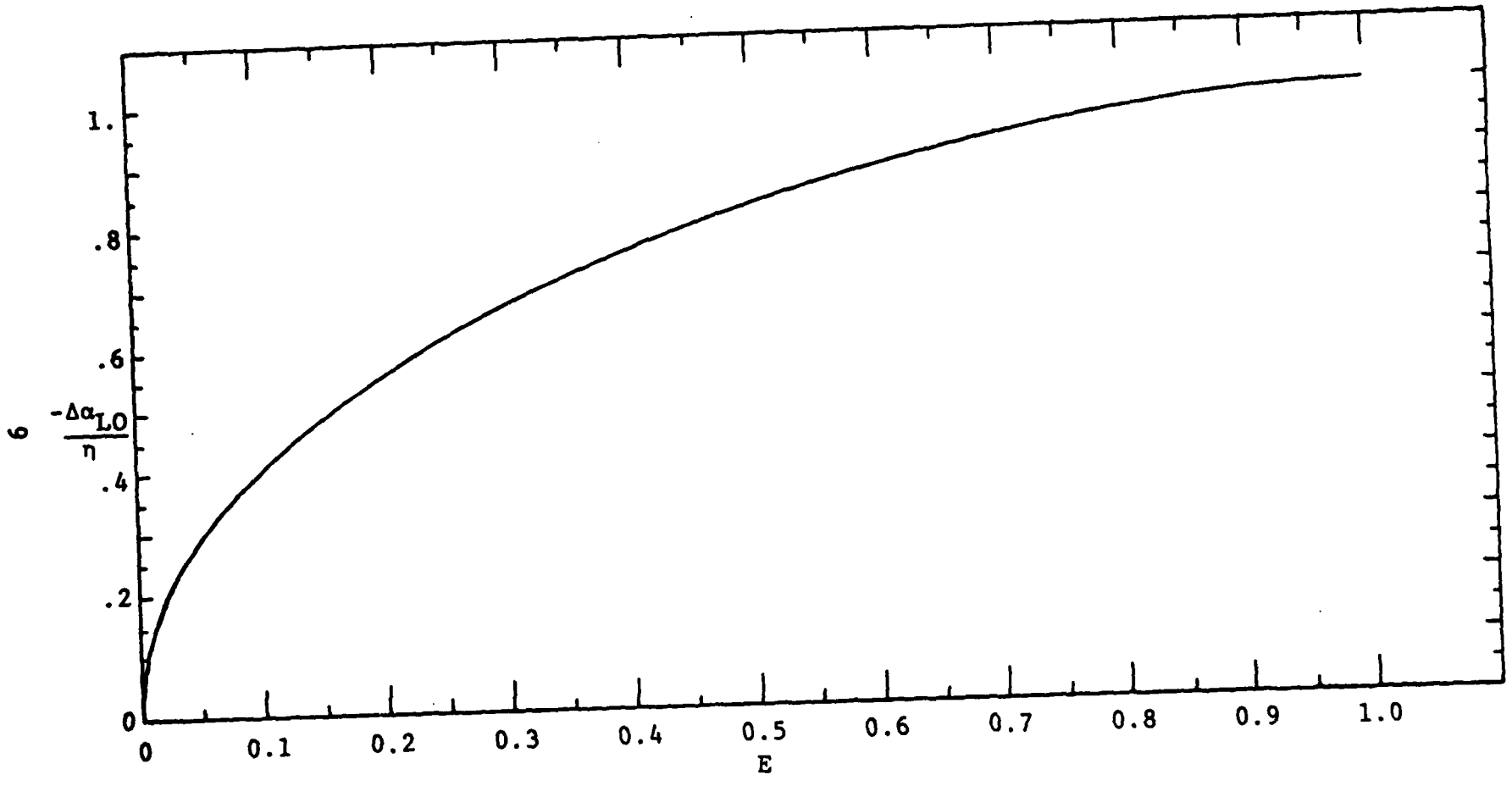

Fig. 2 Effect of flap-chord ratio, E, on $\Delta\alpha_{LO}/\eta$.

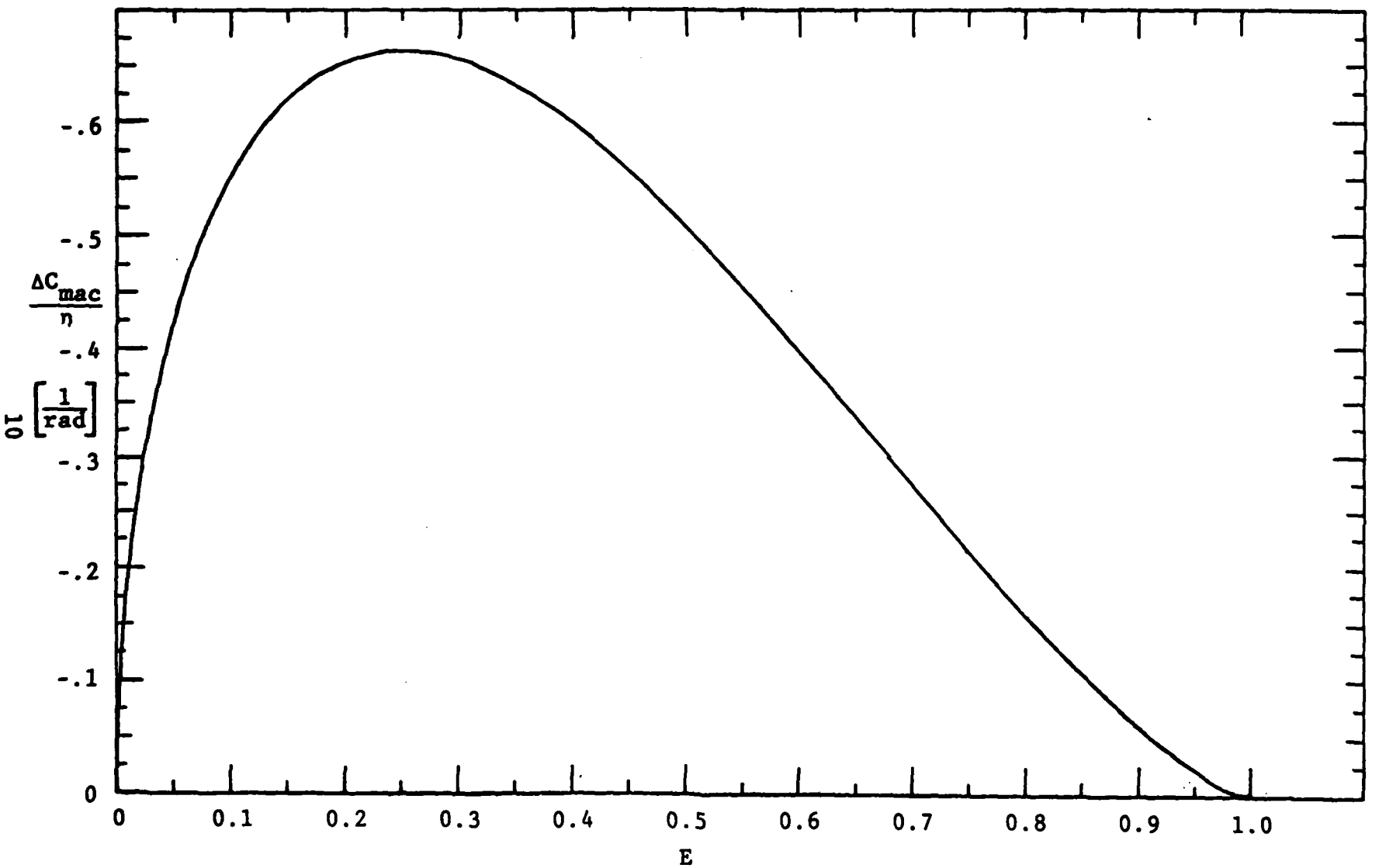

Fig. 3 Effect of flap-chord ratio on $\Delta C_{mac}/\eta$.

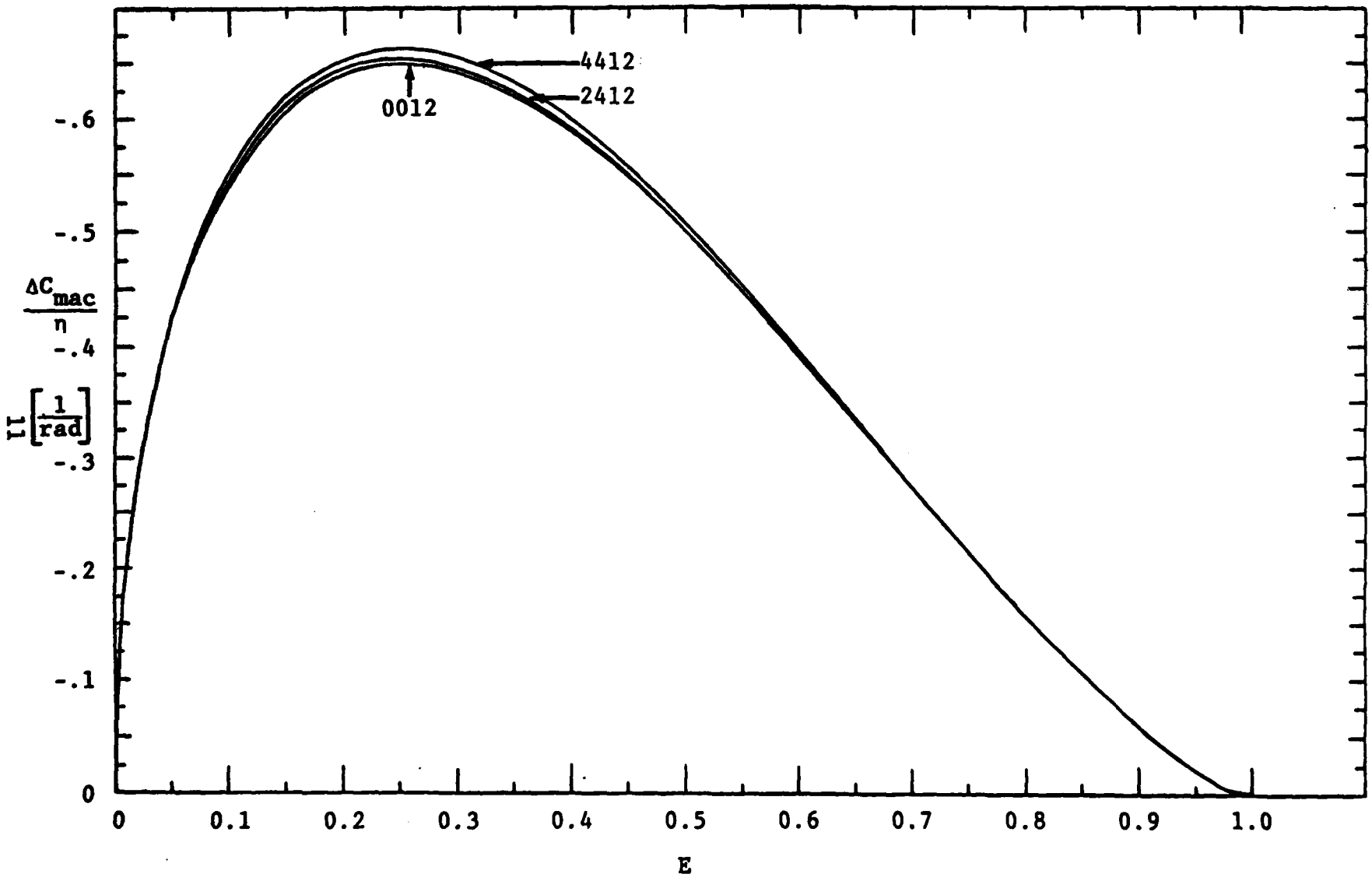

Fig. 4 Effect of camber on $\Delta C_{mac}/\eta$ versus E.

III Wind Tunnel Investigation

Models

The models for wind tunnel testing were constructed by the AFIT Model Fabrication Division. The basic components of a test model are shown in Fig. 5. Components common to all models were the flap deflection mechanism, the side plates, and the rear lift bar. The airfoil component consisted of two sections that varied because of changes in the flap-hinge location. The change in flap-hinge location thereby produced seven different models with flap-hinge locations at 20%, 30%, 40%, 50%, 60%, 70%, and 80% of chord, or expressed in flap-chord ratio, .2, .3, .4, .5, .6, .7, and .8, respectively.

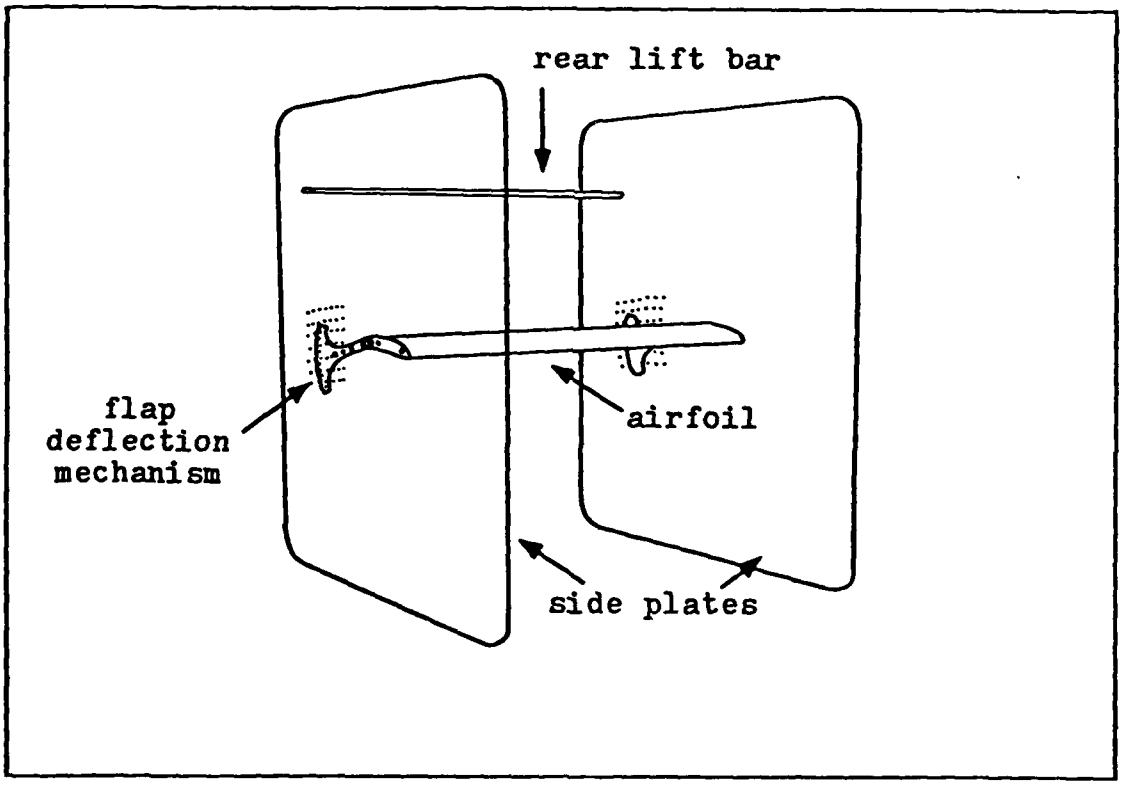

Fig. 5 Basic components of a fully assembled model

The flap deflection mechanism consisted of two identical brass plate. see Fig. 6. Holes B through G served to attach the brass plates to cnly the flap section of the airfoil being tested. Hole A of the brass plates allowed headed screws to be freely inserted, through both the side and brass plates, into treaded holes in the airfoil flap section. This established an axis of rotation about which the flap section was moved. Holes 1 through 7 of the brass plates made it possible to set the flap at prescribed angles of deflection when used in conjunction with corresponding holes in the side plates. Appendix D gives a detailed explanation of how the brass plates were used to establish a desired flap setting.

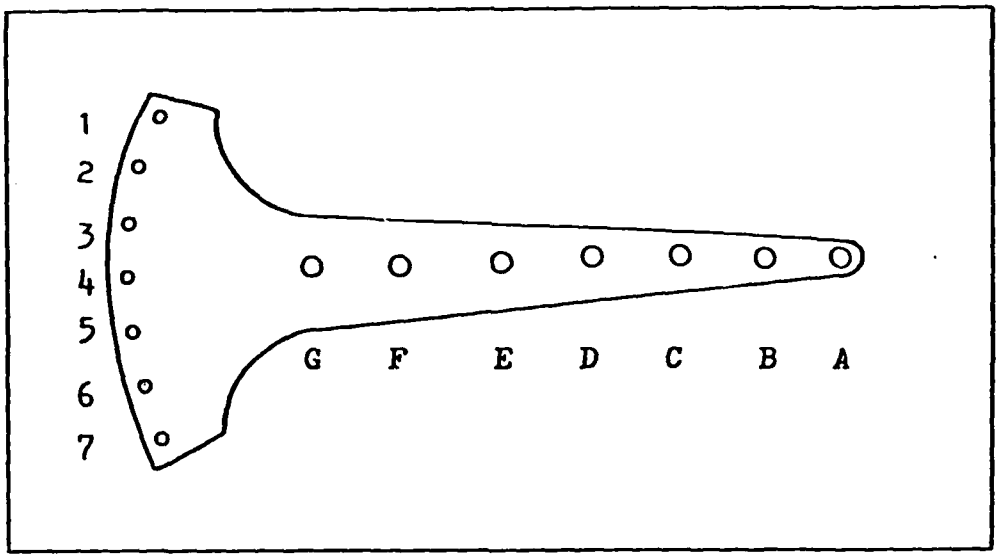

Fig. Brass flap deflection plate with flap attachment holes (B-G), flap deflection holes (1-7), and flap-hinge hole (A).

The two side plates brought all the components together to form a fully assembled model ready for testing. The side plates were constructed of 3/8-inch clear plexiglass with beveled edges and rounded corners. These plates served three

additional functions. First, they served as end plates to simulate two-dimensional flow. Secondly, they captured the airflow far enough upstream of the airfoil's influence so that the tunnel's free stream value for the dynamic pressure could be used in the two dimensional analysis. Finally, the light weight and transparency of the plexiglass side plates facilitated the change from one model to another and allowed viewing of the model during testing.

The rear lift bar was constructed from tubular aluminum with the cross section shown in Fig. 7. This bar was connected to the rear lift wire of the wind tunnel. The bar design for rear lift wire attachment eliminated possible interference problems between the deflecting flap and the rear wire attachment mechanism. It did minimize the number of model measurements needed to set angles of attack and/or flap deflections. It also kept tunnel calibrations to a minimum since only one in-tunnel calibration of a model was required to be able to set any angle of attack and flap deflection combination. Additionally, it eliminated any construction or structural problems associated with having the rear lift attachment mechanism as part of the airfoil. While the bar eliminated many possible problems and minimized many operational problems, it was not wholly satisfactory. The shape of the bar as shown in Fig. 7 led to data errors which had to be accounted for as discussed in Section IV.

The seven NACA 4412 airfoils used for the investigation were made of solid aluminum based epoxy resin. Each airfoil consisted of two matched but separate sections; a front

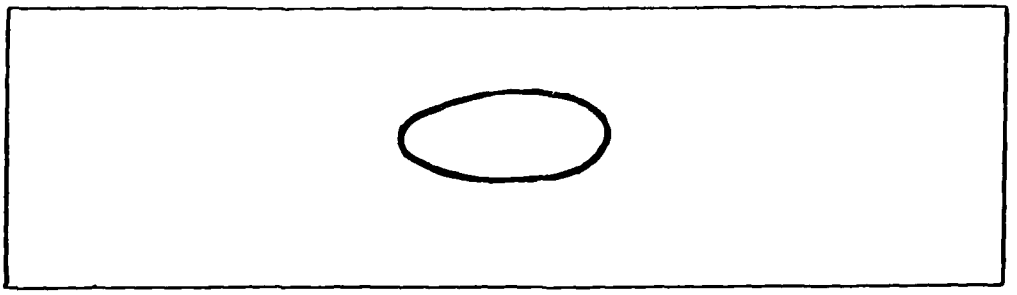

Fig. 7 Cross section of lift bar drawn to actual size.

section that remained fixed, and a flap section which rotated relative to the side plates and the front section. Figure 8 shows the seven airfoils and the difference in size of the flap section among airfoils. Each front section had two attachment fittings in the leading edge for the drag and front lift wires. The matched airfoil sections, which formed 4412s when put together at zero flap deflection, were made from different one piece 4412s because of the chord distance and front section surface lost when a flap section was cut and shaped. Thus, a flap section of E = .6 was matched with an appropriately shaped front section that resulted from producing a flap section with at least a flap-chord ratio of .1 less than .6. The one piece 4412s came from a mold made from a wooden 4412 airfoil of two foot span and nine inch chord. The mold insured that each model was the same for all practical purposes. The similarity of models was checked through model measurement prior to testing. It was confirmed by the excellent agreement between models for α_{LO} and the slope of the C_ℓ versus α curve.

See Appendix C for detailed model geometry and measurements.

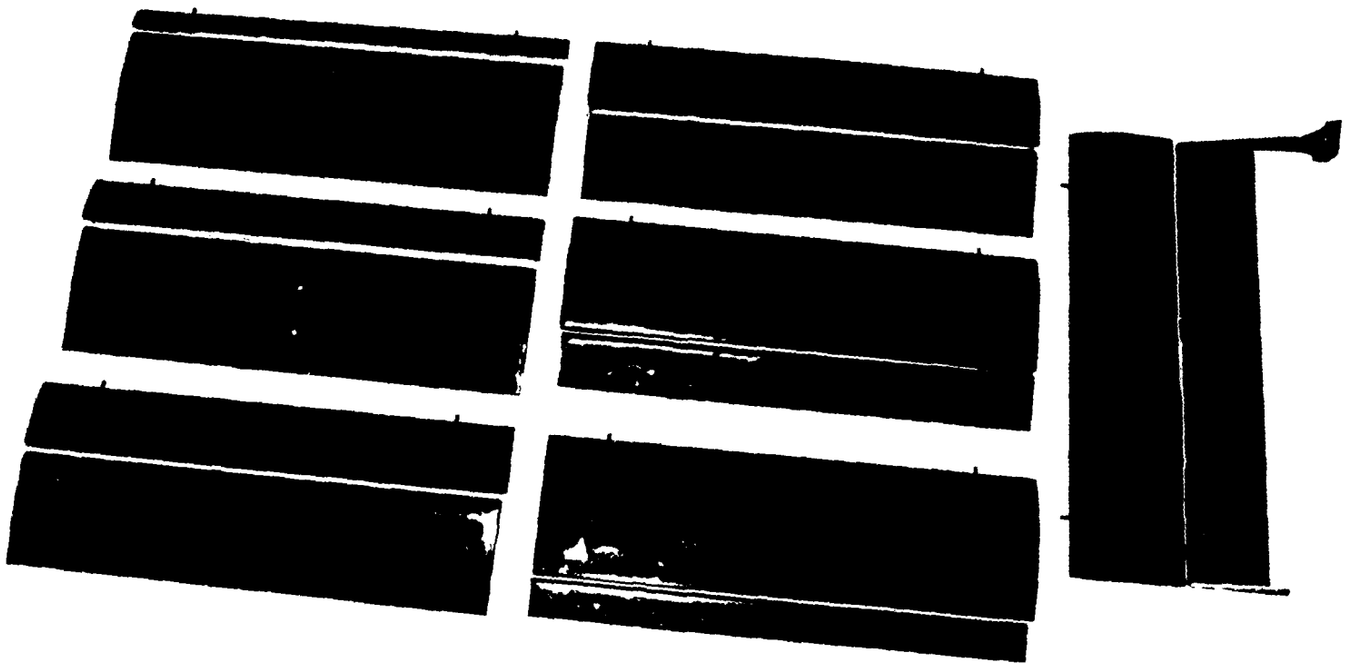

Fig. 8 Investigation airfoils showing the different sizes of the flap section. From top to bottom, left to right: E = .8, .7, .6, .5, .3, .2, and .4.

Wind Tunnel

The AFIT Five-Foot Wind Tunnel was used for the wind tunnel investigation. It is an open return, closed test section wind tunnel with a 5 ft circular cross section as shown in Fig. 9. The two counter rotating 12 ft fans of the wind tunnel are powered by four 400-horsepower direct current motors easily capable of producing the tunnel's top empty speed of 350 mph. The speed limit prevents further cracking of the fan blades at high power settings. The aerodynamic forces on the models were determined by using the wind tunnel's wire balance measuring system consisting of three springless scales connected to the model through separate wire systems. The wind tunnel's wire balance system was checked and aligned prior to beginning the runs for each model.

Installation

Prior to installation in the wind tunnel, the holes in the side plates were covered with tape on the sides facing the tunnel wall to prevent 3-D effects and the gaps between the front airfoil section and the flap section were sealed with modeling clay. Each model was then carefully measured on a surface plate using an inclinometer and a height gage. The measurements were used to determine the angle of balance for the wire system. The angle of balance then determined the distances necessary for setting angles of attack for the model. Appendix C contains a more detailed explanation of the model geometry and calculations involved.

The model was then installed in the test section. Instal-

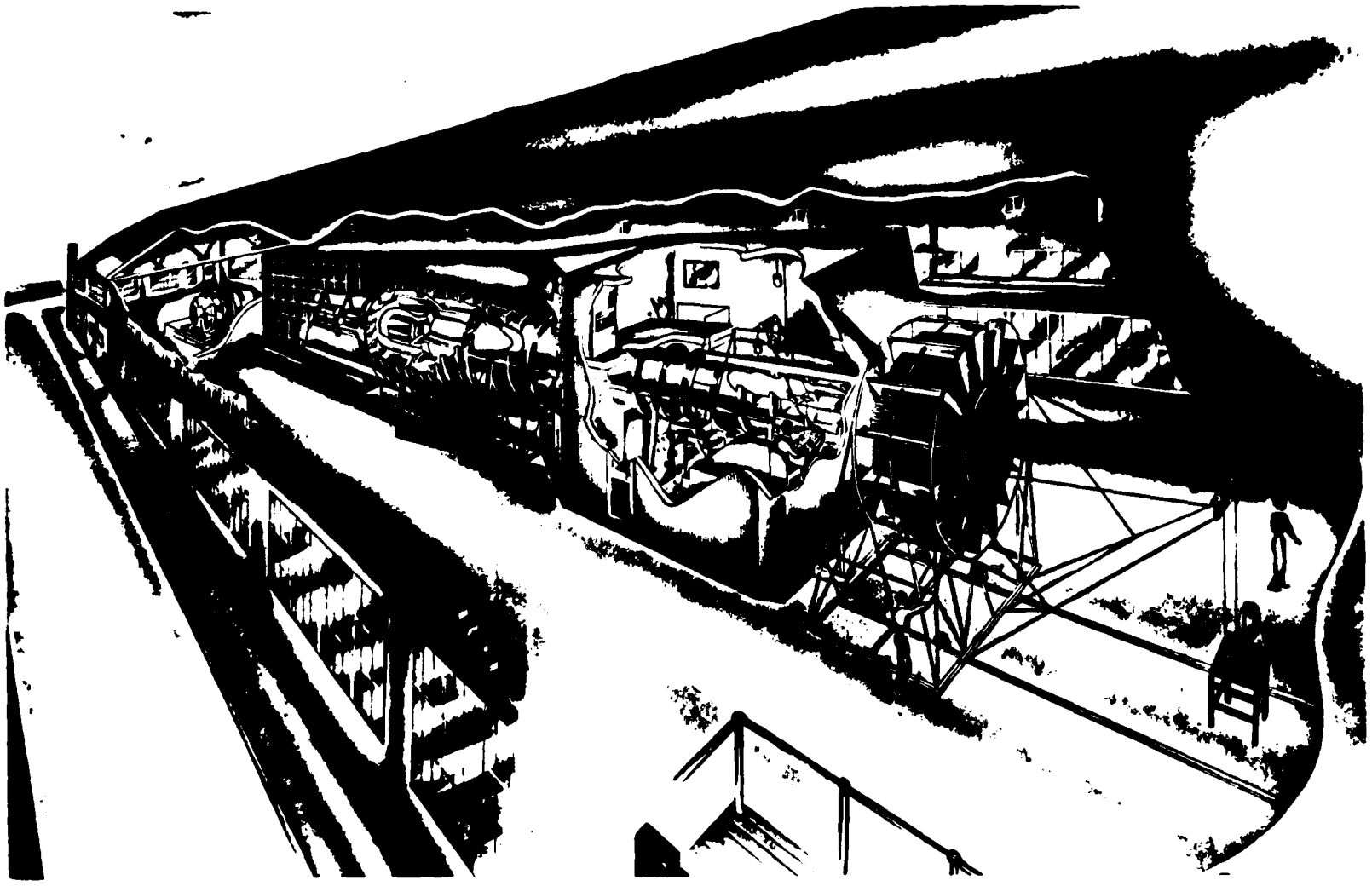

Fig. 9 AFIT Five-Foot Wind Tunnel setup.

lation was accomplished by connecting the model's attachment fittings to plates permanently connected to the appropriate tunnel wire system. These connections allowed the model to rotate freely at each connection and thereby accurately transmit the aerodynamic forces produced on the model to the wire system and then to the scales for a direct measurement. The two trunnions on the leading edge were connected to the drag and front lift wires while the attachment fitting on the rear lift bar was connected to the rear lift wire. Figures 10a and 10b show a model installed in the wind tunnel.

After installing the model, the wind tunnel instruments used to set the model at a particular angle of attack were carefully calibrated prior to taking data. The calibration used an inclinometer to measure accurately the model's angle of attack with respect to the tunnel axis.

Investigation Procedure

After calibrating an installed model, it was ready for testing. The investigation objective required that enough data be gathered to plot both the change in zero-lift angle of attack divided by flap deflection ($\Delta\alpha_{LO}/\eta$) versus flap-hinge location (E) and the change in the moment coefficient about the aerodynamic center divided by flap deflection ($\Delta C_{mac}/\eta$) versus E. Data for $\Delta\alpha_{LO}/\eta$ versus E was obtained by first setting the flap at 0°, 4°, or 8°, and the taking data for angles of attack of -6°, -4°, -2°, 0°, 2°, 4°, 6°, 8°, and 10°. Data for $\Delta C_{mac}/\eta$ versus E was obtained by having the model set at 0° angle of attack with the flap

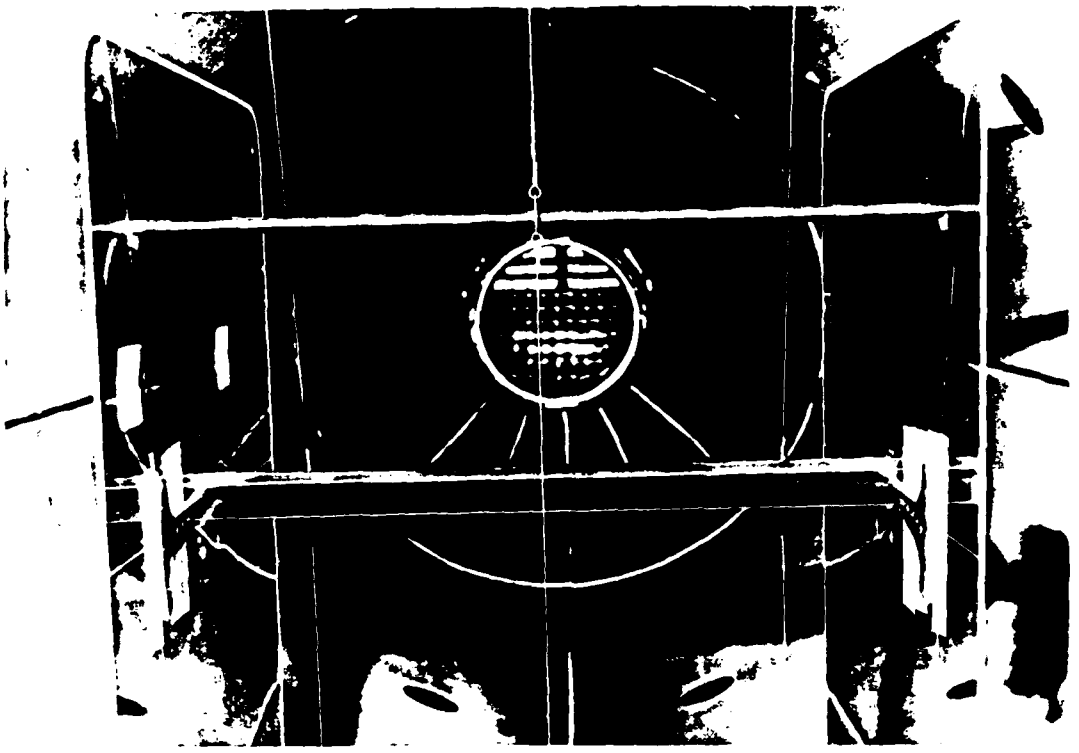

Fig. 10a Rear view of installed model.

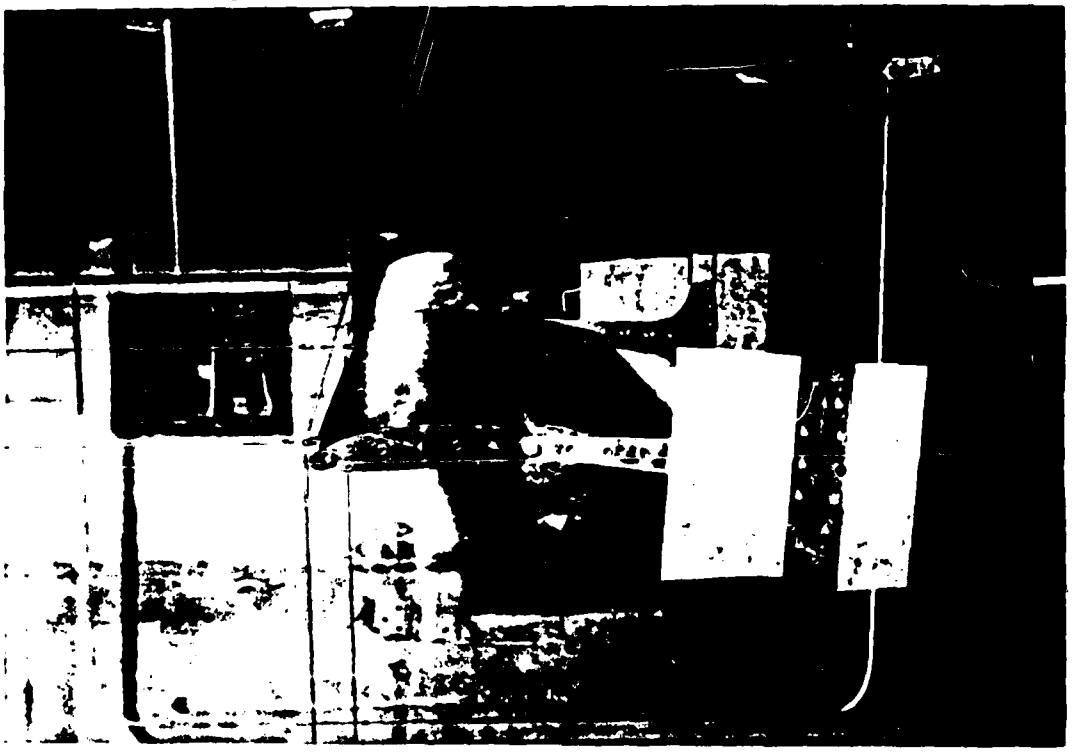

Fig. 10b Side view of installed model.

deflected at settings from 0° to 18°. Overlap in gathering the data occurred as shown in Table I since data for $\Delta\alpha_{LO}/\eta$ versus E at 0° angle of attack was also used as data for $\Delta C_{mac}/\eta$ versus E.

A typical sequence of events used to gather data for a model is given in Table I. A typical change from one flap setting to another, an event in Table I, obtained data for $\Delta C_{mac}/\eta$ and $\Delta\alpha_{LO}/\eta$ and went as follows: The model's flap setting was changed by one degree which also required re-sealing the gaps between the front airfoil section and flap section; and taping over any uncovered holes in the side plates. Next, the model and tunnel were inspected to insure no loose objects remained in the tunnel. The tunnel doors were then secured, after which the tunnel operator aligned the model and took three before-static readings. He also ensured a current barometer and temperature reading were taken. The tunnel air was turned on and brought up to the testing dynamic pressure of three inches of water. The operator adjusted the model as the airflow increased to keep it properly aligned. With the model properly aligned and the dynamic pressure at three inches, the operator took five wind-on readings. The tunnel air was then turned off and the flow allowed to go to zero. The tunnel operator again ensured the model was aligned properly and took three after-static readings. The process for an event as listed in Table I was then complete and the tunnel could again be entered to change the model's flap setting. Data for $\Delta\alpha_{LO}/\eta$ also required changes

TABLE I

Typical event sequence and data gathered

Sequence of events	Flap Setting in degrees	Angles of attack in degrees	Data gathered for	
			$\Delta\alpha_{LO}/\eta$	$\Delta C_{mac}/\eta$
1	0	-6,-4,-2,0,2,4,6,8,10	x	x
2	1	0		x
3	2	0		x
4	3	0		x
5	4	-6,-4,-2,0,2,4,6,8,10	x	x
6	5	0		x
7	6	0		x
8	7	0		x
9	8	-6,-4,-2,0,2,4,6,8,10	x	x
10	9	0		x
11	10	0		x
12	11	0		x
13	12	0		x
14	13	0		x
15	15	0		x
16	16	0		x
17	17	0		x
18	18	0		x

in angle of attack for the flap settings of 0°, 4°, and 8°. The changes in angle of attack were accomplished from outside the test section and allowed the tunnel air to remain on from one angle of attack to another. Five wind-on readings were taken for each angle of attack while three static readings were taken for each angle of attack during the before-statics and after-statics portions of the event.

Tuft studies were conducted on the .2, .4, .5, .6, and .8 E models after obtaining the force data for that individual model. These visual studies indicated the extent of separation on the airfoil's upper surface and were used later to eliminate data for those particular angles of attack and flap settings which showed separation. Appendix E gives the results of the tuft studies.

Data

The data readings for any one setting of angle of attack and flap deflection usually consisted of three before-static readings, five wind-on readings, and three after-static readings, The multiple readings helped to identify bad data and reduce scatter through averaging. Additionally, repeat readings were taken to verify the consistency and repeatability of the data. The static readings determined the loads on the model when the airflow was zero while the wind-on readings determined the loads with air flowing over the model.

Each time a reading was taken, the respective loads on all three scales (drag, rear lift, and front lift) were printed on separate paper tapes. The readings on each tape

were transferred to respective tables with line entries containing static and wind-on readings gathered for a particular angle of attack and flap setting combination. An average static value for any combination was obtained by averaging all the static readings for that combination. An average wind-on reading consisted of only averaging the five wind-on readings for a particular event. In other words, any set of five wind-on readings were averaged and treated as a separate result from any other five wind-on readings. The aerodynamic forces on the model for any particular combination of angle of attack and flap setting were found by subtracting the wind-on averages from the static averages to give drag forces, rear lift forces, and front lift forces. Appendix F contains the raw data (data attainable directly from the scale tapes) obtained during the investigation for each of the seven models.

IV Results

Data Reduction

The data in Appendix F was first reduced to obtain lift coefficient versus angle of attack graphs for each of the models. The lift coefficient (C_ℓ) for a particular angle of attack (α), flap setting, and model was obtained by adding the forces from the raw front lift and rear lift tables and then dividing by the dynamic pressure times the wing span times the chord length (qbc). Since lift data for changing angles of attack were obtained for flap deflections of 0°, 4°, and 8°, this produced three C_ℓ versus α plots for each model. Each plot intersected the α axis where the lift coefficient was zero, this determined the value of the zero-lift angle of attack (α_{LO}) for a specific flap deflection (η) of 0°, 4°, or 8°. Three changes in zero-lift angle of attack divided by the flap deflection ($\Delta\alpha_{LO}/\eta$) were then obtained by subtracting α_{LO} at $0°\eta$ from α_{LO} at $4°\eta$ and then dividing by 4°, α_{LO} at $4°\eta$ from α_{LO} at $8°\eta$ and dividing by 4°, and finally α_{LO} at $0°\eta$ from α_{LO} at $8°\eta$ and dividing by 8°. These values of $\Delta\alpha_{LO}/\eta$ were then plotted versus the value of the flap-chord ratio (E) for the model data being reduced and against the theoretical curve from Fig. 2. This gave Fig. 11 which compares experiment to theory for $\Delta\alpha_{LO}/\eta$ versus E.

The raw wind-tunnel data was also reduced to obtain the change of moment coefficient about the aerodynamic center divided by flap deflection ($\Delta C_{mac}/\eta$) for each model. By

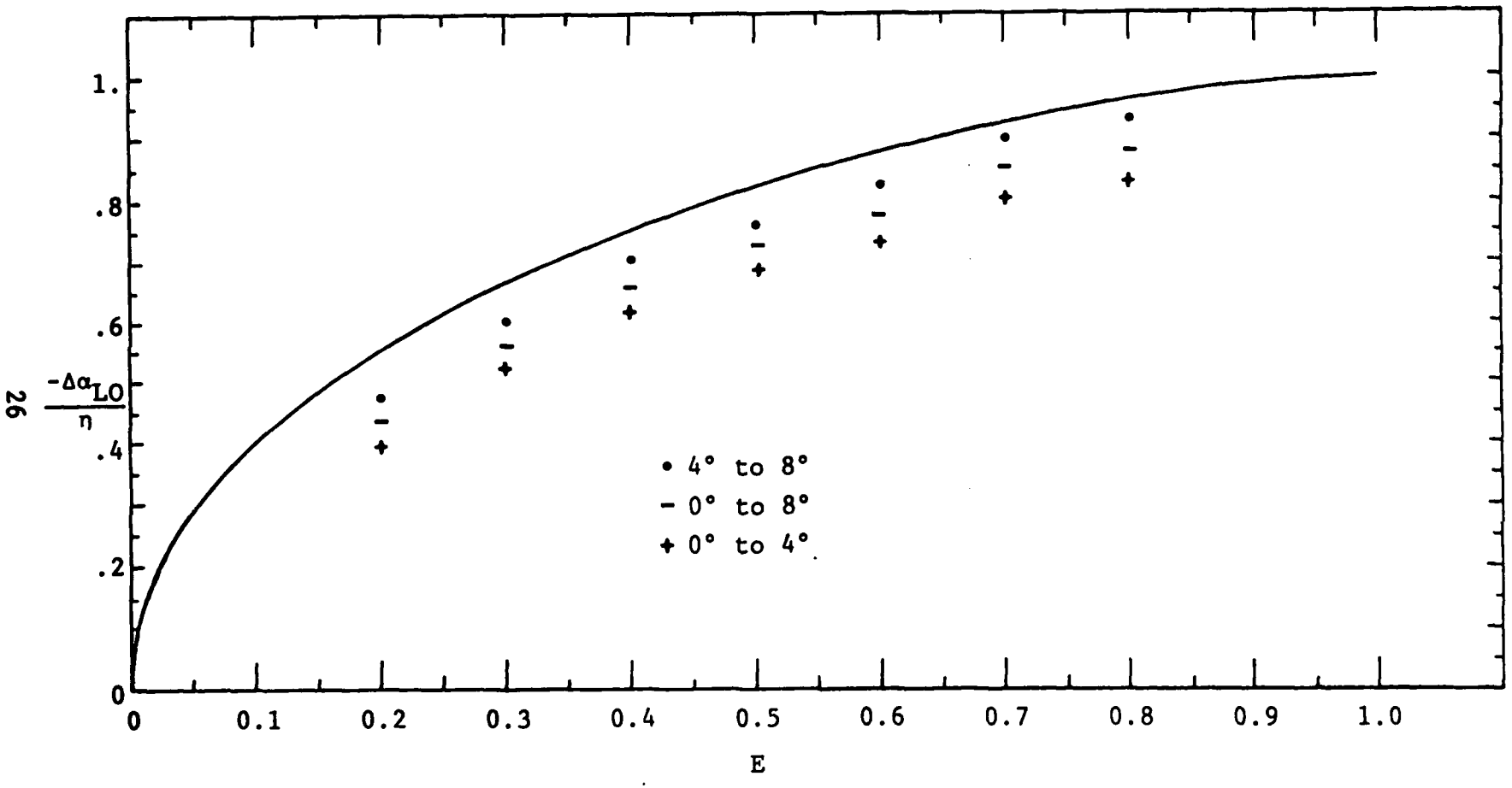

Fig. 11 Experiment versus theory for $\Delta\alpha_{LO}/\eta$ versus E.

summing moments from the rear lift and front lift forces about an assumed aerodynamic center of .245c and then dividing by qbc^2, the C_{mac} was obtained. This was done for data at zero degrees angle of attack and varying flap deflections to obtain a graph of C_{mac} versus η. $\Delta C_{mac}/\eta$ was then obtained by simply measuring the slope of the C_{mac} versus η line. This value was then plotted for the particular model falp-chord ratio against the theoretical curve in Fig. 4 to produce Fig. 12 which again compares experiment to theory.

Comparison of Experimental Data to Theoretical Predictions

Figure 11 shows the experimental data plotted with the theoretical curve for $\Delta\alpha_{LO}/\eta$ versus E. Here the experimental data compares favorably with the theoretical curve from both a trend and numerical standpoint. However, for the small flap deflections used, only one experimental curve was expected instead of three. This seems to imply that the data could be biased in some manner.

Figure 12 shows the experimental data plotted with the theoretical curve for $\Delta C_{mac}/\eta$ versus E. Here, the experimental data indicates the same general trend as the theoretical curve but the positive numbers for E = .6, .7, and .8 are not possible unless again the data has been biased. Since it has already been established in Section II that the theoretical curves are, for all practical purposes, the same for cambered and uncambered flapped airfoils, it is reasonable to assume that the experimental data gathered for a cambered flapped airfoil should be almost the same as the uncambered data. The

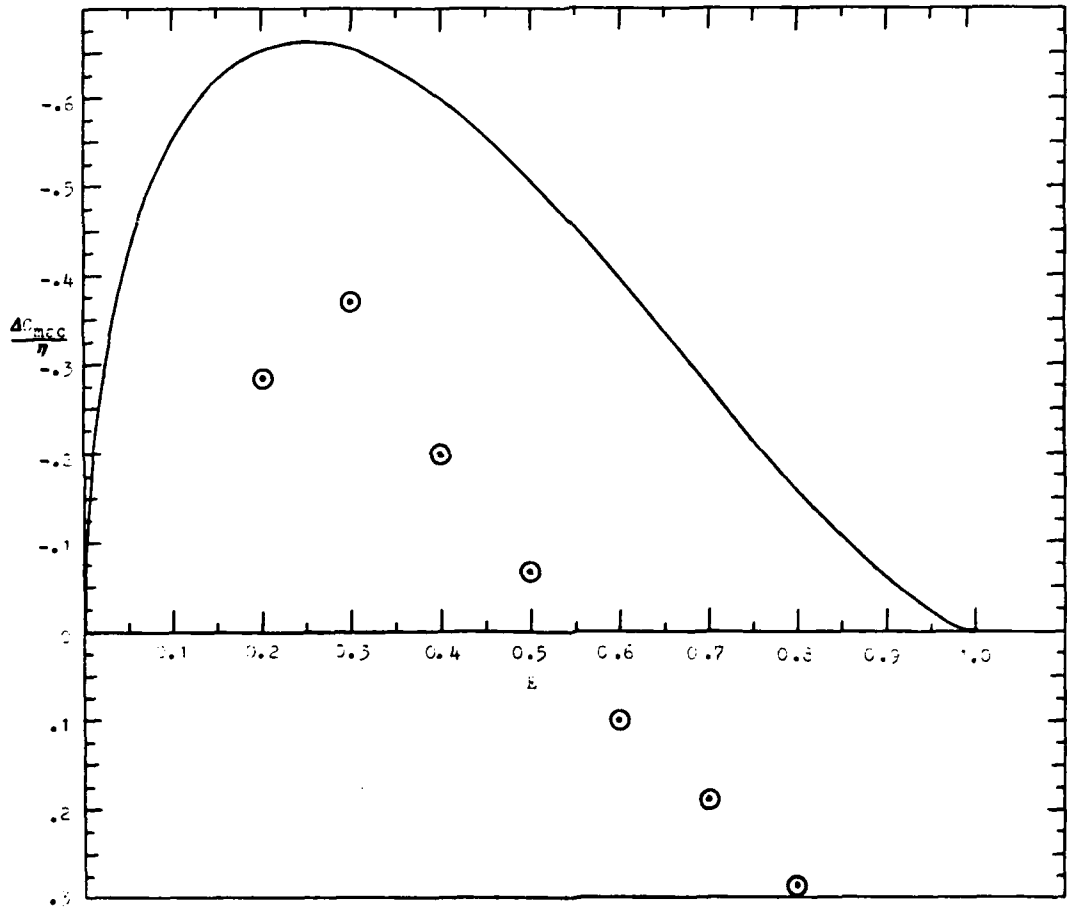

Fig. 12 Experiment versus theory for $\Delta C_{mac}/\eta$ versus E.

experimental data in both Figs. 11 and 12 are overall lower than the results given by Schlichting (Ref 4:65) for an uncambered airfoil with hinged flaps. This also indicates that the data could be biased in some manner.

Corrections for the experimental data were not found. Therefore, the experimental data presented only serves to confirm the general trend of the theoretical predictions.

V Conclusions and Recommendations

Conclusions

The experimental data gathered during the investigation was biased in some manner to produce results which at best can only be used to confirm the trend of the theoretical predictions of the change in the zero-lift angle of attack divided by flap deflection ($\Delta\alpha_{LO}/\eta$) versus the flap-hinge location (E) and the change in the moment coefficient about the aerodynamic center divided by flap deflection ($\Delta C_{mac}/\eta$) versus E. The data can not be used to meet the thesis objective of predicting $\Delta\alpha_{LO}/\eta$ versus E and $\Delta C_{mac}/\eta$ versus E for a NACA 4412 airfoil.

While there is no direct evidence as to what was biasing the experiment, there are several indirect items which point to a major problem. That major problem would seem to be the rear lift bar. If we assume the models were reasonable reproductions of the 4412 airfoil, then, a downward force was produced to counteract the airfoil's lift. The downward force had to be occurring because from Ref 5 the zero-lift angle of attack for a 4412 airfoil is approximately 3.9°, while this investigation had a zero-lift angle of attack of approximately 2° as demonstrated from the C_ℓ versus α graphs in Appendix H. This is a large difference which implies that something was shifting the C_ℓ versus α graph to the right/producing a downward force. That much change could come from another lifting surface which the rear lift bar definitely was as shown by the

cross sectional view in Fig. 7. The rear lift bar was also located in a position where it could be influenced by downwash changes from changes in the amount of flap deflection. This could account for the large changes in the slope of the C_ℓ versus α graphs as the flap was deflected. Take for example the model with E = .8, the slope, in units 1/radian, of the C_ℓ versus α graph goes from 5.809 with $0°\eta$ to 5.602 with $4°\eta$, and to 5.204 with $8°\eta$. In other words, the amount of flap deflection changed the forces on the rear lift bar which in turn effected the model results. The statements in this paragraph imply that the rear lift bar was influencing/biasing the experiment. Unfortunately, no way has been found to make acceptable corrections involving the rear lift bar from the data gathered during the investigation.

Recommendations

If the investigation is accomplished again using the same basic airfoils and model, I would like to recommend some changes which may prove useful. First, eliminate the rear lift bar by modifying the airfoil to accommodate a sting for connecting the rear lift wire to the model or by replacing the rear lift bar with one of cylindrical shape. Both changes have inherent problems but the rear lift bar used in this investigation is unacceptable and must be changed or eliminated. Second, modify the side plates to make them larger and round. Although no evidence exists as to any effect the side plates had on the investigation, the plates are aligned into the free stream differently when the angle of attack is changing which could be

causing different forces on the plates themselves and therefore the model as the angle of attack changes. Third, cut down the flap deflection mechanism so that only flap deflections of 0° to 12° can be accomplished. This provides more than enough data points to plot and eliminates wasted effort since the tuft studies showed that little data is gained above 12°η before separation on the upper surface occurs. Also round off the edges of the flap deflection mechanism and cut down the size of the mechanism along the attachment holes so that the mechanism disturbs the flow as little as possible. Fourth, find someway to seal the gaps on the whole airfoil besides modeling clay. The clay can never be put on the same way twice; tape or wax might be two other possibilities. Finally, the manner in which the investigation is conducted could be changed to help produce successful results. The investigation could be conducted at a higher dynamic pressure than 3 inches of water to provide a Reynolds number of the same magnitude that Abbott and Doenhoff had for their experiments with the 4412. This may involve changing the side plates to a different material than plexiglass or providing stiffeners for the plexiglass to accommodate the increase in tunnel speed. It would be very useful to find the drag and lift of any side plates through wind-tunnel testing so that they can be accurately accounted for during the investigation. When taking data, angle of attack changes could be accomplished in one degree increments and with flap deflections of 0°, 2°, 4°, 6°, and 8°. This increase in data should result in more accurate curves and

and provide a better representation of the actual situation. These recommendations are based on problems encountered during this investigation and hopefully will prove useful if the investigation is accomplished again.

Bibliography

1. McCormick, B.W.,Jr. Aerodynamics of V/STOL Flight. New York: Academic Press, Inc., 1967.

2. Kuethe, A.M. and C.Y. Chow. Foundations of Aerodynamics: Bases of Aerodynamic Design.(Third Edition) New York: John Wiley and Sons, Inc., 1976.

3. Jumper, E.J. Examining a Rule of Thumb For the Relation Between Camber and Zero-Lift Angle of Attack. Reprint from Aeronautics Digest- Fall/Winter 1980. USAFA-TR-81-4, USAF Academy, Colorado.

4. Schlichting, H. and E. Truckenbrodt. Aerodynamics of the Airplane. New York: McGraw-Hill, Inc., 1979.

5. Abbott, I.H. and A.E. Von Doenhoff. Theory of Wing Sections Including a Summary of Airfoil Data. New York: Dover Publications, Inc. 1959.

6. Pope, A. and J.J. Harper. Low-Speed Wind Tunnel Testing. New York: John Wiley and Sons, Inc. 1966.

Appendix A

Analytical Solution for α_{LO} and C_{mac}

Thin-airfoil theory gives $\alpha_{LO} = \frac{-1}{\pi}\int_0^{\pi} \frac{dz}{dx}(\cos\theta - 1)\,d\theta$ and $C_{mac} = \frac{1}{2}\int_0^{\pi} \frac{dz}{dx}(\cos 2\theta - \cos\theta)\,d\theta$. These equations can be analytically integrated for an NACA 4412 airfoil to give numbers for α_{LO} and C_{mac}.

The camber line of a 4 digit NACA airfoil consists of two parabolic arcs tangent at the camber line's maximum ordinate. The equations defining the camber line are

$$\frac{z}{c} = \frac{m}{p^2}\left[2p\frac{x}{c} - \left[\frac{x}{c}\right]^2\right] \tag{18}$$

forward of maximum ordinate and

$$\frac{z}{c} = \frac{m}{(1-p)^2}\left[(1-2p) + 2p\frac{x}{c} - \left[\frac{x}{c}\right]^2\right] \tag{19}$$

aft of the maximum ordinate where m equals the maximum ordinate of the camber line expressed as a fraction of the chord and p equals the chord wise position of the maximum ordinate in tenths of the chord. The 4 digit NACA airfoil numbering system gives the values of m and p. The first digit divided by 100 is m and the second digit divided by 10 is p. (Ref 5: 113,114)

The integral equations from Section I to be solved are

$$\alpha_{LO} = \frac{-1}{\pi}\int_0^{\pi} \frac{dz}{dx}(\cos\theta - 1)\,d\theta \tag{12}$$

and

$$C_{mac} = \frac{1}{2}\int_0^{\pi} \frac{dz}{dx} (\cos 2\theta - \cos \theta)\, d\theta \qquad (13)$$

The only other piece of information needed to accomplish the integration is the function relating x and θ which is $x = .5c(1 - \cos \theta)$. Thus, finding $\frac{dz}{dx}$ from equations 18 and 19 and substituting for $\frac{dz}{dx}$ and x in equation 12

$$\alpha_{LO} = \frac{-1}{\pi}\left[\int_0^{\beta} \left[\frac{2m}{p} - \frac{2mx}{p^2 c}\right](\cos \theta - 1)\, d\theta + \int_{\beta}^{\pi} \left[\frac{2mp}{(1-p)^2} - \frac{2mx}{(1-p)^2 c}\right](\cos \theta - 1)\, d\theta\right] \qquad (20)$$

where β is the angle corresponding to the maximum ordinate. Using the 4412 values for m and p, and substituting for x again

$$\alpha_{LO} = \frac{-1}{\pi}\left[\int_0^{\beta} [.2 - .25(1 - \cos \theta)] (\cos \theta - 1)\, d\theta + \int_{\beta}^{\pi} \left[\frac{.8}{9} - \frac{1-\cos \theta}{9}\right](\cos \theta - 1)\, d\theta\right] \qquad (21)$$

The angle β corresponding to m and p can be found easily by substituting in the value for x at the maximum ordinate into the equation $x = .5c(1 - \cos \theta)$. Thus, for the 4412, $.4c = .5c(1 - \cos \beta)$ which implies that $\cos \beta = .2$ and therefore $\beta = 1.3694384$ radians. By expanding the integral and putting the numerical value of β into equation 21

$$\alpha_{LO} = \frac{-1}{\pi}\left[\int_0^{1.369} [.2(\cos\theta - 1) - .25(2\cos\theta - 1 - \cos^2\theta)]\, d\theta \right.$$

$$\left. + \int_{1.369}^{\pi} \left[\frac{.8}{9}(\cos\theta - 1) - \frac{1}{9}(2\cos\theta - 1 - \cos^2\theta)\right] d\theta\right] \qquad (22)$$

After integrating equation 22

$$\alpha_{LO} = \frac{-1}{\pi}\left[\left[.2(\sin\theta - \theta) - .5\sin\theta + .25\theta + .25\left[\frac{\theta}{2} + \frac{\sin 2\theta}{4}\right]\right]\Bigg|_0^{1.369}\right.$$

$$\left. + \left[\frac{.8}{9}(\sin\theta - \theta) - \frac{2}{9}\sin\theta + \frac{\theta}{9} + \frac{1}{9}\left[\frac{\theta}{2} + \frac{\sin 2\theta}{4}\right]\right]\Bigg|_{1.369}^{\pi}\right] \qquad (23)$$

By putting in the limits for θ, we arrive at

$$\alpha_{LO} = \frac{-1}{\pi}(.227795) = -.0725094 \text{ radians} = -4.1544826 \text{ degrees}$$

Following the same steps as for α_{LO}

$$C_{mac} = \frac{1}{2}\left[\int_0^{1.369} [.2(\cos 2\theta - \cos\theta) - .25(1 - \cos\theta)(\cos 2\theta - \cos\theta)]\, d\theta \right.$$

$$\left. + \int_{1.369}^{\pi} \left[\frac{.8}{9}(\cos 2\theta - \cos\theta) - \frac{1}{9}(1 - \cos\theta)(\cos 2\theta - \cos\theta)\right] d\theta\right] \qquad (24)$$

$$C_{mac} = \frac{1}{2}\left[\left[.2\left[\frac{\sin 2\theta}{2} - \sin\theta\right] - .25\left[\frac{\sin 2\theta}{2} - \sin\theta + \frac{\theta}{2} + \frac{\sin 2\theta}{4}\right]\right.\right.$$

$$\left. + .125\left[\sin\theta + \frac{\sin 3\theta}{3}\right]\right]\Bigg|_0^{1.369} + \left[\frac{.8}{9}\left[\frac{\sin 2\theta}{2} - \sin\theta\right]\right.$$

$$\left.\left. - \frac{1}{9}\left[\frac{\sin 2\theta}{2} - \sin\theta + \frac{\theta}{2} + \frac{\sin 2\theta}{4}\right] + .0555556\left[\sin\theta + \frac{\sin 3\theta}{3}\right]\right]\Bigg|_{1.369}^{\pi}\right] \qquad (25)$$

$$C_{mac} = \frac{1}{2}(-.2124781) = -.1062391$$

Appendix B

Computer Program

This appendix contains the listing of the computer program used to find the theoretical predictions for zero-lift angle of attack (α_{L0}), moment coefficient about the aerodynamic center (C_{mac}), change in α_{L0} divided by flap deflection ($\Delta\alpha_{L0}/\eta$) versus the flap-chord ratio (E), and $\Delta C_{mac}/\eta$ versus E as given in Section II. Comment cards in the program define the variables, parameters, and limitations. The program used numerical integration to calculate the predictions.

The program did not attempt to keep computer time to a minimum or provide a program which needed a minimal number of segments to obtain accurate results. The objective was simply to obtain accurate results as demonstrated by the comparison between the analytic solution and the program solution for α_{L0} and C_{mac} at the top of page 6. It should be pointed out that the method used in this program, the trapezoidal rule of integration, does have inherent errors and requires a relatively large number of segments to achieve accurate results. The accuracy could be improved and the number of segments needed to compute an accurate solution could be reduced by using a different numerical integration method. Since the mean camber line of the NACA 4412 airfoil is a parabolic arc, Simpson's Rule which uses parabolic arcs could be used to produce better accuracy with fewer segments when compared to the results of this program.

```
3 NOV 82 20:19:00   HARRIS FORTRAN 77 S&U OPTIMIZING COMPILER      01414-00
MODULE NAME:  *MAIN*

  1:        PROGRAM FLAP
  2: C      DESIGNED BY HOWARD PRICE, AUG 82, THESIS WORK ON VARYING HINGED
  3: C      FLAP.
  4:        INTEGER I,J,K,L,LE,LETA,N,NA,NACA4D,NE,NFS,NP,NPTS,LL
  5:        REAL AF,AFN,ALO,ALO2,A3,A4,CMAC,CMAC2,DEL1,DEL2,DEL1T,DEL2T,DS,DX,
 6:       $DXN,DXT,DZ,DZDX,DZN,DZT,E,ET,ETA,FC,FC1,FC2,M,P,PX,PZ,SA,SAN,SF,
 7:       $SL,STH,S2TH,THETA,X,XC,XCN,XF,XN,X1,X2,X3,Z,ZN,ZP
  8: C      DIMENSIONS FOR POINT/SEGMENT PROPERTIES OF AIRFOIL CAMBERLINE AND
  9: C      # OF FLAP CHORD RATIOS. CHANGE DIMENSIONS FOR MORE THAN 800
 10: C      SEGMENTS OR 100 FLAP CHORD RATIOS.
 11:        DIMENSION AF(801),AFN(801),DEL1(101,10),DEL2(101,10),DS(800),DZ(80
 12:       $1),DZDX(800),E(101),ETA(10),PX(801),PZ(801),THETA(801),SA(801),SA
 13:       $N(801),SF(801),SL(801),X(801),XN(801),Z(801),ZN(801)
 14: C      INPUT #(NA) OF AIRFOIL CAMBERLINES TO BE ANALYZED
 15:        READ(7,*)NA
 16: C      MAIN CONTROL LOOP
 17:        DO 16 K=1,NA
 18: C        INPUT # OF SEGMENTS(N), AIRFOIL #(NACA4D), CHORD LENGTH(XC)
 19:          READ(7,*)N,NACA4D,XC
 20: C        # OF POINTS(NPTS),CAMBER(M), MAX CAMBER LOCATION(P)
 21:          NPTS=N+1
 22: C        GET CAMBER FROM NACA4D #
 23:          M=NACA4D/1000.
 24:          M=AINT(M)
 25:          M=.01*M
 26: C        GET MAX CAMBER LOCATION FROM NACA4D #
 27:          P=NACA4D/100.
 28:          P=AINT(P)
 29:          P=.1*(P-(M*1000.))
 30: C        POINT(NP) OF MAX CAMBER
 31:          NP=(P*N)+1
 32: C        X COMPONENT(DX) OF EVERY SEGMENT
 33:          DX=XC/N
 34: C        NACA 4 DIGIT AIRFOILS CONSIST OF 2 PARABOLIC ARCS TANGENT AT MAX
 35: C        CAMBER POINT. DO LOOP 1 COMPUTES UP TO NP USING 1 ARC WHILE DO
 36: C        LOOP 2 COMPUTES FROM NP TO TRAILING EDGE POINT(NPTS) USING 2ND
 37: C        ARC. COORDINATE SYSTEM HAS LEADING EDGE POINT AT ORIGIN AND NPTS
 38: C        ON X AXIS AT XC FROM ORIGIN.
 39:          DO 1 J=1,NP
 40: C          COORDINATE(X(J)) OF POINT ON X AXIS. Z(PX(J)) X(J) IS OF XC.
 41:            X(J)=(J-1)*DX
 42:            PX(J)=X(J)/XC
 43:            IF(P.GT.0.)THEN
 44: C            FOR CAMBERED AIRFOIL, ARC EQUATION FINDS HEIGHT(Z(J)) OF A
 45: C            POINT ON CAMBERLINE IN %(PZ(J)) OF XC.
 46:              PZ(J)=M*((2.*P*PX(J))-(PX(J)**2))/(P**2)
 47:            ELSE
 48: C            SYMMETRICAL AIRFOIL,HEIGHT OF CAMBERLINE IS 0.
 49:              PZ(J)=0.
 50:            END IF
```

```
3 NOV 82 20:19:00   HARRIS FORTRAN 77 SAU OPTIMIZING COMPILER      01414-00
MODULE NAME:  FLAP

 51:            Z(J)=XC*PZ(J)
 52: C          DISTANCE(SL(J))FROM POINT 1 TO POINT J.
 53:            SL(J)=SQRT((X(J)**2)+(Z(J)**2))
 54: C          ANGLE(SA(J)) WITH X AXIS OF LINE FROM POINT 1 TO POINT J
 55: C          SA IN RADIANS
 56: C          CHANGE IN Z(DZ(J)) FROM POINT TO POINT
 57:            IF(J.EQ.1)THEN
 58: C            FRONT CONDITIONS
 59:              SA(J)=0.
 60:              DZ(J)=0.
 61:            ELSE
 62:              SA(J)=ATAN(Z(J)/X(J))
 63:              DZ(J)=Z(J)-Z(J-1)
 64:            END IF
 65: C          X(J) TRANSFORMATION ANGLE(THETA(J)) IN RADIANS
 66:            THETA(J)=ACOS(1.-(2.*X(J)/XC))
 67:      1   CONTINUE
 68:          DO 2 J=NP+1,N
 69:            X(J)=X(J-1)+DX
 70:            PX(J)=X(J)/XC
 71:            PZ(J)=M*(1.-(2.*P)+(2.*P*PX(J))-(PX(J)**2))/((1.-P)**2)
 72:            Z(J)=XC*PZ(J)
 73:            DZ(J)=Z(J)-Z(J-1)
 74:            THETA(J)=ACOS(1.-(2.*X(J)/XC))
 75:            SL(J)=SQRT((X(J)**2)+(Z(J)**2))
 76:            SA(J)=ATAN(Z(J)/X(J))
 77:      2   CONTINUE
 78: C        REAR CONDITIONS
 79:          X(NPTS)=XC
 80:          THETA(NPTS)=3.14159265
 81:          SL(NPTS)=XC
 82:          SA(NPTS)=0.
 83:          Z(NPTS)=0.
 84:          DZ(NPTS)=Z(NPTS)-Z(N)
 85: C        INITIALIZE ANGLE OF ZERO LIFT(ALO) AND COEFFICIENT OF MOMENT
 86: C        ABOUT AERODYNAMIC CENTER(CMAC)
 87:          ALO=0.
 88:          CMAC=0.
 89: C        NUMERICAL SUMMATION PROCESS/LOOP FOR ALO AND CMAC
 90:          DO 3 I=1,N
 91: C          SLOPE(DZDX(I)) OF EACH SEGMENT
 92:            DZDX(I)=DZ(I+1)/DX
 93: C          LENGTH(DS(I))OF EACH SEGMENT
 94:            DS(I)=SQRT((DZ(I+1)**2)+(DX**2))
 95: C          INTERMEDIATES IN ALO AND CMAC EQUATIONS
 96:            STH=SIN(THETA(I+1))-SIN(THETA(I))
 97:            S2TH=SIN(2.*THETA(I+1))-SIN(2.*THETA(I))
 98:            ALO=(DZDX(I)*(STH+THETA(I)-THETA(I+1)))+ALO
 99:            CMAC=(DZDX(I)*(-STH+(S2TH/2.)))+CMAC
100:      3   CONTINUE
```

```
3 NOV 82 20:19:00   HARRIS FORTRAN 77 SAU OPTIMIZING COMPILER      01414-00
MODULE NAME:  FLAP

101: C        FINAL ALO IN DEGREES
102:          ALO=(-ALO/3.14159265)*(180./3.14159265)
103: C        FINAL CMAC
104:          CMAC=CMAC/2.
105: C        OUTPUT WITHOUT FLAP DEFLECTION
106:          PRINT'("1")'
107:          PRINT'("0",33X,"ALPHA(LO) EQUALS ",F10.7," .  CMAC EQUALS ",
108:       $  F10.7,".")',ALO,CMAC
109:          PRINT'(38X," FIXED FLAP CHORD RATIOS")'
110:          PRINT'(38X," VARYING FLAP DEFLECTIONS")'
111: C        L = DIMENSION VARIABLE, LE = LOOP COUNTER TO CHANGE FLAP CHORD
112: C        RATIO E.
113:          L=0
114:          DO 13 LE=0,100
115:            L=L+1
116:            E(L)=.01*LE
117: C          NE = HINGE POINT, NFS = # OF FLAP SEGMENTS.
118:            NE=NPTS-((LE*N)/100)
119:            NFS=NPTS-NE
120:            DO 6 I=1,NFS
121: C            DXT = X PROJECTION OF I FLAP SEGMENTS.
122: C            DZT = Z PROJECTION OF I FLAP SEGMENTS.
123:              DXT=I*DX
124:              DZT=0.
125:              DO 5 J=1,I
126:                DZT=DZ(J+NE)+DZT
127:       5        CONTINUE
128: C            SF = DIST FROM HINGE POINT TO A FLAP POINT, A FLAP LINE.
129: C            AF = ANGLE WITH Z AXIS SF MAKES.
130:              SF(I)=SQRT((DXT**2)+(DZT**2))
131:              AF(I)=1.5707963+ASIN(DZT/SF(I))
132:       6      CONTINUE
133: C          XE = FLAP CHORD LENGTH X PROJECTION, FC = FLAP CHORD LENGTH.
134:            XE=E(L)*XC
135:            FC=SQRT((XE**2)+(Z(NE)**2))
136: C          NFS = END POINT CONDITIONS, NE = 1 MEANS ENTIRE AIRFOIL IS
137: C          A FLAP, NE = NPTS MEANS THE AIRFOIL HAS NO FLAP.
138:            SF(NFS)=FC
139:            IF(NE.EQ.1)THEN
140:              AF(NFS)=1.5707963
141:            ELSE IF(NE.EQ.NPTS)THEN
142:              AF(NFS)=1.5707963
143:            ELSE
144:              AF(NFS)=1.5707963-ATAN(Z(NE)/XF)
145:            END IF
146: C          SETUP OUTPUT TABLE.
147:            PRINT'("0",20X,"FOR A FLAP CHORD RATIO OF ",F6.3,
148:       $    ", THE FLAP DEFLECTS ABOUT POINT",I4,
149:       $    " AND GIVES THE FOLLOWING DATA:")',E(L),NE
150:            PRINT'(22X,"ETA",2X,"ALPHA(LO)",4X,"CMAC",3X,
```

```
3 NOV 82 20:19:00   HARRIS FORTRAN 77 SAU OPTIMIZING COMPILER      01414-00
MODULE NAME:  FLAP

151:       $     "DEL(ALPHA(LO))/ETA",2X,"DEL(CMAC)/ETA")'
152:             LL=0
153:             DO 12 JJ=1,10
154:               LL=LL+1
155: C             LL = DIMENSION VARIABLE, JJ =LOOP CONTROL FOR AMOUNT OF FLAP
156: C             DEFLECTION. LETA = DEFLECTION IN DEGREES, ETA = RADIANS.
157:               LETA(LL)=JJ
158:               ETA=LETA(LL)*3.14159265/180.
159: C             GEOMETRY FINDS NEW COORDINATES FOR FLAPPED AIRFOIL.
160: C             BETWEEN FLAP CHORD AND X AXIS, X1 = PROJECTION ONTO X AXIS
161: C             AFN = NEW ANGLE A FLAP LINE MAKES WITH Z AXIS, A3 = ANGLE
162: C             OF FLAP CHORD ABOVE X AXIS. FC1 = LENGTH OF FLAP CHORD
163: C             ABOVE X AXIS, FC2 = LENGTH OF FLAP CHORD BELOW X AXIS.
164:               AFN(NFS)=AF(NFS)-ETA
165:               A3=1.5707963-AFN(NFS)
166:               X1=Z(NE)/TAN(A3)
167:               FC1=SQRT((X1**2)+(Z(NE)**2))
168:               FC2=FC-FC1
169: C             Z2 = PROJECTION ONTO Z AXIS OF FLAP CHORD BELOW X AXIS.
170:               Z2=FC2*SIN(A3)
171: C             X2 = PROJECTION ONTO X AXIS OF FLAP CHORD BELOW X AXIS
172:               X2=Z2/TAN(A3)
173: C             X3 = PROJECTION OF NEW CHORD LINE ONTO X AXIS, XCN = LENGTH
174: C             OF NEW CHORD LINE AFTER DEFLECTION, A4 = ANGLE BETWEEN NEW
175: C             CHORD LINE AND X AXIS.
176:               X3=X1+X2+X(NE)
177:               XCN=SQRT((X3**2)+(Z2**2))
178:               A4=ATAN(Z2/X3)
179: C             COMPUTE NEW COORDINATES AND ANGLES WITH THE NEW CHORD LINE
180: C             BEING THE NEW X AXIS. LOOP 7 TAKES CARE OF POINTS UP TO
181: C             HINGE POINT,8 AND 9 DO POINTS FROM HINGE PT TO END POINT.
182:               DO 7 J=1,NE
183:                 IF(J.EQ.1)THEN
184:                   SAN(J)=0.
185:                   XN(1)=0.
186:                   ZN(1)=0.
187:                 ELSE
188:                   SAN(J)=SA(J)+A4
189:                   XN(J)=SL(J)*COS(SAN(J))
190:                   ZN(J)=SL(J)*SIN(SAN(J))
191:                   DXN=XN(J)-XN(J-1)
192:                   DZN=ZN(J)-ZN(J-1)
193:                   DZDX(J-1)=DZN/DXN
194:                 END IF
195:       7       CONTINUE
196:               DO 8 J=1,NFS
197:                 AFN(J)=AF(J)+A4-ETA
198:                 XN(J+NE)=XN(NE)+(SF(J)*SIN(AFN(J)))
199:                 ZN(J+NE)=ZN(NE)-(COS(AFN(J))*SF(J))
200:       8       CONTINUE
```

```
3 NOV 82 20:19:00   HARRIS FORTRAN 77 SAU OPTIMIZING COMPILER      01414-00
MODULE NAME:  FLAP

201:              XN(NPTS)=XCN
202:              ZN(NPTS)=0.
203:              DO 9 J=NE+1,NPTS
204:                DXN=XN(J)-XN(J-1)
205:                DZN=ZN(J)-ZN(J-1)
206:                DZDX(J-1)=DZN/DXN
207:     9        CONTINUE
208: C            NEW TRANSFORMATION ANGLES.
209:              DO 10 J=1,N
210:                THETA(J)=ACOS(1.-(2.*XN(J)/XCN))
211:    10        CONTINUE
212:              ALO2=0.
213:              CMAC2=0.
214:              THETA(NPTS)=3.14159265
215: C            NEW ALO AND CMAC.
216:              DO 11 I=1,N
217:                STH=SIN(THETA(I+1))-SIN(THETA(I))
218:                S2TH=SIN(2.*THETA(I+1))-SIN(2.*THETA(I))
219:                ALO2=(DZDX(I)*(STH+THETA(I)-THETA(I+1)))+ALO2
220:                CMAC2=(DZDX(I)*(-STH+(S2TH/2.)))+CMAC2
221:    11        CONTINUE
222: C            ACCOUNT FOR NEW ALO BEING COMPUTED IN DIFFERENT COORDINATE
223: C            SYSTEM AND CONVERT TO DEGREES.
224:              ALO2=((-ALO2/3.14159265)-A0)*(180./3.14159265)
225:              CMAC2=CMAC2/2.
226: C            FIND CHANGE IN ALO/FLAP DEFLECTION FOR E.
227:              DEL1(L,LL)=(ALO2-ALO)/LETA(LL)
228: C            FIND CHANGE IN CMAC/FLAP DEFLECTION FOR E.
229:              DEL2(L,LL)=(CMAC2-CMAC)/ETA
230: C            OUTPUT
231:              PRINT'(22X,I2,3X,F9.4,3X,F7.4,4X,F9.4,10X,F9.4)',LETA(LL),
232:       $      ALO2,CMAC2,DEL1(L,LL),DEL2(L,LL)
233:    12      CONTINUE
234:    13    CONTINUE
235: C          OUTPUT IN A DIFFERENT FORM.
236:           PRINT'("1")'
237:           PRINT'(39X," FIXED FLAP DEFLECTION")'
238:           PRINT'(38X," VARYING FLAP-CHORD RATIO")'
239:           DO 15 I=1,LL
240:             PRINT'("0")'
241:             PRINT'(22X,"FOR A FLAP DEFLECTION OF",I4,"DEGREES:")',LETA(I)
242:             PRINT'(22X"E(FLAP-CHORD RATIO)",2X,"DEL ALPHA(LO)/ETA",3X,
243:       $     "DEL CMAC/ETA")'
244:             DO 14 J=1,L
245:               PRINT'(30X,F5.3,14X,F6.3,12X,F5.3)',E(J),DEL1(J,I),DEL2(J,I)
246:    14       CONTINUE
247:    15    CONTINUE
248:    16  CONTINUE
249:        END
```

Appendix C

Model Geometry

The side plates were two and one-half feet square with each corner rounded to an arc with a four inch radius. The rear lift bar dimensions were 1.15 inches in chord length and .5 inches in thickness, see Fig. 7. See Abbott and Von Doenhoff (Ref 5:113,114, and 414) for cross section dimensions of the NACA 4412 airfoil.

Table II gives the airfoil measurements needed to compute C_{ℓ}s and C_{mac}s for each model.

TABLE II

Airfoil measurements

Model E	Chord length (inches)	Wing span (feet)	Distance from trunnion screw to leading edge of airfoil (inches)
.2	8.9	1.992	.3
.3	8.9	1.992	.31
.4	8.88	1.992	.31
.5	8.88	1.987	.33
.6	8.89	1.992	.3
.7	8.88	1.99	.3
.8	8.9	1.99	.3

The model's angle of attack was set by moving the rear lift wire forward or backward and increasing or decreasing the length of the rear wire from the scale to the rear lift

bar attachment fitting. The angle of balance in Fig. 13 determined the distance forward or backward the rear lift wire had to move for a specific angle of attack while the shortening or lengthening of the wire was determined during calibration. Table III gives the balance angles and model measurements, shown in Fig. 13, that determined them. Table III shows that the balance angles and model measurements varied barely at all. For that reason, the first model tested with E = .4 determined the angle of balance, and therefore the distances the rear lift wire moved, for the entire investigation.

TABLE III

Balance angles and associated measurements

Model E	Distances in Fig. 13 (inches)			Balance angle (degrees)
	e	f	$g=\sqrt{e^2+f^2}$	
.2	15.737	9.545	18.405	31.238
.3	15.776	9.637	18.487	31.419
.4	15.71	9.516	18.367	31.204
.5	15.726	9.577	18.413	31.341
.6	15.684	9.599	18.388	31.468
.7	15.737	9.572	18.419	31.31
.8	15.741	9.694	18.487	31.627

The distances the rear wire moved are given in Table IV. The distance and direction of movement for a specific angle of attack in Table IV was determined by calculating a new balance angle for each angle of attack. The new balance

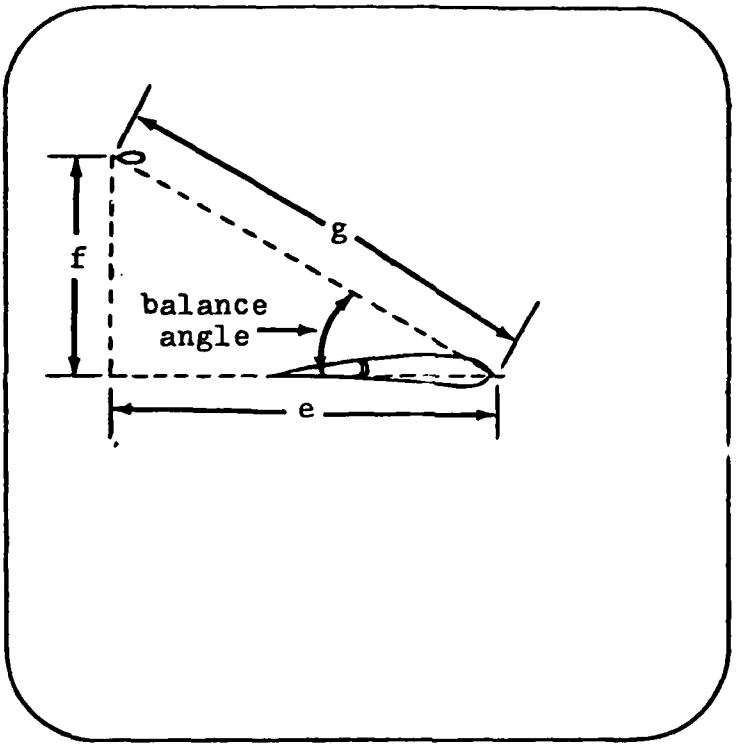

Fig. 13 Balance angle and associated measurements.

e was the horizontal distance and f was the vertical distance from the front trunnion to rear lift wire attachment fitting with $g = \sqrt{e^2+f^2}$.

angle gave a new distance, e in Fig. 13, to the rear fitting from the front trunnion. The difference between the distance e at 0° angle of attack and e at a specific angle of attack gave the distance and direction the rear lift wire was moved. These distances were put on a bar graph and used to set the rear lift wire from the wind-tunnel operator's station during testing that required changing the angle of attack. As stated previously the distances of movement in Table IV were used for the entire investigation and came from the model with E = .4. The same distances were calculated for all the models

and for all practical purposes do not vary. For example, the model with E = .8 gave a maximum difference from the distances in Table IV at the angle of attack of 10° and amounted to only -.031 inches.

TABLE IV

Rear lift wire movement

Angle of attack (degrees)	Balance angle (in degrees)	Horizontal distance e (inches)	Rear lift wire movement + towards airfoil - away from airfoil (inches)
0	31.204	15.71	0
-6	37.204	14.629	1.081
-4	35.204	15.008	.703
-2	33.204	15.368	.342
2	29.204	16.033	-.323
4	27.204	16.336	-.626
6	25.204	16.619	-.909
8	23.204	16.882	-1.172
10	21.204	17.124	-1.414

Appendix D

Flap Deflection Settings

Flap deflections were accomplished by aligning one of the holes (1-7) of the brass plate/flap deflection mechanism in Fig. 6 with one of the holes in the side plate in Fig. 14. Each set of vertical holes were used with a particular model as shown in Fig. 8. Additionally, each set was drilled in a circular arc about the flap-hinge point of the particular model the set was used with. This allowed each hole of a set to be spaced at 6° intervals. The holes (1-7) of the brass plate were drilled in a circular arc about the hinge point A, see Fig. 6, of the brass plate but were separated by 5° instead of 6°. The differences in the increment between holes in the brass plate, 5°, and a set of vertical holes in the side plate, 6°, allowed flap deflections of 0° to 20° either up or down. By numbering each set of vertical holes as shown in Fig. 14 and using the numbering system in Fig. 6 for the holes in the brass plate, Table V was developed to give the flap deflection for particular combinations/alignments of holes in the brass and side plates. Take for example the flap deflection shown in Fig. 14. The set of vertical holes being used tells you that the particular model had a flap-hinge location (E) of .4. The side plate hole number used was 6 and the hole number for the brass plate was 5. For no deflection at all, both numbers must be 4. So, if the brass plate hole number 4 was aligned and set with hole number 6 of the side

plate, the deflection would be 12° downward since the side plate holes were spaced at 6°. But, since the brass plate hole was 5, that had the effect of bringing the flap back upward by 5° to give a flap deflection of 7° downward. The thinking process in the above example can be accomplished to arrive at each of the flap deflections in Table V.

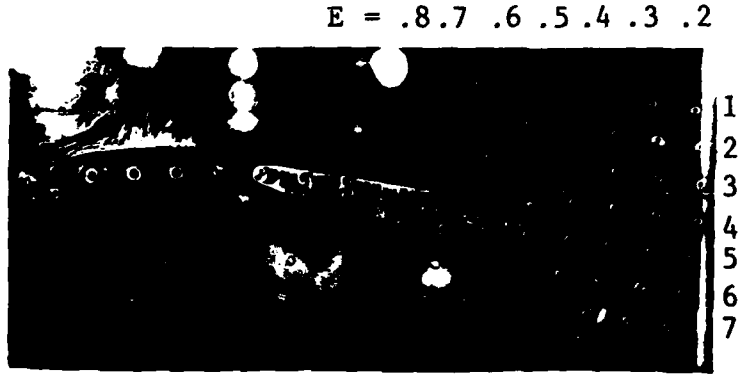

Fig. 14 Side view of flap deflection mechanism in operation. The number above each set of 7 vertical holes designates the model's flap-hinge location used with that set of holes. The vertical numbering system designates the side plate hole numbers.

TABLE V

Hole alignments for flap deflection

Flap setting (degrees)	Hole alignment	
	Brass plate hole # (Fig.6)	Side plate hole # (Fig.14)
0	4	4
1	5	5
2	6	6
3	7	7
4	2	3
5	3	4
6	4	5
7	5	6
8	6	7
9	1	3
10	2	4
11	3	5
12	4	6
13	5	7
15	1	4
16	2	5
17	3	6
18	4	7
-1	3	3
-2	2	2

Note: $\pm$14° flap setting can not be acheived.

Appendix E

Tuft Studies

Tuft studies were accomplished by placing nylon strings on the upper surface of the airfoil, see Fig. 15. Table VI gives the results of the studies by indicating the combination of flap setting and angle of attack at which separation was first noticed. Figures 16 through 21 determined the data for model with E = .8 in Table VI. The figures were obtained by taking pictures through a window on top of the wind tunnel.

TABLE VI

Angles of separation from tuft studies

Model flap-chord ratio (E)	Angle of attack fixed at 0°	Separation angle of attack for flap fixed at		
	Separation flap angle	0°	4°	8°
.2	13°	10°	8°	8°
.4	11°	-	10°	6°
.5	12°	10°	8°	6°
.6	10°	10°	8°	6°
.8	15°	10°	8°	6°

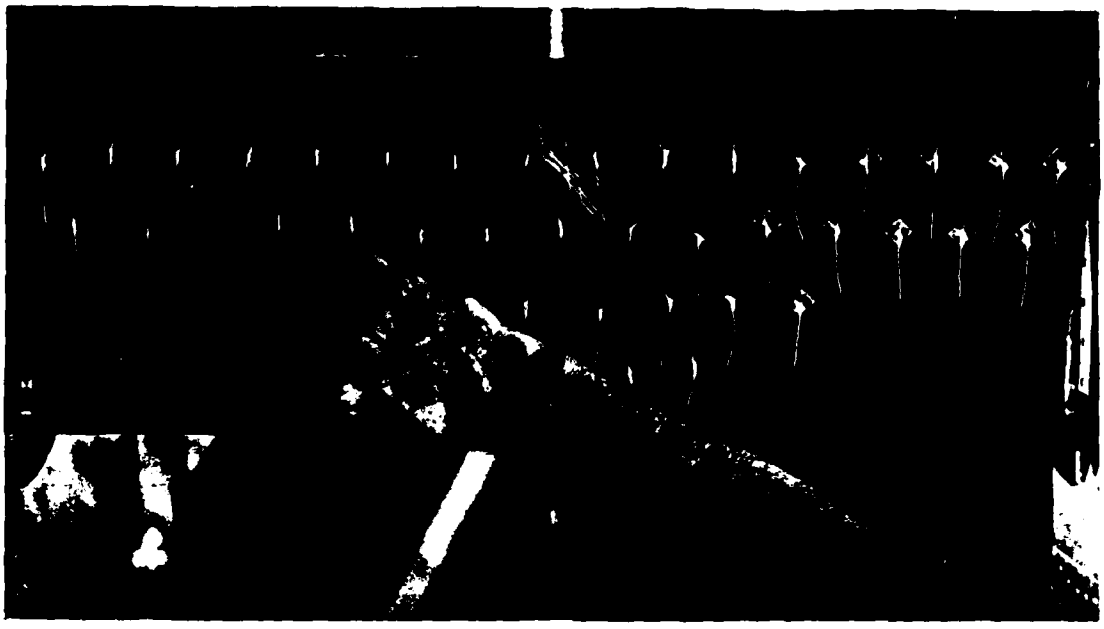

Fig. 15 Tufts being applied to model with E ≈ .8.

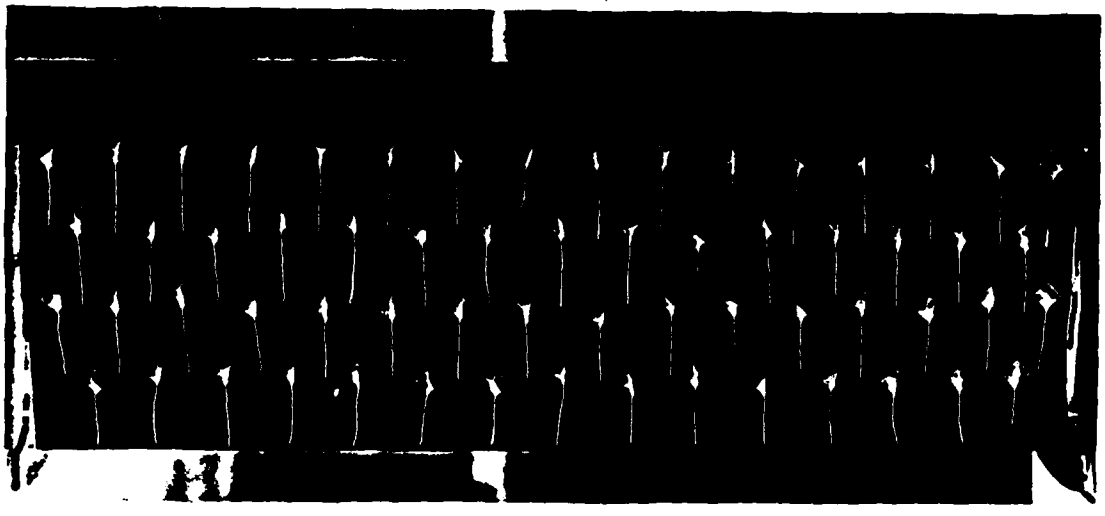

Fig. 16 8° angle of attack and 0° flap deflection. Use this figure for comparison purposes since there was no separation.

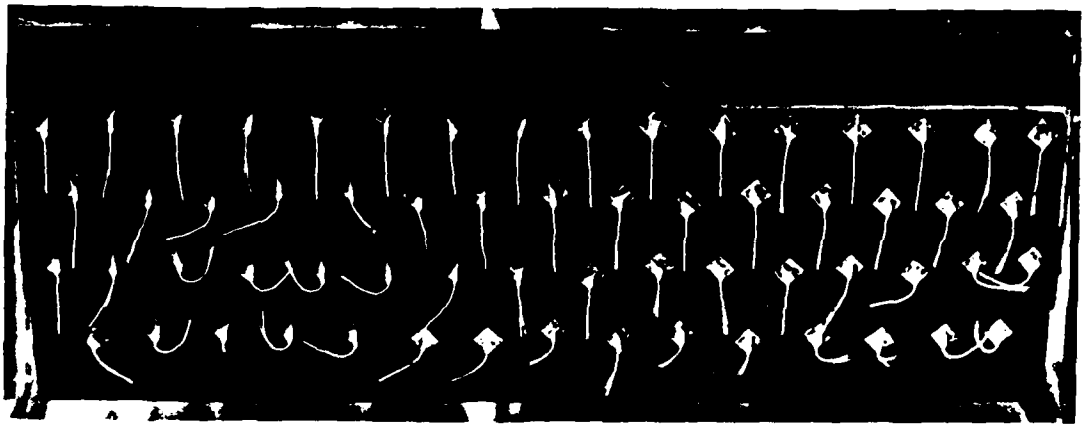

Fig. 17 8° angle of attack and 8° flap deflection. Use this figure for comparison purposes since the flow was well separated.

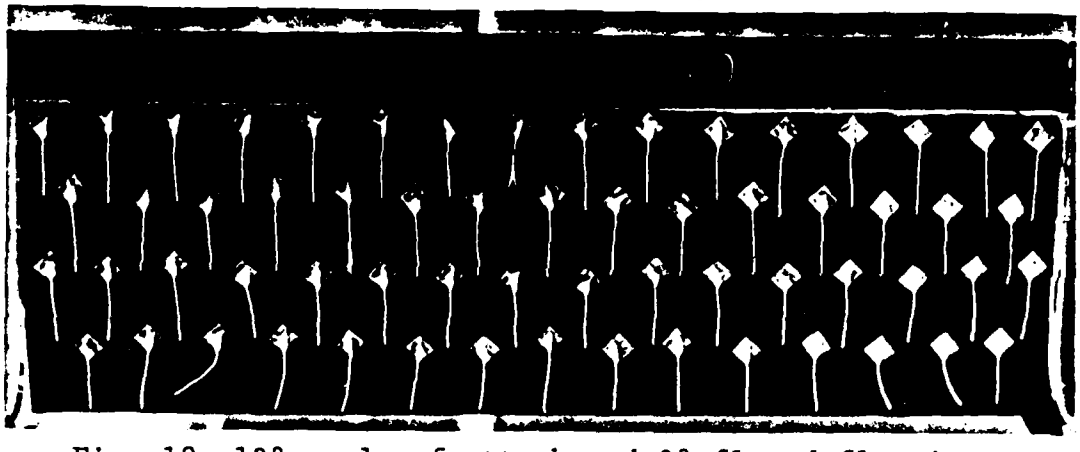

Fig. 18 10° angle of attack and 0° flap deflection. Note lower tufts turned slightly towards side plates indicating very slight separation.

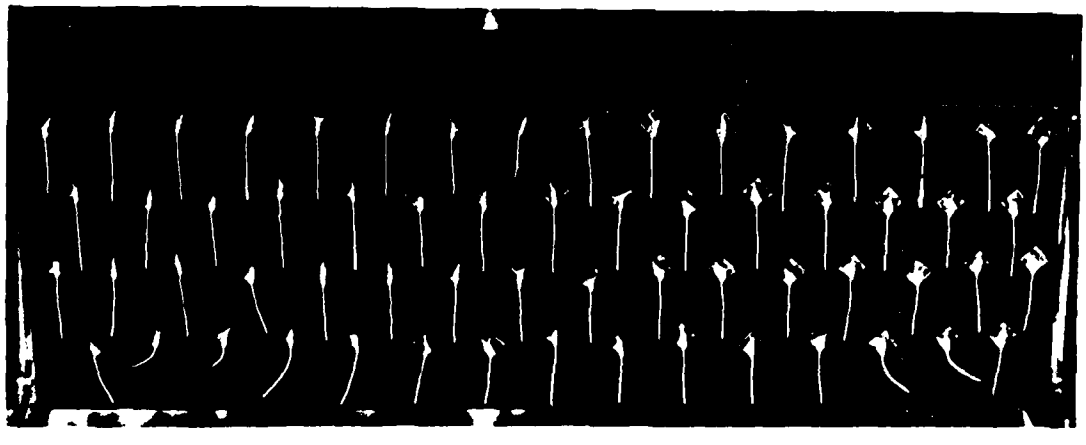

Fig. 19 8° angle of attack and 4° flap deflection.

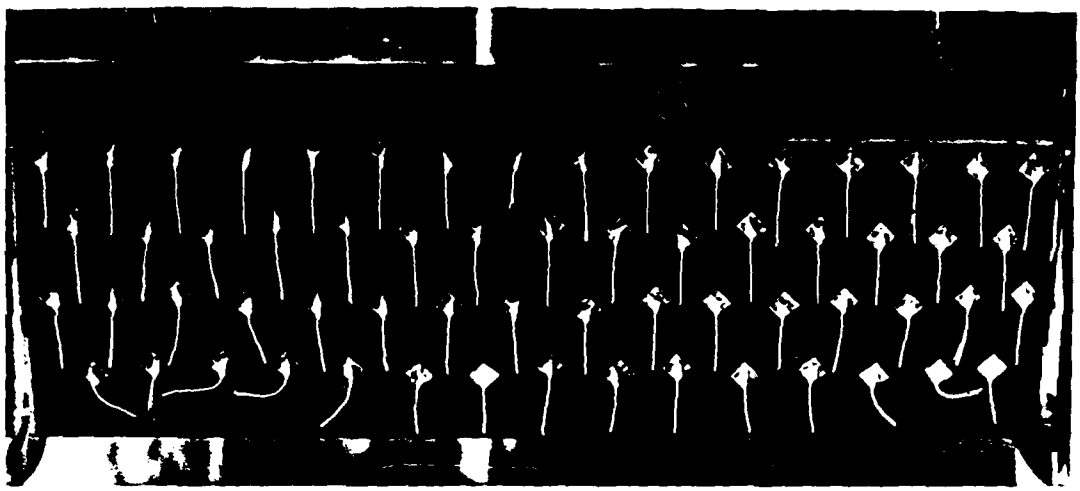

Fig. 20 6° angle of attack and 8° flap deflection.

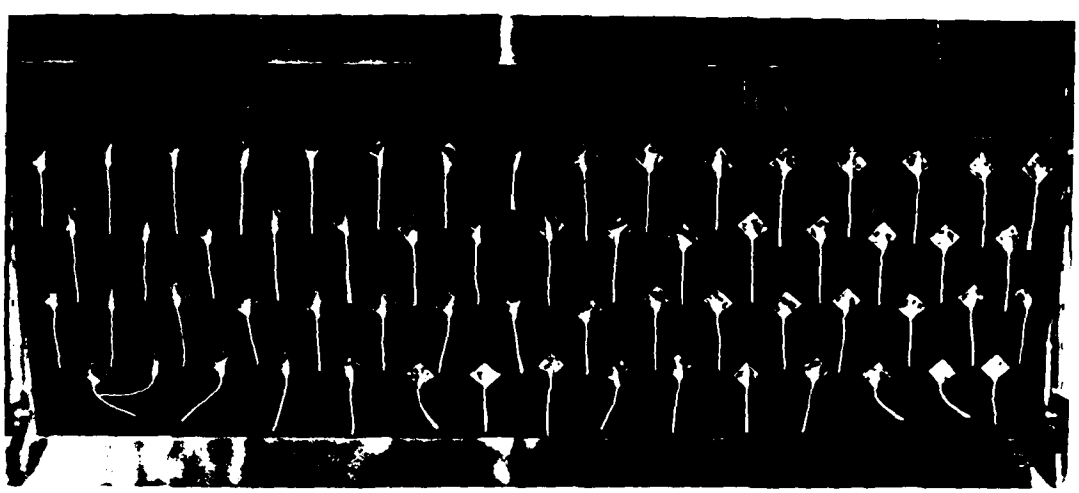

Fig. 21 0° angle of attack and 15° flap deflection.

Appendix F

Raw Tunnel Data

The following tables contain the data taken directly from the wind-tunnel tapes for all seven models. The tables for a particular model are indexed into three parts with part a containing the front lift data, part b the rear lift data, and part c the drag data. The drag tables contain the temperatures in degrees Fahrenheit and the pressures in inches of mercury that occurred during the testing of each model. Angles of attack (α) and flap deflections (η) are in degrees while the forces and wind-on/static readings are in pounds. The force column in each table was computed by subtracting the wind-on average from the static average. The forces were used as explained in Appendix G to calculate the experimental data points.

TABLE VIIa

Raw Front Lift Data for Model with E = .2

Flap Setting	Angle of Attack	Before-Static Readings			Wind-on Readings					After-Static Readings			Static Average	Wind-on Average	Front Lift Force
0	0	39.65	39.62	39.62	34.85	34.82	34.86	34.81	34.88				39.58	34.84	4.74
0	-6	38.72	38.86	38.88	44.55	44.55	44.55	44.52	44.52				38.82	44.34	-5.72
0	-4	39.13	39.15	39.15	41.42	41.40	41.41	41.40	41.39				39.14	41.40	-2.26
0	-2	39.35	39.35	39.35	38.12	38.10	38.05	38.12	38.10				39.35	38.10	1.25
0	0	39.60	39.60	39.60	34.82	34.85	34.86	34.86	34.84				39.58	34.85	4.73
0	2	39.80	39.80	39.80	31.45	31.45	31.40	31.42	31.42				39.80	31.43	8.37
0	4	40.00	40.00	40.00	28.04	28.12	28.19	27.92	28.02				40.00	28.06	11.94
0	6	40.15	40.16	40.16	24.73	24.60	24.69	24.75	24.60				40.16	24.67	15.49
0	8	40.30	40.30	40.31	21.62	21.68	21.62	21.39	21.41				40.30	21.54	18.76
0	10	40.46	40.46	40.46	19.30	19.06	19.19	19.10	18.90				40.46	19.11	21.35
0	10				19.10	19.16	19.34	18.90	19.01				40.46	19.10	21.36
0	6				24.60	24.54	24.62	24.60	24.60				40.16	24.59	15.57
0	2				31.55	31.50	31.48	31.53	31.55				39.80	31.52	8.28
0	0	39.45	39.48	39.46	34.90	34.90	34.90	34.90	34.91	39.62	39.65	39.65	39.58	34.90	4.68
1	0	39.57	39.57	39.57	34.12	34.10	34.12	34.08	34.09	39.47	39.52	39.55	39.54	34.10	5.44
2	0	39.65	39.69	39.66	33.45	33.45	33.48	33.46	33.44	39.42	39.49	39.51	39.57	33.46	6.11
3	0	39.65	39.65	39.66	32.79	32.76	32.82	32.82	32.77	39.45	39.52	39.54	39.58	32.79	6.79
4	0	39.70	39.69	39.71	31.93	31.91	31.92	31.96	31.94	39.68	39.70	39.70	39.65	31.93	7.72
4	-6	38.96	38.96	38.96	41.66	41.69	41.73	41.72	41.75	38.97	38.97	38.97	38.97	41.71	-2.74
4	-4	39.20	39.21	39.21	38.39	38.37	38.40	38.38	38.41	39.20	39.21	39.23	39.21	38.39	.82
4	-2	39.42	39.42	39.43	35.01	35.01	35.01	35.02	35.03	39.40	39.42	39.42	39.42	35.02	4.40
4	0	39.61	39.62	39.62	31.87	31.91	31.89	31.94	31.90	39.60	39.60	39.60	39.65	31.90	7.74
4	2	39.80	39.81	39.81	28.69	28.64	28.64	28.67	28.68	39.80	39.80	39.81	39.81	28.66	11.15
4	4	39.98	39.99	39.99	25.42	25.48	25.48	25.38	25.30	40.00	39.99	40.00	39.99	25.41	14.58
4	6	40.14	40.14	40.15	22.15	22.05	22.08	21.97	22.05	40.14	40.14	40.15	40.14	22.06	18.08
4	8	40.28	40.29	40.29	19.30	19.42	19.25	19.18	19.43	40.29	40.30	40.30	40.29	19.32	20.97
4	10	40.45	40.44	40.45	17.27	17.30	17.39	17.51	17.31	40.45	40.45	40.45	40.45	17.36	23.09
4	0	39.62	39.63	39.64	32.02	32.05	32.10	32.05	32.03	39.63	39.65	39.65	39.65	32.05	7.60
5	0	39.65	39.65	39.65	31.25	31.25	31.26	31.25	31.28	39.50	39.54	39.52	39.60	31.26	8.34
6	0	39.66	39.67	39.67	30.35	30.28	30.27	30.28	30.27	39.44	39.46	39.46	39.56	30.29	9.27
7	0	39.70	39.72	39.71	29.71	29.71	29.76	29.73	29.75	39.45	39.51	39.53	39.60	29.73	9.87
8	0	39.70	39.70	39.71	29.00	28.90	28.91	28.89	28.87	39.66	39.69	39.70	39.64	28.91	10.73
8	-6	38.98	38.98	38.98	38.82	38.80	38.82	38.82	38.83	38.95	38.96	38.96	38.97	38.82	.15
8	-4	39.20	39.22	39.22	35.32	35.33	35.35	35.30	35.32	39.20	39.20	39.21	39.21	35.32	3.89
8	-2	39.42	39.43	39.43	32.10	32.07	32.15	32.09	32.10	39.40	39.40	39.41	39.42	32.10	7.32
8	0	39.60	39.63	39.61	29.13	29.20	29.11	29.15	29.17	39.58	39.58	39.59	39.64	29.15	10.49
8	2	39.81	39.84	39.83	26.16	26.12	26.20	26.08	26.10	39.78	39.79	39.80	39.81	26.13	13.68
8	4	40.00	40.04	40.02	23.01	23.05	23.03	22.95	23.00	39.95	39.96	39.97	39.99	23.01	16.98
8	6	40.15	40.15	40.16	19.95	19.75	19.70	19.69	19.72	40.13	40.14	40.13	40.14	19.76	20.38
8	8	40.30	40.30	40.30	17.56	17.60	17.49	17.62	17.50	40.29	40.29	40.30	40.30	17.55	22.75
8	10	40.45	40.45	40.47	15.24	15.92	15.83	15.81	15.83	40.44	40.45	40.45	40.45	15.83	24.62
8	0	39.65	39.65	39.65	29.07	29.08	29.11	29.10	29.06	39.63	39.63	39.63	39.64	29.08	10.56
9	0	39.68	39.67	39.70	28.41	28.43	28.49	28.50	28.45	39.75	39.77	39.78	39.73	28.46	11.27
10	0	39.65	39.67	39.67	27.76	27.76	27.76	27.71	27.70	39.60	39.63	39.63	39.64	27.74	11.90
11	0	39.68	39.70	39.70	26.95	26.99	26.96	27.00	26.98				39.69	26.98	12.71
12	0	39.62	39.62	39.62	26.32	26.25	26.30	26.28	26.30	39.43	39.52	39.57	39.56	26.29	13.27
13	0	39.70	39.70	39.70	25.78	25.89	25.85	25.92	25.93				39.70	25.87	13.83
15	0	39.71	39.72	39.71	25.02	25.02	25.14	25.04	24.95				39.71	25.03	14.68
16	0	39.68	39.68	39.67	24.23	24.86	24.76	24.96	24.83	39.51	39.58	39.62	39.62	24.83	14.79
17	0	39.69	39.70	39.72	24.41	24.48	24.30	24.32	24.47	39.47	39.56	39.60	39.62	24.40	15.22
18	0	39.71	39.71	39.72	24.25	24.33	24.18	24.28	24.13	39.71	39.74	39.74	39.72	24.23	15.49

TABLE VIIb

Raw Rear Lift Data for Model with E = .2

Flap Setting	Angle of Attack	Before-Static Readings			Wind-on Readings					After-Static Readings			Static Average	Wind-on Average	Rear Lift Force
0	0	19.48	19.48	19.48	19.10	19.06	19.08	19.08	19.09				19.54	19.08	.46
0	-6	20.40	20.22	20.27	23.00	23.02	23.02	23.01	23.02				20.28	23.01	-2.73
0	-4	19.94	19.94	19.94	21.82	21.82	21.84	21.84	21.81				19.94	21.83	-1.89
0	-2	19.67	19.67	19.68	20.49	20.48	20.48	20.51	20.50				19.67	20.49	-.82
0	0	19.50	19.50	19.50	19.12	19.11	19.12	19.13	19.12				19.54	19.12	.42
0	2	19.24	19.24	19.24	17.28	17.30	17.27	17.26	17.27				19.24	17.28	1.96
0	4	19.05	19.05	19.05	15.40	15.27	15.37	15.19	15.21				19.05	15.29	3.76
0	6	18.88	18.89	18.89	13.39	13.60	13.46	13.53	13.67				18.89	13.53	5.36
0	8	18.72	18.72	18.72	12.20	12.23	12.24	12.13	12.13				18.72	12.19	6.53
0	10	18.55	18.55	18.54	11.46	11.40	11.45	11.40	11.35				18.55	11.41	7.14
0	10				11.42	11.42	11.47	11.36	11.40				18.55	11.41	7.14
0	6				13.40	13.44	13.48	13.53	13.59				18.89	13.49	5.40
0	2				17.35	17.35	17.35	17.34	17.33				19.24	17.34	1.90
0	0	19.68	19.65	19.68	19.11	19.12	19.12	19.12	19.12	19.48	19.45	19.48	19.54	19.12	.42
1	0	19.53	19.52	19.52	18.86	18.85	18.87	18.85	18.84	19.44	19.46	19.47	19.49	18.85	.64
2	0	19.51	19.51	19.51	18.75	18.74	18.75	18.76	18.74	19.43	19.46	19.46	19.48	18.75	.73
3	0	19.54	19.54	19.53	18.60	18.56	18.59	18.59	18.58	19.42	19.47	19.48	19.50	18.58	.92
4	0	19.49	19.49	19.48	18.29	18.29	18.32	18.33	18.32	19.45	19.46	19.46	19.50	18.31	1.19
4	-6	20.24	20.24	20.24	21.95	21.95	21.97	21.96	21.96	20.22	20.22	20.22	20.23	21.96	-1.73
4	-4	19.92	19.94	19.94	20.73	20.73	20.75	20.75	20.74	19.92	19.92	19.92	19.93	20.74	-.81
4	-2	19.68	19.68	19.68	19.50	19.49	19.49	19.50	19.49	19.71	19.71	19.70	19.69	19.49	.20
4	0	19.51	19.51	19.51	18.30	18.30	18.30	18.31	18.31	19.52	19.53	19.52	19.50	18.30	1.20
4	2	19.27	19.27	19.27	16.85	16.81	16.79	16.82	16.82	19.26	19.26	19.26	19.27	16.82	2.45
4	4	19.08	19.09	19.10	14.99	15.02	14.99	14.99	14.97	19.05	19.06	19.06	19.07	14.99	4.08
4	6	18.91	18.91	18.92	13.09	13.01	12.99	13.00	13.00	18.92	18.91	18.93	18.92	13.02	5.90
4	8	18.76	18.76	18.76	11.68	11.74	11.69	11.66	11.70	18.75	18.75	18.76	18.76	11.69	7.07
4	10	18.57	18.59	18.59	10.90	10.90	10.92	10.95	10.91	18.55	18.55	18.56	18.57	10.92	7.65
4	0	19.51	19.52	19.52	18.28	18.28	18.27	18.27	18.31	19.46	19.48	19.48	19.50	18.28	1.22
5	0	19.50	19.51	19.51	18.14	18.12	18.12	18.12	18.11	19.44	19.46		19.48	18.12	1.36
6	0	19.49	19.49	19.49	17.84	17.81	17.77	17.80	17.82	19.48	19.50	19.50	19.49	17.81	1.68
7	0	19.47	19.47	19.47	17.60	17.60	17.61	17.61	17.62	19.38	19.42	19.43	19.44	17.61	1.83
8	0	19.47	19.47	19.46	17.44	17.41	17.40	17.40	17.39	19.42	19.42	19.43	19.48	17.41	2.07
8	-6	20.21	20.22	20.22	20.86	20.85	20.85	20.84	20.84	20.19	20.19	20.20	20.21	20.85	-.64
8	-4	19.91	19.92	19.90	19.59	19.59	19.59	19.59	19.59	19.91	19.90	19.91	19.91	19.59	.32
8	-2	19.68	19.65	19.68	18.45	18.46	18.48	18.48	18.47	19.66	19.67	19.67	19.67	18.47	1.20
8	0	19.51	19.45	19.50	17.46	17.50	17.48	17.49	17.49	19.52	19.52	19.52	19.48	17.48	2.00
8	2	19.26	19.25	19.25	16.18	16.15	16.18	16.14	16.14	19.26	19.24	19.25	19.25	16.16	3.09
8	4	19.06	19.05	19.06	14.65	14.67	14.68	14.66	14.68	19.06	19.06	19.06	19.06	14.67	4.39
8	6	18.91	18.90	18.90	12.66	12.67	12.58	12.66	12.68	18.86	18.86	18.86	18.88	12.65	6.23
8	8	18.72	18.73	18.74	11.20	11.22	11.16	11.21	11.16	18.73	18.74	18.74	18.73	11.19	7.54
8	10	18.55	18.56	18.56	10.34	10.40	10.36	10.33	10.34	18.54	18.55	18.56	18.55	10.35	8.20
8	0	19.47	19.49	19.50	17.39	17.42	17.44	17.42	17.41	19.46	19.47	19.47	19.48	17.42	2.06
9	0	19.49	19.49	19.49	17.26	17.23	17.25	17.24	17.22	19.42	19.44	19.44	19.46	17.24	2.22
10	0	19.50	19.50	19.50	17.05	17.04	17.02	17.03	17.01	19.42	19.45	19.45	19.47	17.03	2.44
11	0	19.48	19.48	19.48	16.80	16.80	16.80	16.80	16.79				19.48	16.80	2.68
12	0	19.50	19.50	19.50	16.58	16.54	16.56	16.55	16.55				19.50	16.56	2.94
13	0	19.45	19.43	19.45	16.38	16.41	16.39	16.41	16.43				19.44	16.40	3.04
15	0	19.50	19.49	19.49	16.13	16.13	16.15	16.13	16.09				19.49	16.13	3.36
16	0	19.47	19.47	19.47	16.02	16.04	16.00	16.07	16.05	19.34	19.38	19.40	19.42	16.04	3.38
17	0	19.44	19.44	19.44	15.88	15.90	15.96	15.85	15.88	19.31	19.36	19.39	19.40	15.87	3.53
18	0	19.45	19.45	19.45	15.85	15.81	15.81	15.83	15.81	19.37	19.40	19.40	19.42	15.32	3.60

TABLE VIIc

Raw Drag Data for Model with E = .2

Avg. Temp.	Avg. Press.	n	α	Before-Static Readings			Wind-on Readings					After-Static Readings			Static Average	Wind-on Average	Drag Force
82.0	29.133	0	0	21.30	21.34	21.34	17.78	17.77	17.74	17.75	17.74				21.30	17.75	3.54
82.0	29.133	0	-6	20.87	21.00	21.03	17.39	17.37	17.35	17.36	17.37				20.97	17.37	3.60
82.0	29.133	0	-4	21.12	21.13	21.18	17.48	17.48	17.49	17.50	17.51				21.14	17.49	3.65
82.0	29.133	0	-2	21.24	21.22	21.22	17.62	17.60	17.61	17.60	17.61				21.23	17.61	3.62
82.0	29.133	0	0	21.38	21.34	21.32	17.65	17.65	17.65	17.64	17.65				21.30	17.65	3.65
82.0	29.133	0	2	21.38	21.39	21.40	17.57	17.57	17.56	17.57	17.57				21.39	17.57	3.82
82.0	29.133	0	4	21.42	21.45	21.45	17.48	17.48	17.48	17.45	17.47				21.44	17.47	3.97
82.0	29.133	0	6	21.48	21.49	21.49	17.25	17.22	17.25	17.26	17.24				21.49	17.24	4.25
82.0	29.133	0	8	21.55	21.55	21.56	16.96	17.02	17.02	16.97	16.98				21.55	16.99	4.56
82.0	29.133	0	10	21.59	21.60	21.61	16.70	16.70	16.72	16.69	16.66				21.60	16.69	4.91
82.0	29.133	0	10				16.65	16.65	16.70	16.66	16.67				21.60	16.67	4.93
82.0	29.133	0	6				17.33	17.28	17.25	17.27	17.26				21.49	17.29	4.21
82.0	29.133	0	2				17.25	17.23	17.21	17.23	17.22				21.39	17.23	3.66
82.0	29.133	0	0	21.13	21.08	21.11	17.71	17.71	17.72	17.72	17.73	21.44	21.42	21.40	21.30	17.72	3.58
78.5	29.099	1	0	21.23	21.25	21.25	17.61	17.61	17.62	17.62	17.61	21.26	21.28	21.29	21.26	17.61	3.65
78.5	29.099	2	0	21.44	21.38	21.39	17.61	17.62	17.63	17.62	17.62	21.24	21.25	21.26	21.33	17.62	3.71
78.5	29.099	3	0	21.31	21.40	21.37	17.62	17.61	17.60	17.60	17.60	21.25	21.26	21.30	21.32	17.61	3.71
78.5	29.099	4	0	21.45	21.41	21.39	17.54	17.57	17.58	17.58	17.56	21.47	21.42	21.40	21.37	17.57	3.80
78.5	29.099	4	-6	21.13	21.14	21.14	17.42	17.45	17.44	17.44	17.43	21.23	21.21	21.20	21.18	17.44	3.74
78.5	29.099	4	-4	21.19	21.28	21.21	17.59	17.57	17.57	17.56	17.56	21.23	21.24	21.24	21.23	17.57	3.66
78.5	29.099	4	-2	21.24	21.25	21.25	17.54	17.56	17.57	17.57	17.56	21.25	21.26	21.25	21.25	17.56	3.69
78.5	29.099	4	0	21.30	21.31	21.32	17.51	17.52	17.54	17.53	17.55	21.31	21.32	21.32	21.37	17.53	3.84
78.5	29.099	4	2	21.38	21.38	21.38	17.49	17.48	17.48	17.48	17.48	21.38	21.39	21.40	21.39	17.48	3.91
78.5	29.099	4	4	21.43	21.44	21.45	17.28	17.30	17.31	17.30	17.28	21.45	21.47	21.48	21.45	17.29	4.16
78.5	29.099	4	6		21.52	21.51	16.96	16.97	16.98	16.96	16.97	21.49	21.48	21.47	21.50	16.97	4.53
78.5	29.099	4	8	21.54	21.55	21.56	16.62	16.66	16.66	16.65	16.66	21.52	21.53	21.53	21.54	16.65	4.89
78.5	29.099	4	10	21.58	21.59	21.60	16.36	16.36	16.38	16.40	16.37	21.58	21.60	21.60	21.59	16.37	5.22
78.5	29.099	4	0	21.39	21.38	21.36	17.71	17.68	17.69	17.68	17.67	21.42	21.39	21.38	21.37	17.69	3.68
80.5	29.150	5	0	21.34	21.34	21.35	17.53	17.56	17.57	17.56	17.57		21.20	21.24	21.28	17.56	3.72
80.5	29.150	6	0	21.32	21.30	21.30	17.45	17.48	17.51	17.51	17.51	20.97	21.01	21.03	21.16	17.49	3.67
80.5	29.150	7	0	21.47	21.43	21.41	17.48	17.49	17.49	17.50	17.48	21.14	21.18	21.21	21.31	17.49	3.82
80.5	29.150	8	0	21.50	21.45	21.43	17.36	17.37	17.39	17.38	17.37	21.46	21.43	21.40	21.39	17.37	4.02
80.5	29.150	8	-6	21.25	21.18	21.18	17.46	17.46	17.45	17.46	17.46	21.23	21.21	21.19	21.21	17.46	3.75
80.5	29.150	8	-4	21.22	21.22	21.21	17.42	17.43	17.46	17.46	17.46	21.21	21.23	21.23	21.22	17.45	3.77
80.5	29.150	8	-2	21.27	21.27	21.25	17.44	17.46	17.46	17.47	17.46	21.26	21.25	21.26	21.26	17.46	3.80
80.5	29.150	8	0	21.32	21.32	21.31	17.42	17.45	17.42	17.44	17.46	21.31	21.30	21.31	21.39	17.44	3.95
80.5	29.150	8	2	21.40	21.39	21.40	17.32	17.32	17.35	17.34	17.34	21.37	21.39	21.39	21.39	17.33	4.06
80.5	29.150	8	4	21.47	21.43	21.47	17.18	17.17	17.14	17.14	17.15	21.43	21.44	21.46	21.45	17.16	4.29
80.5	29.150	8	6	21.50	21.46	21.47	16.68	16.68	16.67	16.67	16.69	21.50	21.50	21.51	21.49	16.68	4.81
80.5	29.150	8	8	21.54	21.56	21.57	16.40	16.41	16.41	16.42	16.40	21.54	21.55	21.55	21.55	16.41	5.14
80.5	29.150	8	10	21.62	21.63	21.63	16.00	16.04	16.04	16.03	16.03	21.60	21.60	21.61	21.62	16.03	5.59
80.5	29.150	8	0	21.42	21.40	21.38	17.55	17.55	17.56	17.55	17.54	21.42	21.39	21.38	21.39	17.55	3.84
82.0	29.128	9	0	21.40	21.39	21.39	17.39	17.39	17.40	17.44	17.44	21.38	21.37	21.37	21.38	17.41	3.97
82.0	29.128	10	0	21.31	21.31	21.31	17.32	17.34	17.34	17.36	17.33	21.30	21.31	21.32	21.31	17.34	3.97
82.0	29.128	11	0	21.46	21.44	21.42	17.23	17.25	17.25	17.27	17.27				21.44	17.25	4.19
82.0	29.128	12	0	21.28	21.29	21.28	17.21	17.22	17.23	17.23	17.21	21.30	21.30	21.32	21.30	17.22	4.08
82.0	29.128	13	0	21.48	21.45	21.44	17.13	17.18	17.18	17.20	17.20				21.46	17.18	4.28
82.0	29.128	15	0	21.38	21.37	21.37	17.02	17.04	17.05	17.05	17.03				21.37	17.04	4.33
82.0	29.128	16	0	21.35	21.38	21.35	16.94	16.96	16.96	16.98	16.96	21.36	21.34	21.34	21.35	16.96	4.39
82.0	29.128	17	0	21.34	21.38	21.38	16.84	16.88	16.86	16.85	16.88	21.35	21.33	21.34	21.35	16.86	4.49
82.0	29.128	18	0	21.50	21.44	21.43	16.76	16.78	16.78	16.78	16.79	21.37	21.37	21.38	21.42	16.78	4.64

TABLE VIIIa

Raw Front Lift Data for Model with E = .3

Flap Setting	Angle of Attack	Before-Static Readings			Wind-on Readings					After-Static Readings			Static Average	Wind-on Average	Front Lift Force
0	0	39.60	39.61		34.50	34.52	34.53	34.53	34.55				39.67	34.53	5.14
0	-6	39.50	39.49	39.50	44.30	44.34	44.34	44.34	44.35				39.50	44.33	-4.83
0	-4	39.40	39.45	39.42	41.17	41.15	41.15	41.15	41.14				39.42	41.15	-1.73
0	-2	40.00	40.00	39.43	37.90	37.88	37.90	37.90	37.90				39.81	37.90	1.91
0	0				34.68	34.70	34.70	34.68	34.70				39.67	34.69	4.98
0	2	40.31	40.30	40.32	31.38	31.36	31.34	31.34	31.38				40.31	31.36	8.95
0	4	40.35	40.19	40.14	28.05	27.98	27.96	27.93	27.93				40.23	27.97	12.26
0	6	40.21	40.22	40.20	24.40	24.28	24.19	24.25	24.25				40.21	24.27	15.94
0	8	40.36	40.39	40.36	21.25	21.29	21.15	21.13	21.16				40.37	21.19	19.18
0	10	40.50	40.50	40.50	19.11	18.98	18.96	18.99	18.95				40.50	19.00	21.50
0	10				18.86	18.98	19.02	19.14	19.20				40.50	19.04	21.46
0	6				24.34	24.33	24.38	24.35	24.37				40.21	24.35	15.86
0	2				31.26	31.35	31.33	31.33	31.26				40.31	31.33	8.98
0	0	39.67	39.63	39.65	34.71	34.70	34.70	34.70	34.72	39.70	39.73	39.73	39.67	34.71	4.96
1	0	39.59	39.60	39.60	33.76	33.76	33.77	33.75	33.73	39.50	39.53	39.56	39.56	33.75	5.81
2	0	39.63	39.65	39.65	32.75	32.76	32.76	32.80	32.81	39.48	39.54	39.56	39.59	32.78	6.81
3	0	39.65	39.65	39.65	31.95	31.98	31.99	32.00	31.96	39.62	39.64	39.65	39.64	31.98	7.66
4	0	39.65	39.66	39.65	30.90	30.88	30.87	30.92	30.89	39.65	39.68	39.67	39.64	30.89	8.75
4	-6	38.90	38.92	38.92	40.57	40.58	40.58	40.54	40.55	38.90	38.91	38.91	38.91	40.56	-1.65
4	-4	39.18	39.19	39.18	37.30	37.30	37.30	37.30	37.30	39.23	39.24	39.24	39.21	37.30	1.91
4	-2	39.42	39.43	39.43	34.20	34.16	34.14	34.12	34.13	39.43	39.43	39.44	39.43	34.15	5.28
4	0	39.61	39.61	39.61	30.99	30.95	30.98	31.03	31.00	39.63	39.65	39.64	39.64	30.99	8.65
4	2	39.82	39.82	39.82	27.23	27.25	27.80	27.89	27.86	39.82	39.84	39.84	39.83	27.81	12.02
4	4	40.01	40.01	40.01	24.70	24.66	24.64	24.57	24.56	40.02	40.03	40.03	40.02	24.63	15.39
4	6	40.18	40.19	40.18	21.67	21.63	21.73	21.78	21.58	40.24	40.25	40.25	40.22	21.68	18.54
4	8	40.34	40.35	40.35	19.10	19.03	19.17	19.39	19.30	40.40	40.40	40.40	40.37	19.20	21.17
4	10	40.54	40.55	40.55	17.65	17.85	17.60	17.45	17.49	40.50	40.50	40.50	40.52	17.61	22.91
4	0	39.63	39.62	39.61	30.76	30.87	30.93	30.93	30.90	39.63	39.64	39.65	39.64	30.88	8.76
5	0	39.66	39.68	39.68	29.85	29.79	29.80	29.85	29.90	39.34	39.43	39.46	39.54	29.84	9.70
6	0	39.67	39.67	39.69	28.80	28.83	28.86	28.80	28.82	39.33	39.43	39.48	39.55	28.82	10.73
7	0	39.69	39.70	39.70	28.01	28.02	28.08	28.07	28.00	39.55	39.60	39.61	39.64	28.04	11.60
8	0	39.68	39.62	39.69	27.13	27.11	27.12	27.10	27.10	39.65	39.67	39.66	39.65	27.11	12.54
8	-6	38.93	38.93	38.93	36.90	36.95	36.94	36.93	36.97	38.81	38.92	38.92	38.91	36.94	1.97
8	-4	39.25	39.26	39.26	33.62	33.58	33.60	33.60	33.60	39.20	39.21	39.21	39.23	33.60	5.63
8	-2	39.42	39.42	39.43	30.40	30.34	30.33	30.33	30.40	39.42	39.44	39.44	39.43	30.36	9.07
8	0	39.63	39.63	39.65	27.03	27.00	27.00	27.04	26.99	39.63	39.65	39.65	39.65	27.01	12.64
8	2	39.87	39.89	39.88	24.15	24.07	24.08	24.15	24.12	39.83	39.84	39.84	39.86	24.11	15.75
8	4	40.06	40.07	40.07	21.34	21.40	21.40	21.36	21.40	40.01	40.02	40.02	40.04	21.38	18.66
8	6	40.26	40.27	40.27	19.12	18.84	19.15	18.90	19.09	40.25	40.26	40.27	40.26	19.02	21.24
8	8	40.41	40.41	40.41	17.40	17.30	17.41	17.47	17.30	40.41	40.43	40.43	40.42	17.38	23.04
8	10	40.55	40.55	40.55	16.23	16.38	16.38	16.25	16.15	40.55	40.56	40.56	40.55	16.28	24.27
8	0	39.63	39.65	39.65	27.05	27.15	27.15	27.15	27.15	39.60	39.61	39.62	39.65	27.13	12.52
9	0	39.67	39.70	39.68	26.11	26.16	26.15	26.07	26.11	39.65	39.67	39.67	39.67	26.12	13.55
10	0	39.70	39.70	39.71	25.38	25.39	25.45	25.36	25.29	39.62	39.65	39.65	39.67	25.37	14.30
11	0	39.70	39.70	39.70	24.63	24.60	24.72	24.76	24.73	39.54	39.57	39.60	39.64	24.69	14.95
12	0	39.75	39.75	39.77	23.61	23.61	23.69	23.68	23.68				39.72	23.65	16.07
12	0				23.86	23.75	23.80	23.75	23.75	39.66	39.69	39.69	39.72	23.78	15.94
13	0	39.70	39.71	39.71	23.35	23.23	23.21	23.32	23.35	39.58	39.45	39.50	39.58	23.29	16.29
15	0	39.69	39.72	39.70	22.85	22.75	22.75	22.73	22.72				39.70	22.76	16.94
15	0				22.96	23.00	23.05	22.90	22.98	39.65	39.68	39.68	39.70	22.98	16.72
16	0	39.70	39.71	39.71	22.03	22.15	22.28	22.25	22.15	39.66	39.68	39.66	39.69	22.17	17.52
17	0	39.71	39.71	39.72	21.99	21.97	22.14	21.92	21.88	39.45	39.50	39.51	39.60	21.98	17.62
18	0	39.71	39.72	39.72	22.23	22.23	22.07	21.91	22.14	39.52	39.58	39.58	39.64	22.12	17.52

TABLE VIIIb

Raw Rear Lift Data for Model with E = .3

Flap Setting	Angle of Attack	Before-Static Readings			Wind-on Readings					After-Static Readings			Static Average	Wind-on Average	Rear Lift Force
0	0	19.36	19.43		19.80	19.81	19.81	19.80	19.80				19.34	19.80	-.46
0	-6	20.40	20.41	20.41	23.28	23.30	23.30	23.29	23.29				20.41	23.29	-2.88
0	-4	19.96	19.92	19.92	22.14	22.15	22.15	22.14	22.14				19.93	22.14	-2.21
0	-2	19.87	19.87	19.62	21.01	21.01	21.01	21.01	21.01				19.79	21.01	-1.22
0	0				19.85	19.86	19.85	19.85	19.85				19.34	19.85	-.51
0	2	19.66	19.65	19.65	18.47	18.47	18.45	18.47	18.47				19.65	18.47	1.18
0	4	19.04	18.90	18.93	16.76	16.73	16.74	16.74	16.72				18.96	16.74	2.22
0	6	18.76	18.76	18.77	14.77	14.78	14.72	14.74	14.74				18.76	14.75	4.01
0	8	18.59	18.59	18.60	13.10	13.13	13.09	13.09	13.09				18.59	13.10	5.49
0	10	18.44	18.42	18.44	12.11	12.09	12.08	12.07	12.07				18.43	12.08	6.34
0	10				12.05	12.08	12.07	12.13	12.12				18.43	12.09	6.34
0	6				14.79	14.75	14.74	14.76	14.78				18.76	14.76	4.00
0	2				18.50	18.49	18.47	18.48	18.46				19.65	18.48	1.17
0	0	19.33	19.32	19.33	19.85	19.86	19.86	19.86	19.87	19.30	19.31	19.32	19.34	19.86	-.52
1	0	19.35	19.36	19.36	19.59	19.60	19.59	19.60	19.60	19.31	19.32	19.34	19.34	19.60	-.26
2	0	19.36	19.36	19.35	19.32	19.31	19.32	19.33	19.33	19.29	19.33	19.34	19.34	19.32	.02
3	0	19.36	19.35	19.35	19.08	19.09	19.08	19.09	19.09	19.33	19.35	19.35	19.34	19.09	.26
4	0	19.36	19.37	19.36	18.77	18.77	18.76	18.77	18.76	19.31	19.31	19.31	19.35	18.77	.58
4	-6	20.08	20.08	20.09	21.95	21.96	21.95	21.94	21.94	20.07	20.08	20.08	20.08	21.95	-1.87
4	-4	19.79	19.79	19.79	20.82	20.82	20.82	20.82	20.83	19.77	19.78	19.77	19.78	20.82	-1.04
4	-2	19.55	19.56	19.55	19.80	19.79	19.79	19.78	19.78	19.54	19.54	19.54	19.55	19.79	-.24
4	0	19.35	19.36	19.36	18.78	18.77	18.77	18.78	18.78	19.34	19.35	19.34	19.35	18.78	.57
4	2	19.11	19.11	19.11	17.65	17.66	17.66	17.66	17.68	19.11	19.11	19.11	19.11	17.66	1.45
4	4	18.92	18.92	18.92	16.34	16.32	16.31	16.31	16.29	18.92	18.92	18.92	18.92	16.31	2.61
4	6	18.76	18.76	18.76	14.68	14.67	14.68	14.70	14.63	18.75	18.75	18.75	18.76	14.67	4.09
4	8	18.59	18.59	18.59	12.82	12.84	12.88	12.93	12.91	18.58	18.58	18.58	18.59	12.88	5.71
4	10	18.41	18.41	18.41	11.29	11.85	11.27	11.75	11.74	18.43	18.42	18.43	18.42	11.78	6.64
4	0	19.34	19.36	19.36	18.74	18.76	18.76	18.72	18.76	19.34	19.35	19.35	19.35	18.76	.59
5	0	19.33	19.34	19.34	18.46	18.45	18.45	18.46	18.46	19.20	19.24	19.26	19.29	18.46	.83
6	0	19.34	19.34	19.33	18.15	18.15	18.16	18.14	18.15	19.19	19.24	19.26	19.28	18.15	1.13
7	0	19.33	19.32	19.32	17.89	17.90	17.89	17.90	17.90	19.26	19.29	19.30	19.30	17.90	1.40
8	0	19.32	19.32	19.31	17.64	17.62	17.63	17.63	17.63	19.31	19.32	19.32	19.34	17.63	1.71
8	-6	20.09	20.10	20.10	20.63	20.65	20.65	20.65	20.66	20.10	20.10	20.11	20.10	20.65	-.55
8	-4	19.75	19.75	19.75	19.56	19.57	19.57	19.57	19.57	19.82	19.77	19.77	19.77	19.57	.20
8	-2	19.52	19.52	19.53	18.55	18.55	18.55	18.54	18.56	19.51	19.51	19.52	19.52	18.55	.97
8	0	19.34	19.34	19.34	17.59	17.60	17.60	17.60	17.58	19.34	19.34	19.34	19.34	17.59	1.75
8	2	19.09	19.09	19.09	16.67	16.66	16.66	16.67	16.67	19.09	19.10	19.10	19.09	16.67	2.42
8	4	18.89	18.89	18.89	15.66	15.65	15.66	15.65	15.65	18.91	18.91	18.91	18.90	15.65	3.25
8	6	18.72	18.73	18.73	14.34	14.28	14.33	14.30	14.33	18.73	18.73	18.73	18.73	14.32	4.41
8	8	18.55	18.56	18.56	12.62	12.60	12.64	12.64	12.64	18.56	18.56	18.56	18.56	12.63	5.93
8	10	18.42	18.42	18.42	11.37	11.43	11.46	11.40	11.40	18.42	18.42	18.42	18.42	11.41	7.01
8	0	19.33	19.34	19.34	17.60	17.61	17.62	17.62	17.62	19.37	19.38	19.37	19.34	17.61	1.73
9	0	19.36	19.36	19.35	17.33	17.33	17.34	17.32	17.33	19.29	19.29	19.30	19.33	17.33	2.00
10	0	19.33	19.33	19.33	17.09	17.08	17.09	17.07	17.06	19.28	19.31	19.31	19.32	17.08	2.24
11	0	19.33	19.33	19.31	16.84	16.83	16.85	16.86	16.86	19.24	19.27	19.29	19.30	16.85	2.45
12	0	19.33	19.33	19.32	16.06	16.08	16.06	16.02	16.06				19.32	16.07	3.35
12	0				16.12	16.01	16.07	16.06	15.99	19.31	19.32	19.32	19.32	16.05	3.27
13	0	19.33	19.31	19.32	15.95	15.91	15.91	15.89	16.00	19.17	19.20	19.23	19.26	15.93	3.33
15	0	19.33	19.33	19.33	16.20	16.17	16.18	16.18	16.17				19.31	16.13	3.13
15	0				16.21	16.23	16.21	16.21	16.25	19.28	19.29	19.30	19.31	16.22	3.09
16	0	19.31	19.31	19.31	15.42	15.42	15.43	15.47	15.40	19.26	19.28	19.30	19.30	15.43	2.87
17	0	19.30	19.30	19.30	15.30	15.04	15.35	15.36	15.31	19.22	19.25	19.26	19.27	15.27	4.00
13	0	19.32	19.32	19.32	15.41	15.01	14.92	14.88	15.07	19.23	19.26	19.26	19.29	15.06	4.23

TABLE VIIIc

Raw Drag Data for Model with E = .3

Avg. Temp.	Avg. Press.	n	α	Before-Static Readings			Wind-on Readings					After-Static Readings			Static Average	Wind-on Average	Drag Force
77.0	29.050	0	0	21.47	21.40		17.70	17.70	17.73	17.74	17.75				21.41	17.72	3.69
77.0	29.050	0	-6	21.02	21.06	21.06	17.35	17.37	17.38	17.39	17.38				21.05	17.37	3.68
77.0	29.050	0	-4	21.13	21.16	21.17	17.62	17.62	17.61	17.60	17.60				21.15	17.61	3.54
77.0	29.050	0	-2	21.18	21.22	21.24	17.76	17.74	17.72	17.74	17.75				21.21	17.74	3.47
77.0	29.050	0	0				17.82	17.84	17.85	17.85	17.84				21.41	17.84	3.57
77.0	29.050	0	2	21.38	21.36	21.33	17.83	17.83	17.84	17.84	17.84				21.36	17.84	3.52
77.0	29.050	0	4	21.57	21.57	21.64	17.69	17.73	17.71	17.71	17.71				21.59	17.71	3.88
77.0	29.050	0	6	21.57	21.56	21.58	17.40	17.39	17.42	17.40	17.42				21.57	17.41	4.16
77.0	29.050	0	8	21.62	21.64	21.66	17.16	17.16	17.16	17.17	17.17				21.64	17.16	4.43
77.0	29.050	0	10	21.68	21.69	21.69	16.90	16.88	16.89	16.88	16.89				21.69	16.89	4.39
77.0	29.050	0	10				16.90	16.91	16.91	16.92	16.93				21.69	16.91	4.73
77.0	29.050	0	6				17.49	17.46	17.45	17.45	17.47				21.57	17.46	4.11
77.0	29.050	0	2				17.75	17.73	17.79	17.78	17.77				21.36	17.77	3.59
77.0	29.050	0	0	21.37	21.36	21.38	17.89	17.35	17.85	17.84	17.86	21.40	21.42	21.45	21.41	17.86	3.55
70.5	29.355	1	0	21.46	21.44	21.43	17.96	17.34	17.83	17.83	17.82	21.36	21.35	21.36	21.40	17.84	3.56
70.5	29.355	2	0	21.48	21.45	21.44	17.69	17.72	17.71	17.72	17.72	21.33	21.35	21.37	21.40	17.71	3.69
70.5	29.355	3	0	21.48	21.45	21.44	17.68	17.71	17.72	17.72	17.71	21.48	21.45	21.44	21.46	17.71	3.75
73.0	29.357	4	0	21.41	21.42	21.42	17.65	17.68	17.68	17.68	17.69	21.52	21.48	21.48	21.39	17.68	3.71
73.0	29.357	4	-6	21.07	21.09	21.09	17.55	17.54	17.56	17.55	17.55	21.13	21.14	21.14	21.11	17.55	3.56
73.0	29.357	4	-4	21.15	21.17	21.17	17.65	17.65	17.65	17.65	17.66	21.22	21.23	21.24	21.20	17.65	3.55
73.0	29.357	4	-2	21.30	21.31	21.30	17.70	17.70	17.70	17.69	17.69	21.27	21.28	21.27	21.29	17.70	3.59
73.0	29.357	4	0	21.34	21.35	21.35	17.70	17.71	17.71	17.72	17.71	21.35	21.36	21.36	21.39	17.71	3.68
73.0	29.357	4	2	21.42	21.44	21.44	17.66	17.66	17.66	17.65	17.65	21.41	21.42	21.43	21.43	17.66	3.77
73.0	29.357	4	4	21.48	21.51	21.49	17.59	17.59	17.56	17.56	17.54	21.49	21.50	21.50	21.50	17.57	3.93
73.0	29.357	4	6	21.53	21.55	21.54	17.29	17.29	17.30	17.31	17.30	21.70	21.68	21.66	21.61	17.30	4.31
73.0	29.357	4	8	21.62	21.62	21.62	16.92	16.93	16.95	16.98	16.98	21.70	21.70	21.70	21.66	16.95	4.71
73.0	29.357	4	10	21.79	21.77	21.77	16.69	16.72	16.66	16.63	16.63	21.64	21.67	21.67	21.72	16.67	5.05
73.0	29.357	4	0	21.33	21.36	21.37	17.27	17.25	17.26	17.27	17.25	21.35	21.38	21.38	21.39	17.26	3.53
73.0	29.357	5	0	21.48	21.45	21.46	17.61	17.60	17.60	17.61	17.62	21.32	21.34	21.35	21.40	17.51	3.89
73.0	29.357	6	0	21.52	21.52	21.49	17.55	17.52	17.60	17.57	17.58	21.32	21.35	21.37	21.43	17.57	3.86
73.0	29.357	7	0	21.52	21.51	21.52	17.50	17.52	17.53	17.52	17.53	21.34	21.37	21.38	21.44	17.52	3.92
73.0	29.357	8	0	21.39	21.41	21.44	17.42	17.44	17.43	17.43	17.43	21.51	21.48	21.48	21.42	17.43	3.99
73.0	29.357	8	-6	21.22	21.20	21.20	17.53	17.54	17.53	17.51	17.51	21.26	21.22	21.21	21.22	17.52	3.77
73.0	29.357	8	-4	21.27	21.27	21.28	17.51	17.51	17.51	17.50	17.52	21.27	21.28	21.28	21.28	17.51	3.77
73.0	29.357	8	-2	21.28	21.33	21.31	17.60	17.60	17.58	17.57	17.56	21.33	21.33	21.36	21.32	17.58	3.74
73.0	29.357	8	0	21.35	21.37	21.37	17.52	17.50	17.51	17.49	17.48	21.39	21.38	21.38	21.42	17.50	3.92
73.0	29.357	8	2	21.60	21.55	21.55	17.36	17.35	17.35	17.36		21.45	21.45	21.46	21.51	17.36	4.13
73.0	29.357	8	4	21.60	21.60	21.59	17.16	17.18	17.18	17.17	17.18	21.51	21.53	21.54	21.56	17.17	4.39
73.0	29.357	8	6	21.68	21.65	21.64	16.97	17.01	16.98	17.00	17.01	21.73	21.72	21.74	21.69	16.99	4.70
73.0	29.357	8	8	21.70	21.70	21.70	16.56	16.57	16.60	16.59	16.57	21.73	21.73	21.73	21.72	16.98	5.14
73.0	29.357	8	10	21.73	21.73	21.73	16.22	16.24	16.24	16.22	16.22	21.77	21.78	21.77	21.75	16.23	5.52
73.0	29.357	8	0	21.50	21.48	21.49	17.62	17.60	17.60	17.60	17.59	21.37	21.40	21.39	21.42	17.59	3.92
76.2	29.302	9	0	21.37	21.44	21.43	17.31	17.32	17.35	17.36	17.32	21.49	21.44	21.44	21.44	17.34	4.10
76.2	29.308	10	0	21.39	21.37	21.43	17.37	17.38	17.41	17.39	17.38	21.41	21.42	21.42	21.41	17.39	4.02
76.2	29.308	11	0	21.41	21.41	21.40	17.39	17.37	17.39	17.38	17.37	21.39	21.39	21.41	21.40	17.38	4.02
76.2	29.308	12	0	21.47	21.47	21.47	16.93	16.97	16.95	16.97	16.97				21.47	16.96	4.51
76.2	29.308	12	0				17.08	17.05	17.07	17.08	17.04	21.47	21.45	21.47	21.47	17.06	4.41
76.2	29.308	13	0	21.46	21.43	21.41	16.86	16.85	16.86	16.86	16.90	21.34	21.33	21.37	21.39	16.87	4.52
76.2	29.308	13	0	21.47	21.43	21.43	16.78	16.80	16.79	16.79	16.80				21.46	16.79	4.57
76.2	29.308	15	0				17.02	17.01	17.00	16.98	16.99	21.47	21.47	21.47	21.46	17.00	4.45
76.2	29.308	15	0				16.41	16.43	16.44	16.45	16.43	21.51	21.49	21.50	21.48	16.43	5.05
75.2	29.308	16	0	21.50	21.44	21.43	16.36	16.29	16.37	16.33	16.34	21.30	21.30	21.30	21.32	16.34	4.38
75.2	29.308	17	0	21.33	21.34	21.33	16.22	16.13	16.14	16.08	16.17	21.39	21.36	21.36	21.42	16.15	5.27
75.2	29.308	18	0	21.50	21.47	21.46											

TABLE IXa

Raw Front Lift Data for Model with E = .4

Flap Setting	Angle of Attack	Before-Static Readings			Wind-on Readings					After-Static Readings			Static Average	Wind-on Average	Front Lift Force
0	0	39.95	39.97	39.97	35.13	35.12	35.08	35.13	35.12	40.13	40.12	40.14	40.02	35.12	4.90
0	-6	39.22	39.22	39.22	45.05	45.03	45.06	45.05	45.05	39.33	39.33	39.34	39.28	45.05	-5.77
0	-4	39.49	39.50	39.51	41.89	41.89	41.90	41.87	41.86	39.58	39.60	39.60	39.55	41.88	-2.33
0	-2	39.70	39.72	39.72	38.45	38.45	38.46	38.49	38.50	39.80	39.80	39.82	39.76	38.47	1.29
0	0	39.94	39.95	39.96	35.26	35.21	35.20	35.17	35.18	39.98	40.02	40.00	40.02	35.20	4.82
0	2	40.17	40.18	40.17	31.86	31.85	31.84	31.82	31.84	40.23	40.22	40.23	40.20	31.84	8.36
0	4	40.35	40.35	40.35	28.68	28.62	28.65	28.61	28.65	40.40	40.42	40.41	40.38	28.64	11.74
0	6	40.51	40.52	40.52	25.35	25.26	25.30	25.18	25.26	40.56	40.56	40.58	40.54	25.27	15.27
0	8	40.68	40.69	40.70	22.48	22.35	22.41	22.35	22.28	40.72	40.73	40.74	40.71	22.37	18.34
0	10	40.85	40.84	40.84	19.81	20.01	20.04	19.92	19.83	40.85	40.86	40.85	40.85	19.92	20.93
0	0	40.02	40.05	40.05	35.17	35.13	35.15	35.10	35.15	40.06	40.06	40.06	40.02	35.14	4.88
1	0	40.03	40.03	40.03	33.98	34.00	33.98	34.02	33.98	39.96	40.01	40.03	40.02	33.99	6.03
2	0	40.06	40.05	40.08	32.79	32.80	32.81	32.81	32.77	39.94	39.98	40.00	40.02	32.80	7.22
3	0	40.05	40.06	40.06	31.61	31.63	31.61	31.62	31.65	39.95	39.99	40.00	40.02	31.62	8.40
4	0	40.07	40.07	40.08	30.52	30.55	30.45	30.52	30.55	40.12	40.12	40.13	40.06	30.52	9.54
4	-6	39.31	39.31	39.31	40.65	40.69	40.65	40.68	40.68	39.35	39.36	39.36	39.33	40.67	-1.34
4	-4	39.56	39.57	39.58	37.45	37.38	37.36	37.36	37.36	39.59	39.59	39.59	39.58	37.38	2.20
4	-2	39.76	39.76	39.76	34.05	34.00	34.01	34.08	34.07	39.80	39.81	39.82	39.79	34.04	5.75
4	0	40.00	40.00	40.00	30.61	30.50	30.59	30.60	30.54	40.03	40.02	40.04	40.06	30.57	9.49
4	2	40.22	40.23	40.23	27.18	27.20	27.23	27.23	27.26	40.23	40.23	40.23	40.23	27.22	13.01
4	4	40.37	40.39	40.38	24.38	24.46	24.30	24.38	24.32	40.40	40.40	40.40	40.39	24.37	16.02
4	6	40.55	40.55	40.55	21.37	21.46	21.33	21.44	21.53	40.55	40.56	40.57	40.56	21.43	19.13
4	8	40.73	40.72	40.73	19.07	18.87	18.90	19.05	19.10	40.73	40.73	40.74	40.73	19.00	21.23
4	10	40.88	40.88	40.89	17.79	17.68	17.73	17.65	17.85	40.88	40.88	40.89	40.88	17.74	23.14
4	0	40.06	40.06	40.06	30.50	30.51	30.50	30.58	30.52	40.05	40.05	40.06	40.06	30.52	9.54
5	0	40.05	40.06	40.06	29.50	29.47	29.47	29.44	29.44	39.80	39.90	39.94	39.97	29.46	10.51
6	0	40.08	40.08	40.09	28.26	28.25	28.22	28.18	28.25	39.86	39.94	39.96	40.00	28.23	11.77
7	0	40.12	40.12	40.13	27.20	27.21	27.18	27.21	27.23	39.80	39.90	39.94	40.00	27.21	12.79
8	0	40.12	40.12	40.13	25.87	25.95	25.96	25.88	25.90	40.12	40.13	40.15	40.08	25.91	14.17
8	-6	39.36	39.37	39.37	36.13	36.14	36.13	36.13	36.15	39.26	39.27	39.29	39.32	36.14	3.18
8	-4	39.60	39.63	39.64	32.82	32.81	32.77	32.78	32.80	39.57	39.57	39.58	39.60	32.80	6.80
8	-2	39.83	39.85	39.86	29.44	29.47	29.56	29.50	29.46	39.75	39.75	39.76	39.80	29.49	10.31
8	0	40.05	40.07	40.06	26.14	26.11	26.09	25.98	26.01	40.00	40.00	40.01	40.08	26.07	14.01
8	2	40.25	40.25	40.27	23.00	22.85	22.80	22.78	22.85	40.21	40.22	40.22	40.24	22.86	17.38
8	4	40.42	40.43	40.43	20.00	20.22	20.00	20.04	20.10	40.39	40.40	40.40	40.41	20.07	20.34
8	6	40.58	40.59	40.60	18.05	18.00	17.86	17.95	17.89	40.55	40.56	40.58	40.58	17.95	22.63
8	8	40.75	40.75	40.76	16.62	16.92	16.84	16.65	16.85	40.74	40.75	40.74	40.75	16.78	23.97
8	10	40.90	40.91	40.91	16.26	16.27	16.33	16.38	16.34	40.95	40.96	40.95	40.93	16.32	24.61
9	0	40.06	40.08	40.09	26.02	26.10	26.05	26.18	26.16	40.16	40.10	40.10	40.08	26.11	13.92
9	0	40.10	40.10	40.10	24.92	25.07	25.05	25.05	25.10	39.86	39.95	39.97	40.01	25.04	14.92
10	0	40.10	40.11	40.12	23.58	23.62	23.61	23.54	23.80	39.94	40.00	40.02	40.05	23.63	16.42
11	0	40.10	40.11	40.12	22.96	22.98	23.00	23.00	23.00	40.10	40.11	40.12	40.11	22.99	17.12
12	0	40.12	40.12	40.12	21.49	21.43	21.46	21.55	21.49	39.99	40.01	40.05	40.07	21.48	18.59
13	0	40.10	40.10	40.11	20.83	20.63	20.92	20.86	20.65	39.75	39.81	39.85	39.95	20.78	19.12
15	0	40.14	40.14	40.15	19.54	19.26	19.26	19.34	19.54	39.90	39.95	39.98	40.04	19.39	20.65
16	0	40.15	40.16	40.15	19.66	20.29	19.91	20.24	20.14	40.06	40.06	40.09	40.11	20.05	20.06
17	0	40.13	40.13	40.13	20.16	20.02	20.10	20.09	19.76	40.03	40.08	40.07	40.10	20.03	20.02
18	0	40.15	40.15	40.15	19.45	19.50	19.26	18.92	19.01	39.85	39.90	39.93	40.02	19.23	20.79

TABLE IXb

Raw Rear Lift Data for Model with E = .4

Flap Setting	Angle of Attack	Before-Static Readings			Wind-on Readings					After-Static Readings			Static Average	Wind-on Average	Rear Lift Force
0	0	19.46	19.42	19.45	19.36	19.34	19.34	19.36	19.36	19.44	19.44	19.45	19.42	19.35	.12
0	-6	20.27	20.28	20.28	23.24	23.23	23.24	23.25	23.23	20.25	20.25	20.25	20.26	23.23	-2.97
0	-4	19.95	19.94	19.94	21.94	21.95	21.95	21.94	21.93	19.95	19.92	19.94	19.94	21.94	-2.00
0	-2	19.69	19.70	19.70	20.63	20.64	20.65	20.63	20.63	19.69	19.68	19.68	19.69	20.64	-.95
0	0	19.50	19.49	19.49	19.39	19.37	19.35	19.33	19.33	19.51	19.51	19.51	19.47	19.35	.12
0	2	19.23	19.23	19.23	17.75	17.75	17.74	17.76	17.77	19.24	19.23	19.24	19.23	17.25	1.48
0	4	19.07	19.07	19.07	15.99	15.98	15.98	15.96	15.95	19.06	19.06	19.06	19.07	15.97	3.10
0	6	18.91	18.91	18.91	14.03	13.98	13.96	13.91	13.96	18.90	18.90	18.90	18.91	13.97	4.94
0	8	18.73	18.73	18.73	12.62	12.58	12.59	12.57	12.56	18.73	18.73	18.73	18.73	12.58	6.15
0	10	18.56	18.56	18.56	11.63	11.70	11.69	11.66	11.64	18.58	18.58	18.57	18.57	11.66	6.91
0	0	19.47	19.49	19.45	19.34	19.25	19.26	19.24	19.25	19.46	19.48	19.48	19.47	19.27	.20
1	0	19.49	19.49	19.49	19.11	19.11	19.08	19.08	19.08	19.44	19.46	19.47	19.47	19.09	.38
2	0	19.47	19.47	19.47	18.82	18.80	18.82	18.82	18.79	19.40	19.43	19.44	19.45	18.81	.64
3	0	19.49	19.48	19.48	18.56	18.54	18.54	18.55	18.53	19.43	19.46	19.46	19.47	18.54	.93
4	0	19.49	19.49	19.48	18.31	18.31	18.26	18.28	18.29	19.42	19.44	19.44	19.47	18.29	1.18
4	-6	20.28	20.28	20.28	21.89	21.89	21.88	21.89	21.89	20.23	20.34	20.24	20.26	21.89	-1.63
4	-4	19.96	19.96	19.97	20.70	20.70	20.69	20.69	20.70	19.95	19.96	19.95	19.96	20.70	-.74
4	-2	19.70	19.70	19.71	19.48	19.48	19.49	19.50	19.50	19.66	19.67	19.66	19.68	19.49	.19
4	0	19.49	19.49	19.49	18.29	18.28	18.30	18.31	18.29	19.47	19.48	19.48	19.47	18.29	1.18
4	2	19.23	19.23	19.23	16.92	16.95	16.94	16.94	16.96	19.23	19.23	19.23	19.23	16.94	2.29
4	4	19.07	19.07	19.07	15.63	15.64	15.58	15.63	15.61	19.06	19.06	19.06	19.07	15.62	3.45
4	6	18.90	18.90	18.90	13.71	13.74	13.22	13.80	13.81	18.89	18.89	18.89	18.90	13.76	5.14
4	8	18.72	18.72	18.72	12.09	12.03	12.04	12.08	12.11	18.71	18.71	18.71	18.72	12.07	6.65
4	10	18.55	18.56	18.56	11.16	11.15	11.15	11.15	11.20	18.55	18.55	18.55	18.55	11.16	7.39
4	0	19.47	19.48	19.49	18.22	18.22	18.22	18.24	18.22	19.48	19.47	19.48	19.47	18.22	1.25
5	0	19.48	19.48	19.48	18.02	17.99	18.01	18.01	17.98	19.37	19.42	19.44	19.45	18.00	1.45
6	0	19.48	19.48	19.48	17.68	17.66	17.67	17.66	17.67	19.37	19.42	19.43	19.44	17.67	1.77
7	0	19.46	19.44	19.46	17.42	17.41	17.41	17.41	17.42	19.35	19.40	19.42	19.42	17.41	2.01
8	0	19.46	19.46	19.46	17.10	17.10	17.10	17.08	17.08	19.40	19.41	19.41	19.46	17.09	2.37
8	-6	20.27	20.26	20.25	20.48	20.48	20.48	20.48	20.49	20.26	20.25	20.25	20.26	20.48	-.22
8	-4	19.94	19.94	19.95	19.33	19.34	19.34	19.34	19.34	19.92	19.92	19.91	19.93	19.34	.59
8	-2	19.67	19.67	19.68	18.23	18.24	18.26	18.24	18.23	19.68	19.69	19.69	19.68	18.24	1.44
8	0	19.48	19.48	19.48	17.14	17.13	17.13	17.10	17.12	19.47	19.48	19.48	19.46	17.12	2.34
8	2	19.22	19.23	19.23	15.97	15.97	15.94	15.97	15.97	19.22	19.23	19.23	19.23	15.96	3.27
8	4	19.05	19.05	19.05	14.81	14.83	14.83	14.86	14.88	19.04	19.05	19.05	19.05	14.84	4.21
8	6	18.89	18.89	18.88	13.46	13.40	13.38	13.36	13.37	18.88	18.88	18.88	18.88	13.39	5.49
8	8	18.72	18.72	18.71	11.63	11.73	11.69	11.62	11.66	18.68	18.69	18.69	18.70	11.67	7.03
8	10	18.55	18.54	18.54	10.67	10.68	10.68	10.68	10.66	18.53	18.53	18.53	18.54	10.67	7.87
8	0	19.48	19.49	19.49	17.08	17.08	17.08	17.10	17.10	19.46	19.47	19.47	19.46	17.09	2.37
9	0	19.47	19.47	19.47	16.80	16.85	16.82	16.82	16.84	19.32	19.37	19.39	19.42	16.83	2.59
10	0	19.45	19.45	19.45	16.52	16.52	16.53	16.49	16.55	19.33	19.38	19.39	19.41	16.52	2.89
11	0	19.46	19.44	19.45	15.99	16.00	16.32	16.29	16.28	19.39	19.42	19.42	19.43	16.18	3.25
12	0	19.45	19.45	19.45	15.63	15.55	15.91	15.93	15.92	19.33	19.37	19.38	19.41	15.79	3.62
13	0	19.45	19.45	19.44	15.24	15.27	15.25	15.74	15.72	19.27	19.30	19.32	19.37	15.73	3.64
15	0	19.45	19.44	19.44	15.37	15.35	15.35	15.35	15.37	19.34	19.36	19.38	19.40	15.36	4.04
16	0	19.43	19.41	19.42	15.30	15.39	15.33	15.34	15.35	19.34	19.41	19.39	.40	15.34	4.06
17	0	19.45	19.44	19.44	15.26	15.26	15.27	15.28	15.21	19.34	19.38	19.41	.41	15.26	4.15
18	0	19.42	19.40	19.42	15.10	15.08	15.01	14.96	14.96	19.26	19.30	19.3-	.35	15.02	4.33

TABLE IXc

Raw Drag Data for Model with E = .4

Avg. Temp.	Avg. Press.	n	α	Before-Static Readings			Wind-on Readings					After-Static Readings			Static Average	Wind-on Average	Drag Force
80.0	29.240	0	0	21.33	21.33	21.33	17.58	17.59	17.62	17.59	17.60	21.44	21.44	21.45	21.36	17.60	3.76
80.0	29.240	0	-6	20.07	21.10	21.10	17.31	17.31	17.30	17.30	17.31	21.21	21.20	21.19	21.15	17.31	3.84
80.0	29.240	0	-4	21.16	21.17	21.15	17.46	17.47	17.47	17.48	17.49	21.25	21.20	21.24	21.20	17.47	3.73
80.0	29.240	0	-2	21.21	21.23	21.22	17.57	17.57	17.57	17.56	17.57	21.29	21.29	21.30	21.26	17.57	3.69
80.0	29.240	0	0	21.28	21.28	21.28	17.60	17.59	17.60	17.58	17.60	21.35	21.35	21.34	21.36	17.59	3.77
80.0	29.240	0	2	21.36	21.37	21.37	17.60	17.59	17.60	17.60	17.60	21.42	21.44	21.44	21.40	17.60	3.80
80.0	29.240	0	4	21.41	21.43	21.43	17.51	17.51	17.52	17.50	17.50	21.49	21.47	21.51	21.49	17.51	3.95
80.0	29.240	0	6	21.44	21.44	21.44	17.23	17.24	17.27	17.24	17.26	21.52	21.53	21.56	21.49	17.25	4.24
80.0	29.240	0	8	21.51	21.51	21.51	17.04	17.02	17.03	17.04	17.03	21.57	21.58	21.58	21.54	17.03	4.51
80.0	29.240	0	10	21.55	21.57	21.58	16.79	16.81	16.84	16.80	16.81	21.61	21.68	21.61	21.60	16.81	4.79
80.0	29.240	0	0	21.35	21.35	21.35	17.81	17.82	17.82	17.82	17.32	21.42	21.44	21.42	21.36	17.32	3.54
78.5	29.254	1	0	21.34	21.35	21.34	17.55	17.58	17.58	17.58	17.58	21.36	21.36	21.37	21.35	17.57	3.74
78.5	29.254	2	0	21.38	21.39	21.38	17.55	17.56	17.56	17.56	17.56	21.33	21.35	21.36	21.37	17.56	3.81
78.5	29.254	3	0	21.36	21.36	21.36	17.45	17.49	17.48	17.48	17.49	21.33	21.36	21.37	21.36	17.48	3.88
78.5	29.254	4	0	21.40	21.39	21.39	17.44	17.47	17.45	17.47	17.48	21.45	21.46	21.46	21.41	17.46	3.95
78.5	29.254	4	-6	21.23	21.18	21.20	17.38	17.38	17.39	17.39	17.39	21.17	21.15	21.16	21.18	17.39	3.79
78.5	29.254	4	-4	21.26	21.29	21.25	17.45	17.47	17.47	17.47	17.46	21.22	21.22	21.22	21.24	17.46	3.78
78.5	29.254	4	-2	21.31	21.31	21.31	17.51	17.50	17.51	17.50	17.50	21.26	21.27	21.27	21.29	17.50	3.79
78.5	29.254	4	0	21.34	21.35	21.36	17.52	17.51	17.51	17.51	17.50	21.38	21.39	21.38	21.41	17.51	3.90
78.5	29.254	4	2	21.44	21.44	21.44	17.38	17.38	17.40	17.41	17.43	21.51	21.50	21.50	21.47	17.40	4.07
78.5	29.254	4	4	21.48	21.49	21.49	17.29	17.30	17.28	17.28	17.29	21.51	21.51	21.51	21.50	17.29	4.21
78.5	29.254	4	6	21.52	21.53	21.53	16.92	16.94	16.92	16.94	16.94	21.55	21.57	21.56	21.54	16.93	4.61
78.5	29.254	4	8	21.59	21.60	21.60	16.63	16.64	16.63	16.66	16.68	21.62	21.63	21.62	21.61	16.65	4.96
78.5	29.254	4	10	21.62	21.63	21.65	16.30	16.31	16.31	16.31	16.33	21.66	21.67	21.68	21.65	16.31	5.34
78.5	29.254	4	0	21.43	21.44	21.43	17.71	17.71	17.70	17.71	17.70	21.41	21.42	21.48	21.41	17.71	3.70
78.5	29.254	5	0	21.37	21.37	21.35	17.42	17.46	17.46	17.46	17.45	21.29	21.32	21.34	21.34	17.45	3.89
78.5	29.254	6	0	21.40	21.41	21.40	17.35	17.38	17.37	17.37	17.38	21.31	21.34	21.35	21.37	17.37	4.00
78.5	29.254	7	0	21.47	21.43	21.44	17.28	17.30	17.31	17.31	17.31	21.28	21.32	21.34	21.38	17.30	4.08
82.0	29.241	8	0	21.44	21.44	21.45	17.13	17.15	17.17	17.17	17.17	21.49	21.47	21.48	21.41	17.16	4.25
82.0	29.241	8	-6	21.22	21.19	21.19	17.32	17.32	17.37	17.32	17.37	21.12	21.13	21.14	21.17	17.37	3.80
82.0	29.241	8	-4	21.26	21.29	21.28	17.43	17.44	17.43	17.43	17.43	21.21	21.22	21.21	21.24	17.43	3.81
82.0	29.241	8	-2	21.31	21.27	21.35	17.38	17.38	17.41	17.39	17.37	21.24	21.25	21.27	21.28	17.39	3.89
82.0	29.241	8	0	21.37	21.37	21.37	17.18	17.20	17.19	17.18	17.20	21.32	21.33	21.33	21.41	17.19	4.22
82.0	29.241	8	2	21.43	21.45	21.44	17.13	17.12	17.10	17.11	17.11	21.39	21.40	21.41	21.42	17.11	4.31
82.0	29.241	8	4	21.49	21.50	21.50	16.79	16.82	16.84	16.83	16.84	21.44	21.44	21.44	21.47	16.82	4.65
82.0	29.241	8	6	21.51	21.52	21.50	16.57	16.53	16.53	16.52	16.51	21.48	21.43	21.51	21.50	16.53	4.97
82.0	29.241	8	8	21.58	21.57	21.59	16.03	16.06	16.06	16.04	16.04	21.55	21.56	21.58	21.57	16.05	5.52
82.0	29.241	8	10	21.41	21.37	21.39	15.69	15.68	15.68	15.71	15.69	21.73	21.71	21.71	21.55	15.69	5.38
82.0	29.241	8	0	21.41	21.37	21.39	17.41	17.41	17.40	17.43	17.42	21.47	21.45	21.45	21.41	17.41	4.00
82.0	29.241	9	0	21.42	21.42	21.44	17.10	17.14	17.14	17.16	17.15	21.29	21.32	21.35	21.37	17.14	4.23
82.0	29.241	10	0	21.43	21.44	21.43	16.87	16.89	16.90	16.90	16.94	21.35	21.37	21.38	21.40	16.90	4.50
82.0	29.241	11	0	21.41	21.37	21.39	16.85	16.86	16.92	16.94	16.94	21.40	21.42	21.42	21.40	16.90	4.50
82.0	29.241	12	0	21.44	21.44	21.44	16.62	16.64	16.72	16.75	16.75	21.39	21.40	21.41	21.42	16.70	4.72
82.0	29.241	13	0	21.39	21.39	21.39	16.67	16.65	16.73	16.71	16.65	21.27	21.27	21.21	21.32	16.68	4.64
82.0	29.241	15	0	21.41	21.37	21.38	16.39	16.42	16.43	16.43	16.43	21.32	21.32	21.36	21.36	16.42	4.94
82.0	29.241	16	0	21.43	21.40	21.41	16.00	15.97	16.01	16.00	15.98	21.38	21.36	21.39	21.40	15.99	5.41
82.0	29.241	17	0	21.38	21.33	21.39	15.92	15.94	15.93	15.92	15.94	21.40	21.38	21.37	21.38	15.94	5.44
82.0	29.241	18	0	21.41	21.37	21.40	15.56	15.56	15.50	15.53	15.50	21.27	21.28	21.31	21.34	15.53	5.31

TABLE Xa

Raw Front Lift Data for Model with E = .5

Flap Setting	Angle of Attack	Before-Static Readings			Wind-on Readings					After-Static Readings			Static Average	Wind-on Average	Front Lift Force
0	0	39.69	39.69	39.69	35.22	35.20	35.20	35.18	35.21	39.65	39.66	39.68	39.66	35.20	4.46
0	-6	38.95	38.95	38.95	44.79	44.80	44.79	44.78	44.80	38.96	38.96	38.97	38.96	44.79	-2.33
0	-4	39.21	39.22	39.21	41.92	41.93	41.90	41.87	41.87	39.22	39.22	39.23	39.22	41.90	-2.68
0	-2	39.43	39.45	39.45	38.69	38.73	38.70	38.70	38.70	39.52	39.42	39.43	39.43	38.70	.73
0	0	39.65	39.67	39.66	35.17	35.13	35.13	35.10	35.12	39.65	39.65	39.65	39.66	35.13	4.53
0	2	39.85	39.84	39.86	31.90	31.90	31.90	31.95	31.92	39.84	39.84	39.84	39.84	31.91	7.93
0	4	40.02	40.02	40.02	28.75	28.68	28.80	28.75	28.75	40.00	40.02	40.02	40.02	28.75	11.27
0	6	40.19	40.19	40.18	25.45	25.32	25.34	25.34	25.41	40.17	40.17	40.18	40.17	25.37	14.80
0	8	40.35	40.34	40.35	22.38	22.36	22.26	22.34	22.34	40.31	40.32	40.32	40.33	22.34	17.99
0	10	40.47	40.48	40.50	20.01	20.07	19.99	20.04	19.92	40.46	40.46	40.48	40.48	20.01	20.47
0	6	40.17	40.16	40.17	25.51	25.54	25.48	25.42	25.48	40.15	40.16	40.15	40.17	25.49	14.68
0	2	39.84	39.84	39.84	32.10	32.05	32.11	32.10	32.15	39.83	39.82	39.82	39.84	32.10	7.74
0	0	39.65	39.65	39.67	35.34	35.40	35.37	35.35	35.30	39.63	39.64	39.63	39.66	35.35	4.31
1	0	39.70	39.70	39.70	33.55	33.57	33.64	34.00	33.94	39.71	39.71	39.72	39.71	33.74	5.97
2	0	39.72	39.73	39.72	32.52	32.52	32.51	32.55	32.56	39.70	39.72	39.73	39.72	32.53	7.19
3	0	39.23	39.23	39.23	31.15	31.17	31.17	31.17	31.17	39.70	39.72	39.73	39.72	31.17	8.55
4	0	39.62	39.68	39.69	29.98	29.85	29.85	29.83	29.86	39.41	39.42	39.42	39.62	29.87	9.75
4	-6	38.95	38.95	38.96	40.02	40.02	39.98	40.00	39.95	38.94	38.94	38.94	38.95	39.99	-1.04
4	-4	39.24	39.23	39.25	36.74	36.75	36.75	36.75	36.77	39.20	39.19	39.20	39.22	36.75	2.47
4	-2	39.52	39.55	39.55	33.43	33.46	33.42	33.46	33.50	39.45	39.44	39.45	39.50	33.45	6.05
4	0	39.65	39.65	39.65	30.09	30.05	30.09	30.08	30.06	39.63	39.64	39.64	39.62	30.07	9.55
4	2	39.85	39.85	39.85	26.85	26.94	26.96	26.90	26.95	39.82	39.82	39.82	39.84	26.92	12.92
4	4	40.05	40.05	40.05	23.67	23.69	23.68	23.79	23.75	40.00	40.01	40.01	40.02	23.72	16.31
4	6	40.26	40.27	40.27	20.75	20.76	20.83	20.74	20.69	40.17	40.18	40.19	40.22	20.75	19.47
4	8	40.50	40.51	40.50	18.60	18.73	18.68	18.55	18.55	40.32	40.34	40.34	40.42	18.62	21.80
4	10	40.54	40.55	40.55	17.65	17.78	17.75	17.74	17.74	40.48	40.49	40.49	40.52	17.73	22.79
4	0	39.70	39.68	39.69	29.94	29.91	29.90	29.91	29.94	39.65	39.65	39.65	39.62	29.92	9.70
4	6				20.74	20.76	20.76	20.74	20.69				40.22	20.74	19.48
4	2				26.99	26.92	26.93	26.91	26.95				39.84	26.94	12.90
5	0	39.68	39.69	39.70	28.70	28.71	28.74	28.80	28.72	39.74	39.77	39.78	39.73	28.73	11.00
6	0	39.72	39.73	39.73	27.32	27.32	27.39	27.40	27.35	39.67	39.70	39.70	39.71	27.36	12.35
7	0	39.74	39.73	39.75	26.22	26.23	26.25	26.25	26.32	39.52	39.57	39.59	39.65	26.25	13.45
8	0	39.75	39.75	39.75	24.96	25.12	25.06	25.02	25.03	39.72	39.73	39.73	39.69	25.04	14.65
8	0	39.68	39.70	39.69	25.10	25.05	25.08	25.02	25.02	39.70	39.71	39.73	39.69	25.05	14.64
8	-6	38.94	38.93	38.94	34.79	34.81	34.83	34.79	34.81	38.94	38.95	38.95	38.94	34.81	4.13
8	-4	39.20	39.21	39.20	31.65	31.65	31.61	31.60	31.59	39.20	39.22	39.20	39.21	31.62	7.59
8	-2	39.45	39.45	39.45	28.41	28.40	28.41	28.42	28.45	39.43	39.43	39.43	39.44	28.42	11.02
8	0	39.63	39.63	39.63	25.06	25.06	25.00	25.01	25.09	39.66	39.66	39.67	39.69	25.04	14.65
8	2	39.82	39.84	39.83	22.01	21.97	21.85	22.11	21.93	39.85	39.85	39.85	39.85	21.97	17.88
8	4	40.04	40.04	40.05	18.64	18.60	18.68	18.68	18.78	40.05	40.05	40.06	40.05	18.68	21.37
8	6	40.15	40.15	40.15	16.23	16.76	16.65	16.64	16.70	40.20	40.20	40.20	40.19	16.70	23.49
8	8	40.32	40.33	40.33	16.84	16.55	16.59	16.65	16.85	40.45	40.44	40.45	40.39	16.70	23.69
8	10	40.50	40.50	40.50	16.77	16.80	16.81	16.62	16.80	40.52	40.52	40.53	40.51	16.76	23.75
8	6	40.19	40.17	40.19	16.93	16.85	16.80	17.05	17.00	40.24	40.24	40.24	40.19	16.93	23.26
8	2	39.84	39.85	39.85	21.89	21.91	22.04	22.00	22.00	39.87	39.87	39.89	39.85	21.98	17.87
8	0	39.65	39.65	39.66	25.05	25.10	25.20	25.06	25.10	39.68	39.67	39.68	39.69	25.10	14.59
9	0	39.70	39.71	39.71	23.79	23.75	23.76	23.77	23.76	39.70	39.72	39.72	39.71	23.77	15.94
10	0	39.70	39.71	39.70	22.33	22.45	22.40	22.40	22.38	39.68	39.70	39.70	39.70	22.39	17.31
11	0	39.75	39.75	39.75	21.18	21.02	21.12	21.15	21.13	39.65	39.70	39.70	39.72	21.12	18.60
12	0	39.69	39.69	39.70	19.94	20.05	20.01	19.94	20.17	39.72	39.73	39.75	39.71	20.02	19.69
13	0	39.74	39.75	39.75	18.83	18.80	18.75	18.76	18.86	39.66	39.70	39.70	39.72	18.80	20.92

TABLE Xb

Raw Rear Lift Data for Model with E = .5

Flap Setting	Angle of Attack	Before-Static Readings			Wind-on Readings					After-Static Readings			Static Average	Wind-on Average	Rear Lift Force
0	0	19.28	19.28	19.27	19.77	19.78	19.78	19.78	19.78	19.30	19.29	19.31	19.29	19.78	-.49
0	-6	20.05	20.05	20.05	23.34	23.35	23.34	23.32	23.34	20.05	20.04	20.05	20.05	23.34	-3.29
0	-4	19.73	19.74	19.73	22.29	22.29	22.28	22.27	22.27	19.73	19.72	19.72	19.73	22.28	-2.55
0	-2	19.47	19.47	19.48	21.07	21.09	21.09	21.10	21.10	19.49	19.49	19.49	19.48	21.09	-1.61
0	0	19.27	19.27	19.27	19.73	19.72	19.72	19.72	19.72	19.27	19.28	19.28	19.29	19.72	-.43
0	2	19.02	19.03	19.03	18.31	18.31	18.32	18.32	18.30	19.04	19.04	19.04	19.05	18.31	.74
0	4	18.87	18.87	18.86	16.50	16.49	16.52	16.52	16.50	18.88	18.88	18.88	18.87	16.51	2.37
0	6	18.71	18.71	18.71	14.65	14.61	14.58	14.59	14.63	18.71	18.72	18.72	18.72	14.61	4.11
0	8	18.52	18.52	18.53	13.09	13.08	13.06	13.09	13.07	18.53	18.54	18.54	18.53	13.08	5.45
0	10	18.35	18.35	18.35	12.19	12.20	12.18	12.20	12.18	18.37	18.37	18.38	18.36	12.19	6.17
0	6	18.72	18.72	18.72	14.59	14.57	14.56	14.55	14.55	18.75	18.75	18.75	18.72	14.56	4.16
0	2	19.06	19.06	19.06	18.31	18.29	18.30	18.31	18.32	19.06	19.06	19.06	19.05	18.31	.74
0	0	19.29	19.29	19.29	19.85	19.85	19.86	19.83	19.82	19.30	19.30	19.30	19.29	19.84	-.55
1	0	19.27	19.27	19.27	19.44	19.45	19.46	19.48	19.48	19.25	19.26	19.26	19.26	19.46	-.20
2	0	19.28	19.27	19.27	19.19	19.19	19.19	19.21	19.22	19.24	19.25	19.26	19.26	19.20	.06
3	0	19.27	19.27	19.27	18.92	18.92	18.91	18.91	18.92	19.23	19.24	19.25	19.26	18.92	.34
4	0	19.28	19.28	19.28	18.63	18.64	18.63	18.63	18.64	19.31	19.31	19.32	19.29	18.63	.66
4	-6	20.06	20.06	20.06	22.07	22.07	22.03	22.04	22.03	20.08	20.08	20.08	20.07	22.05	-1.98
4	-4	19.72	19.72	19.73	20.92	20.93	20.93	20.93	20.94	19.74	19.74	19.75	19.73	20.93	-1.20
4	-2	19.33	19.33	19.33	19.79	19.79	19.79	19.79	19.80	19.48	19.48	19.48	19.41	19.79	-.38
4	0	19.28	19.27	19.27	18.70	18.70	18.70	18.71	18.71	19.30	19.30	19.29	19.29	18.70	.59
4	2	19.02	19.02	19.03	17.43	17.45	17.47	17.45	17.45	19.05	19.05	19.05	19.04	17.45	1.59
4	4	18.84	18.84	18.84	16.11	16.12	16.11	16.14	16.13	18.86	18.86	18.87	18.85	16.12	2.73
4	6	18.59	18.59	18.59	14.46	14.46	14.48	14.46	14.44	18.72	18.73	18.72	18.66	14.46	4.20
4	8	18.38	18.38	18.38	12.68	12.71	12.72	12.67	12.68	18.53	18.54	18.54	18.46	12.69	5.77
4	10	18.34	18.34	18.34	11.74	11.79	11.77	11.78	11.77	18.36	18.37	18.37	18.35	11.77	6.58
4	0	19.26	19.27	19.27	18.60	18.59	18.59	18.58	18.60	19.30	19.30	19.30	19.29	18.59	.70
4	6				14.43	14.41	14.40	14.40	14.38				18.66	14.40	4.26
4	2				17.44	17.42	17.41	17.44	17.42				19.04	14.43	4.61
5	0	19.27	19.26	19.26	18.36	18.37	18.37	18.38	18.38	19.21	19.23	19.24	19.25	18.37	.88
6	0	19.25	19.24	19.25	18.06	18.05	18.05	18.05	18.04	19.20	19.22	19.22	19.23	18.05	1.18
7	0	19.25	19.25	19.25	17.74	17.74	17.73	17.73	17.75	19.19	19.22	19.23	19.23	17.74	1.49
8	0	19.26	19.25	19.25	17.47	17.50	17.48	17.47	17.47	19.19	19.22	19.22	19.25	17.48	1.77
8	0	19.24	19.24	19.24	17.49	17.47	17.47	17.46	17.46	19.21	19.21	19.21	19.25	17.47	1.74
8	-6	20.08	20.08	20.08	20.56	20.56	20.57	20.56	20.57	20.05	20.06	20.06	20.07	20.56	-.49
8	-4	19.74	19.75	19.75	19.54	19.55	19.55	19.55	19.56	19.76	19.76	19.76	19.75	19.55	.20
8	-2	19.46	19.46	19.46	18.51	18.52	18.51	18.51	18.52	19.48	19.49	19.49	19.47	18.51	.96
8	0	19.27	19.28	19.28	17.49	17.50	17.49	17.49	17.51	19.26	19.27	19.27	19.25	17.50	1.75
8	2	19.05	19.05	19.05	16.47	16.47	16.44	16.50	16.47	19.03	19.04	19.05	19.05	16.47	2.58
8	4	18.83	18.83	18.84	15.34	15.33	15.35	15.34	15.37	18.84	18.85	18.85	18.84	15.35	3.49
8	6	18.21	18.22	18.22	14.10	14.10	14.09	14.06	14.06	18.68	18.69	18.69	18.70	14.08	4.62
8	8	18.52	18.53	18.52	12.46	12.43	12.42	12.45	12.47	18.45	18.45	18.45	18.49	12.44	6.04
8	10	18.35	18.37	18.37	11.35	11.35	11.33	11.32	11.35	18.36	18.36	18.35	18.36	11.34	7.02
8	6	18.69	18.70	18.70	14.14	14.12	14.12	14.16	14.15	18.69	18.71	18.70	18.70	14.14	4.56
8	2	19.06	19.06	19.06	16.44	16.44	16.46	16.45	16.47	19.05	19.05	19.06	19.05	16.45	2.60
8	0	19.27	19.27	19.27	17.45	17.46	17.46	17.45	17.45	19.19	19.22	19.22	19.24	17.19	2.05
9	0	19.27	19.27	19.27	17.19	17.19	17.19	17.19	17.18	19.19	19.21	19.22	19.23	16.85	2.38
10	0	19.25	19.24	19.24	16.84	16.86	16.85	16.85	16.84	19.17	19.21	19.21	19.22	16.16	3.06
11	0	19.25	19.25	19.25	15.96	16.02	16.05	16.23	16.53	19.19	19.21	19.21	19.23	15.83	3.40
12	0	19.27	19.26	19.26	15.68	15.72	15.75	15.71	16.28	19.17	19.20	19.21	19.22	15.37	3.85
13	0	19.25	19.25	19.25	15.37	15.36	15.36	15.34	15.42						

TABLE Xc

Raw Drag Data for Model with E = .5

Avg. Temp.	Avg. Press.	n	α	Before-Static Readings			Wind-on Readings					After-Static Readings			Static Average	Wind-on Average	Drag Force
69.5	29.359	0	0	21.43	21.42	21.40	17.81	17.82	17.81	17.80	17.30	21.50	21.49	21.49	21.44	17.31	3.63
69.5	29.359	0	-6	21.20	21.20	21.20	17.36	17.37	17.40	17.40	17.39	21.30	21.29	21.27	21.24	17.38	3.86
69.5	29.359	0	-4	21.27	21.26	21.25	17.62	17.61	17.62	17.61	17.62	21.33	21.33	21.33	21.30	17.62	3.68
69.5	29.359	0	-2	21.32	21.30	21.31	17.72	17.71	17.71	17.70	17.71	21.36	21.37	21.35	21.34	17.71	3.63
69.5	29.359	0	0	21.38	21.38	21.38	17.79	17.79	17.79	17.79	17.78	21.45	21.45	21.45	21.44	17.79	3.65
69.5	29.359	0	2	21.45	21.45	21.46	17.74	17.74	17.74	17.75	17.74	21.50	21.50	21.51	21.50	17.74	3.76
69.5	29.359	0	4	21.51	21.50	21.50	17.74	17.73	17.73	17.71	17.71	21.57	21.59	21.59	21.54	17.72	3.82
69.5	29.359	0	6	21.54	21.55	21.55	17.58	17.56	17.55	17.56	17.56	21.62	21.63	21.63	21.60	17.56	4.04
69.5	29.359	0	8	21.58	21.60	21.61	17.41	17.39	17.39	17.40	17.38	21.63	21.63	21.63	21.61	17.39	4.22
69.5	29.359	0	10	21.64	21.64	21.65	16.97	16.98	16.98	16.98	16.98	21.71	21.71	21.70	21.68	16.98	4.70
69.5	29.359	0	6	21.58	21.60	21.58	17.65	17.65	17.66	17.65	17.66	21.62	21.63	21.64	21.60	17.65	3.95
69.5	29.359	0	2	21.48	21.41	21.49	17.93	17.93	17.93	17.93	17.94	21.55	21.55	21.56	21.50	17.93	3.57
69.5	29.359	0	0	21.42	21.42	21.42	17.88	17.89	17.88	17.88	17.88	21.49	21.48	21.48	21.44	17.88	3.56
72.5	29.331	1	0	21.42	21.42	21.42	17.57	17.59	17.60			21.49	21.49	21.50	21.46	17.58	3.33
72.5	29.331	2	0	21.45	21.45	21.45	17.66	17.62	17.66	17.66	17.67	21.49	21.48	21.48	21.47	17.66	3.31
72.5	29.331	3	0	21.48	21.48	21.48	17.57	17.58	17.61	17.61	17.60	21.50	21.48	21.47	21.48	17.59	3.39
66.3	29.399	4	0	21.47	21.47	21.48	17.60	17.58	17.60	17.60	17.62				21.47	17.60	3.87
66.3	29.399	4	-6	21.26	21.24	21.24	17.48	17.48	17.49	17.49	17.48	21.27	21.24	21.24	21.25	17.48	3.77
66.3	29.399	4	-4	21.32	21.32	21.33	17.56	17.56	17.55	17.56	17.56	21.31	21.32	21.31	21.32	17.56	3.76
66.3	29.399	4	-2	21.50	21.52	21.52	17.61	17.61	17.61	17.61	17.62	21.38	21.38	21.38	21.45	17.61	3.84
66.3	29.399	4	0	21.42	21.41	21.42	17.62	17.61	17.61	17.61	17.61	21.43	21.42	21.42	21.47	17.61	3.86
66.3	29.399	4	2	21.49	21.50	21.49	17.55	17.57	17.57	17.57	17.57	21.48	21.48	21.47	21.49	17.57	3.92
66.3	29.399	4	4	21.55	21.56	21.55	17.44	17.43	17.43	17.45	17.45	21.54	21.53	21.53	21.54	17.44	4.10
66.3	29.399	4	6	21.71	21.75	21.73	17.12	17.12	17.12	17.11	17.12	21.57	21.57	21.52	21.65	17.12	4.53
66.3	29.399	4	8	22.08	22.08	22.07	16.94	16.94	16.93	16.92	16.91	21.64	21.64	21.64	21.86	16.93	4.93
66.3	29.399	4	10	21.90	21.87	21.86	16.55	16.57	16.56	16.58	16.56	21.68	21.68	21.68	21.78	16.56	5.22
66.3	29.399	4	0	21.57	21.54	21.52	17.74	17.74	17.73	17.73	17.74	21.51	21.48	21.48	21.47	17.74	3.73
66.3	29.399	4	6				17.29	17.28	17.28	17.28	17.27				21.65	17.28	4.37
66.3	29.399	4	2				17.74	17.72	17.73	17.71	17.72				21.49	17.72	3.77
67.0	29.395	5	0	21.44	21.44	21.44	17.51	17.54	17.53	17.52	17.54	21.46	21.48	21.49	21.46	17.53	3.93
67.0	29.395	6	0	21.55	21.52	21.52	17.42	17.44	17.45	17.46	17.45	21.52	21.50	21.50	21.52	17.44	4.08
67.0	29.395	7	0	21.45	21.46	21.44	17.62	17.62	17.61	17.60	17.61	21.40	21.43	21.45	21.44	17.61	3.83
67.0	29.395	8	0	21.48	21.48	21.49	17.31	17.33	17.34	17.33	17.34	21.55	21.52	21.53	21.46	17.33	4.13
67.0	29.395	8	0	21.41	21.41	21.43	17.30	17.33	17.33	17.32	17.33	21.55	21.51	21.51	21.46	17.32	4.14
67.0	29.395	8	-6	21.18	21.20	21.19	17.38	17.38	17.39	17.39	17.39	21.25	21.23	21.23	21.21	17.39	3.82
67.0	29.395	8	-4	21.27	21.27	21.26	17.41	17.40	17.39	17.40	17.39	21.29	21.29	21.29	21.28	17.40	3.88
67.0	29.395	8	-2	21.32	21.32	21.32	17.41	17.41	17.41	17.42	17.41	21.33	21.32	21.30	21.32	17.41	3.91
67.0	29.395	8	0	21.38	21.38	21.38	17.35	17.33	17.34	17.34	17.35	21.44	21.44	21.43	21.46	17.34	4.12
67.0	29.395	8	2	21.43	21.43	21.43	17.12	17.15	17.13	17.16	17.14	21.49	21.49	21.50	21.46	17.14	4.32
67.0	29.395	8	4	21.51	21.52	21.52	16.98	16.96	16.95	16.96	16.98	21.56	21.56	21.55	21.54	16.96	4.53
67.0	29.395	8	6	21.49	21.50	21.49	16.73	16.73	16.73	16.74	16.73	21.59	21.59	21.60	21.54	16.73	4.31
67.0	29.395	8	8	21.57	21.57	21.57	16.21	16.20	16.20	16.21	16.24	21.90	21.88	21.86	21.68	16.21	5.47
67.0	29.395	8	10	21.64	21.65	21.64	15.72	15.76	15.78	15.76	15.79	21.80	21.78	21.77	21.71	15.77	5.94
67.0	29.395	8	6	21.56	21.57	21.56	16.87	16.86	16.84	16.87	16.87	21.75	21.73	21.75	21.65	16.36	4.39
67.0	29.395	8	2	21.48	21.47	21.47	17.36	17.35	17.38	17.35	17.37	21.59	21.59	21.59	21.53	17.36	4.17
67.0	29.395	8	0	21.41	21.41	21.41	17.54	17.55	17.57	17.56	17.55	21.52	21.51	21.51	21.46	17.55	3.91
72.5	29.331	9	0	21.42	21.42	21.42	17.22	17.21	17.24	17.23	17.22	21.50	21.49	21.49	21.46	17.22	4.24
72.5	29.331	10	0	21.40	21.40	21.40	17.08	17.10	17.10	17.10	17.10	21.47	21.46	21.48	21.44	17.10	4.34
72.5	29.331	11	0	21.47	21.47	21.47	16.94	16.94	16.96	17.00	17.04	21.48	21.46	21.47	21.47	16.98	4.49
72.5	29.331	12	0	21.44	21.44	21.44	16.72	16.74	16.75	16.74	16.86	21.44	21.44	21.44	21.44	16.76	4.68
72.5	29.331	13	0	21.44	21.44	21.43	16.55	16.56	16.55	16.56	16.55	21.48	21.49	21.49	21.46	16.56	4.90

TABLE XIa

Raw Front Lift Data for Model with E = .6

Flap Setting	Angle of Attack	Before-Static Readings			Wind-on Readings					After-Static Readings			Static Average	Wind-on Average	Front Lift Force
0	0	40.00	40.00	40.02	35.07	35.08	35.04	35.08	35.04				40.01	35.06	4.95
0	-6	39.10	39.13	39.12	44.86	44.85	44.85	44.84	44.82				39.12	44.84	-5.72
0	-4	39.53	39.53	39.54	41.78	41.78	41.76	41.76	41.80				39.53	41.78	-2.25
0	-2	39.24	39.25	39.25	38.45	38.45	38.46	38.45	38.45				39.25	38.45	1.30
0	0	39.98	39.99	39.99	35.09	35.08	35.07	35.12	35.10				40.01	35.09	4.92
0	2	40.16	40.17	40.17	31.24	31.20	31.22	31.29	31.69				40.17	31.73	8.44
0	4	40.34	40.35	40.35	28.32	28.29	28.28	28.33	28.33				40.35	28.31	12.04
0	6	40.50	40.50	40.50	25.04	24.75	24.65	24.72	24.72				40.50	24.78	15.72
0	8	40.67	40.69	40.68	21.26	21.36	21.29	21.26	21.25				40.68	21.28	19.40
0	10	40.81	40.82	40.82	19.01	18.96	19.00	18.95	19.10				40.82	19.00	21.82
0	0	40.02	40.02	40.02											
0	10				19.08	19.15	19.27	19.21	19.32				40.82	19.21	21.61
0	6				24.70	24.85	24.71	24.76	24.81				40.50	24.77	15.73
0	2				31.59	31.64	31.65	31.80	31.72				40.17	31.68	8.49
0	0				35.19	35.15	35.16	35.15	35.12	40.00	40.01	40.04	40.01	35.15	4.86
1	0	39.96	39.96	39.98	33.54	33.50	33.53	33.53	33.59	39.99	40.01	40.03	39.99	33.54	6.45
2	0	40.01	40.01	40.01	32.20	32.23	32.22	32.18	32.18	39.93	39.99	40.02	39.99	32.20	7.79
3	0	40.00	40.01	40.00	30.63	30.60	30.64	30.70	30.65	39.91	39.97	40.00	39.98	30.64	9.34
4	0	40.05	40.05	40.06											
4	0	40.05	40.05	40.08											
4	0	40.05	40.05	40.05	29.41	29.45	29.44	29.35	29.38	40.06	40.07	40.10	40.03	29.41	10.62
4	-6	39.32	39.32	39.32	39.17	39.20	39.20	39.23	39.20	39.35	39.36	39.37	39.34	39.20	.14
4	-4	39.53	39.55	39.54	36.08	36.06	36.10	36.05	36.01	39.58	39.60	39.59	39.57	36.06	3.51
4	-2	39.72	39.74	39.73	32.76	32.79	32.79	32.79	32.82	39.74	39.75	39.74	39.74	32.79	6.95
4	0	39.96	39.98	39.99	29.44	29.46	29.49	29.50	29.50	39.96	39.97	39.98	40.03	29.48	10.55
4	2	40.15	40.15	40.16	26.25	26.18	26.25	26.27	26.21	40.15	40.15	40.15	40.15	26.23	13.92
4	4	40.34	40.35	40.35	22.85	22.83	22.98	22.96	22.92	40.34	40.34	40.35	40.35	22.91	17.44
4	6	40.50	40.50	40.51	19.89	19.90	18.83	19.80	19.49	40.50	40.51	40.50	40.50	19.78	20.72
4	8	40.67	40.68	40.69	17.38	17.34	17.05	17.22	17.18	40.66	40.68	40.68	40.68	17.23	23.45
4	10	40.84	40.85	40.85	16.20	16.21	16.39	16.20	16.34	40.85	40.85	40.85	40.85	16.26	24.59
4	0	40.00	40.01	40.02	29.25	29.22	29.28	29.30	29.25	40.02	40.03	40.04	40.03	29.26	10.77
5	0	40.06	40.07	40.07	27.90	27.92	28.00	27.90	27.89	39.69	39.74	39.78	39.90	27.92	11.98
6	0	40.02	40.04	40.03	26.28	26.28	26.25	26.33	26.30	40.02	40.09	40.08	40.05	26.29	13.76
7	0	40.07	40.08	40.06	25.04	24.99	25.04	25.02	25.06	39.78	39.88	39.92	39.97	25.03	14.94
8	0	40.02	40.04	40.03	23.92	23.85	23.85	23.75	23.75	40.07	40.08	40.08	40.04	23.82	16.22
8	-6	39.31	39.31	39.33	33.55	33.55	33.58	33.59	33.61	39.36	39.36	39.38	39.34	33.58	5.76
8	-4	39.58	39.58	39.59	30.29	30.27	30.31	30.23	30.30	39.60	39.60	39.60	39.59	30.28	9.31
8	-2	39.76	39.77	39.80	27.22	27.20	27.13	27.12	27.15	39.80	39.82	39.82	39.80	27.16	12.64
8	0	39.98	40.00	40.00	23.88	23.89	23.81	23.70	23.78	40.03	40.03	40.04	40.04	23.81	16.23
8	2	40.18	40.19	40.20	20.16	20.39	20.28	20.15	20.13	40.22	40.21	40.22	40.20	20.22	19.98
8	4	40.36	40.39	40.37	16.94	16.74	17.12	16.96	16.93	40.38	40.37	40.40	40.38	16.94	23.44
8	6	40.52	40.53	40.53	14.35	14.74	14.41	14.60	14.52	40.55	40.55	40.55	40.54	14.52	26.02
8	8	40.70	40.70	40.70	14.45	14.44	14.50	14.23	14.21	40.70	40.72	40.72	40.71	14.37	26.34
8	10	40.85	40.87	40.86	15.67	16.10	15.93	15.60	16.02	40.86	40.85	40.85	40.86	15.86	25.00
8	0	40.03	40.05	40.05	23.70	23.58	23.59	23.72	23.72	40.03	40.03	40.04	40.04	23.66	16.38
9	0	40.06	40.06	40.06	22.19	22.16	22.21	22.26	22.20	39.60	39.74	39.94	39.91	22.20	17.71
10	0	39.98	40.00	40.00	21.06	20.94	20.85	20.96	20.86	39.59	39.70	39.85	39.85	20.93	18.92
11	0	40.09	40.07	40.09	19.46	19.49	19.53	19.45	19.52	39.90	39.95	39.96	40.01	19.49	20.52
12	0	40.01	40.03	40.03	18.21	18.10	18.02	17.97	17.94	39.79	39.86	39.90	39.94	18.05	21.89
13	0	40.06	40.06	40.06	16.98	16.88	16.89	16.80	16.85	39.92	39.97	39.98	40.01	16.88	23.13
15	0	40.10	40.11	40.12	14.75	14.70	14.77	14.79	14.78	39.97	40.01	40.03	40.06	14.76	25.30
16	0	40.06	40.07	40.08	14.07	14.05	13.97	14.02	14.01	39.80	39.91	39.95	39.98	14.02	25.96
17	0	40.08	40.08	40.08	12.84	12.80	12.35	12.50	12.42	40.09	40.11	40.11	40.09	12.58	27.51

TABLE XIb

Raw Rear Lift Data for Model with E = .6

Flap Setting	Angle of Attack	Before-Static Readings			Wind-on Readings					After-Static Readings			Static Average	Wind-on Average	Rear Lift Force
0	0	19.28	19.27	19.27	18.78	18.77	18.77	18.78	18.78				19.26	18.78	.48
0	-6	20.23	20.24	20.24	22.78	22.78	22.78	22.78	22.76				20.24	22.78	-2.54
0	-4	19.75	19.75	19.75	21.58	21.59	21.59	21.58	21.60				19.75	21.59	-1.84
0	-2	19.50	19.50	19.49	20.23	20.25	20.26	20.24	20.25				19.50	20.25	-.75
0	0	19.29	19.28	19.28	18.77	18.78	18.77	18.80	18.78				19.26	18.78	.48
0	2	19.05	19.06	19.07	16.98	16.99	16.99	17.04	16.96				19.06	16.99	3.07
0	4	18.91	18.91	18.90	14.96	14.98	14.91	14.98	14.97				18.91	14.96	3.95
0	6	18.74	18.74	18.74	13.24	13.14	13.09	13.12	13.12				18.74	13.14	5.60
0	8	18.56	18.56	18.56	11.82	11.86	11.84	11.84	11.82				18.56	11.34	6.72
0	10	18.39	18.39	18.39	11.10	11.10	11.13	11.10	11.15				18.39	11.12	7.27
0	10				11.10	11.19	11.18	11.18	11.22				18.39	11.18	7.21
0	6				13.15	13.06	13.16	13.20	13.12				18.74	13.14	5.60
0	2				17.03	17.01	17.00	17.05	17.04				19.06	17.03	2.03
0	0	19.25	19.24	19.25	18.89	18.87	18.88	18.86	18.86	19.25	19.25	19.25	19.26	18.87	.39
1	0	19.30	19.28	19.28	18.55	18.53	18.55	18.55	18.52	19.24	19.26	19.26	19.27	18.55	.72
2	0	19.49	19.31	19.29	18.36	18.38	18.37	18.35	18.34	19.21	19.25	19.26	19.30	18.36	.94
3	0	19.26	19.28	19.28	18.14	18.11	18.12	18.16	18.11	19.21	19.24	19.25	19.25	18.13	1.12
4	0	19.31	19.29	19.28											
4	0	19.28	19.28	19.28											
4	0	19.28	19.28	19.28	18.01	18.02	18.02	17.98	17.99	19.25	19.26	19.26	19.29	18.00	1.29
4	-6	20.04	20.05	20.05	21.63	21.63	21.64	21.62	21.62	20.07	20.07	20.05	20.06	21.63	-1.57
4	-4	19.79	19.75	19.78	20.45	20.45	20.45	20.46	20.47	19.75	19.75	19.77	19.77	20.46	-.69
4	-2	19.52	19.52	19.52	19.24	19.25	19.25	19.26	19.26	19.51	19.50	19.50	19.51	19.25	.26
4	0	19.31	19.31	19.31	17.94	17.95	17.95	17.96	17.97	19.29	19.30	19.30	19.29	17.95	1.34
4	2	19.08	19.08	19.08	16.59	16.55	16.60	16.59	16.58	19.07	19.07	19.08	19.08	16.58	2.50
4	4	18.89	18.89	18.89	14.79	14.78	14.82	14.87	14.83	18.89	18.89	18.89	18.89	14.82	4.07
4	6	18.74	18.73	18.73	12.95	12.99	12.89	12.89	12.80	18.73	18.73	18.73	18.73	12.90	5.83
4	8	18.56	18.55	18.55	11.39	11.41	11.30	11.37	11.34	18.55	18.55	18.55	18.55	11.36	7.19
4	10	18.39	18.39	18.39	10.56	10.55	10.60	10.54	10.60	18.39	18.39	18.39	18.39	11.57	6.32
4	0	19.31	19.31	19.31	12.93	12.94	12.93	12.95	12.95	19.27	19.27	19.29	19.29	12.94	1.35
5	0	19.48	19.29	19.27	12.65	12.64	12.66	12.64	12.64	19.18	19.20	19.21	19.27	12.65	1.62
6	0	19.26	19.26	19.26	17.36	17.35	17.33	17.35	17.34	19.19	19.23	19.24	19.24	17.35	1.89
7	0	18.97	19.23	19.28	17.10	17.07	17.08	17.08	17.08	19.13	19.19	19.20	19.17	17.08	2.09
8	0	19.28	19.27	19.27	16.93	16.91	16.91	16.89	16.88	19.28	19.29	19.28	19.29	16.90	2.39
8	-6	20.05	20.05	20.05	20.27	20.27	20.27	20.27	20.28	20.05	20.05	20.05	20.05	20.27	-.22
8	-4	19.73	19.73	19.73	19.12	19.13	19.14	19.13	19.13	19.78	19.80	19.79	19.76	19.13	.63
8	-2	19.48	19.49	19.50	18.08	18.06	18.06	18.06	18.06	19.51	19.51	19.51	19.50	18.06	1.44
8	0	19.30	19.30	19.29	16.94	16.96	16.94	16.91	16.92	19.29	19.30	19.30	19.29	16.93	2.36
8	22	19.06	19.04	19.06	15.62	15.65	15.63	15.61	15.59	19.05	19.05	19.06	19.05	15.62	3.43
8	4	18.86	18.86	18.86	14.17	14.12	14.23	14.18	14.14	18.89	18.89	18.89	18.88	14.17	4.71
8	6	18.72	18.72	18.72	12.43	12.54	12.44	12.51	12.47	18.71	18.70	18.70	18.71	12.48	6.23
8	8	18.54	18.54	18.53	10.85	10.35	10.85	10.77	10.76	18.53	13.52	18.52	18.53	10.32	7.71
8	10	18.39	18.39	18.38	10.12	10.14	10.09	10.08	10.16	18.36	18.36	18.37	18.38	10.12	8.26
8	0	19.29	19.29	19.29	16.99	16.92	16.95	16.98	16.97	19.29	19.30	19.29	19.29	16.96	2.33
9	0	19.29	19.29	19.29	16.57	16.58	16.58	16.59	16.57	19.09	19.15	19.20	19.21	16.58	2.64
10	0	19.27	19.28	19.28	16.34	16.31	16.28	16.30	16.28	19.19	13.16	19.20	19.22	16.30	2.92
11	0	19.32	19.31	19.31	16.06	16.04	16.06	16.04	16.05	19.16	19.21	19.22	19.26	16.05	3.21
12	0	19.26	19.26	19.26	15.78	15.76	15.74	15.72	15.73	19.16	19.20	19.22	19.23	15.75	3.48
13	0	19.25	19.25	19.26	15.54	15.52	15.53	15.51	15.52	19.19	19.22	19.23	19.23	15.52	3.71
15	0	19.26	19.26	19.26	14.74	14.71	14.72	14.74	14.36	19.17	19.19	19.20	19.22	14.65	4.57
16	0	19.26	19.27	19.26	14.96	14.96	14.94	14.96	14.96	19.11	19.16	19.19	19.22	14.96	4.26
17	0	19.26	19.25	19.25	14.36	14.37	14.34	14.29	14.25	19.21	19.23	19.23	19.24	14.32	4.92

TABLE XIc

Raw Drag Data for Model with E = .6

Avg. Temp.	Avg. Press.	n	α	Before-Static Readings			Wind-on Readings					After-Static Readings			Static Average	Wind-on Average	Drag Force
77.0	29.344	0	0	21.43	21.40	21.43	17.63	17.65	17.67	17.67	17.66				21.40	17.65	3.74
77.0	29.344	0	-6	20.99	20.97	20.94	17.31	17.34	17.36	17.37	17.38				20.97	17.35	3.62
77.0	29.344	0	-4	21.12	21.16	21.16	17.51	17.53	17.54	17.55	17.54				21.15	17.53	3.62
77.0	29.344	0	-2	21.12	21.21	21.22	17.74	17.72	17.69	17.69	17.69				21.21	17.71	3.50
77.0	29.344	0	0	21.28	21.30	21.29	17.74	17.72	17.73	17.74	17.74				21.40	17.73	3.67
77.0	29.344	0	2	21.37	21.38	21.37	17.64	17.64	17.65	17.65	17.66				21.37	17.65	3.72
77.0	29.344	0	4	21.41	21.42	21.40	17.53	17.52	17.52	17.54	17.55				21.41	17.53	3.88
77.0	29.344	0	6	21.45	21.48	21.49	17.32	17.33	17.31	17.29	17.30				21.47	17.31	4.16
77.0	29.344	0	8	21.53	21.54	21.55	16.91	16.96	16.96	16.97	16.95				21.54	16.35	4.29
77.0	29.344	0	10	21.71	21.68	21.68	16.80	16.80	16.81	16.82	16.81				21.69	16.51	4.33
77.0	29.344	0	0	21.44	21.41	21.41									21.69	16.81	4.33
77.0	29.344	0	10				16.81	16.82	16.81	16.79	16.79				21.47	17.24	4.13
77.0	29.344	0	6				17.20	17.25	17.22	17.32	17.22				21.37	17.23	4.02
77.0	29.344	0	2				17.49	17.52	17.53	17.58	17.61				21.40	17.73	3.85
77.0	29.344	0	-2				17.28	17.25	17.25	17.24	17.24	21.48	21.44	21.43	21.41	17.58	3.85
77.0	29.344	0	-4				17.55	17.59	17.59	17.59	17.59	21.44	21.41	21.41	21.41	17.66	3.73
79.9	29.284	1	0	21.39	21.39	21.40	17.67	17.66	17.66	17.66	17.66	21.39	21.40	21.42	21.39	17.42	3.97
79.9	29.284	2	0	21.36	21.38	21.39	17.39	17.41	17.42	17.45	17.43	21.35	21.35	21.37	21.39		
79.9	29.284	3	0	21.42	21.41	21.41											
79.9	29.284	4	0	21.54	21.50	21.50											
79.9	29.284	4	0	21.48	21.49	21.52											
79.9	29.284	4	0	21.49	21.50	21.49	17.35	17.38	17.39	17.38	17.38	21.50	21.48	21.46	21.43	17.38	4.05
79.9	29.284	4	-6	21.05	21.06	21.07	17.36	17.35	17.35	17.34	17.36	21.25	21.22	21.20	21.20	17.35	3.85
79.9	29.284	4	-4	21.13	21.11	21.12	17.42	17.43	17.43	17.44	17.43	21.25	21.25	21.27	21.27	17.43	3.84
79.9	29.284	4	-2	21.17	21.18	21.16	17.46	17.47	17.46	17.45	17.48	21.28	21.28	21.27	21.27	17.46	3.81
79.9	29.284	4	0	21.25	21.28	21.29	17.47	17.46	17.46	17.50	17.48	21.35	21.35	21.36	21.43	17.47	3.95
79.9	29.284	4	2	21.33	21.35	21.36	17.38	17.36	17.37	17.36	17.37	21.41	21.41	21.43	21.38	17.37	4.01
79.9	29.284	4	4	21.40	21.43	21.43	17.21	17.17	17.19	17.19	17.19	21.47	21.48	21.52	21.46	17.19	4.27
79.9	29.284	4	6	21.45	21.45	21.42	16.79	16.81	16.80	16.81	16.79	21.51	21.52	21.55	21.48	16.80	4.03
79.9	29.284	4	8	21.51	21.52	21.53	16.39	16.41	16.36	16.37	16.36	21.59	21.58	21.59	21.55	16.38	2.17
79.9	29.284	4	10	21.57	21.56	21.58	16.20	16.17	16.20	16.16	16.18	21.63	21.66	21.65	21.61	16.18	5.43
79.9	29.284	4	0	21.37	21.35	21.34	17.53	17.53	17.55	17.54	17.54	21.46	21.44	21.43	21.43	17.54	3.89
79.9	29.284	4	0	21.41	21.40	21.42	17.30	17.31	17.34	17.34	17.33	21.34	21.33	21.35	21.38	17.32	4.06
79.9	29.284	5	0	21.49	21.46	21.46	17.16	17.20	17.20	17.21	17.20	21.46	21.44	21.44	21.46	17.19	4.27
79.9	29.284	6	0	21.42	21.44	21.42	17.15	17.15	17.17	17.16	17.16	21.39	21.39	21.39	21.41	17.16	4.25
79.9	29.284	7	0	21.42	21.42	21.41	17.07	17.08	17.07	17.05	17.05	21.49	21.46	21.46	21.42	17.06	4.36
79.9	29.284	8	0	21.22	21.21	21.20	17.42	17.41	17.42	17.41	17.42	21.26	21.24	21.22	21.23	17.42	3.81
79.9	29.284	8	-6	21.24	21.23	21.25	17.40	17.40	17.41	17.39	17.40	21.26	21.26	21.27	21.25	17.40	3.85
79.9	29.284	8	-4	21.29	21.29	21.29	17.17	17.18	17.18	17.18	17.21	21.31	21.26	21.28	21.29	17.18	4.11
79.9	29.284	8	-2	21.35	21.32	21.33	17.02	17.04	17.04	17.02	17.03	21.38	21.40	21.41	21.42	17.03	4.39
79.9	29.284	8	0	21.41	21.41	21.41	16.74	16.78	16.76	16.74	16.73	21.45	21.45	21.46	21.43	16.75	4.68
79.9	29.284	8	2	21.48	21.47	21.47	16.43	16.41	16.42	16.46	16.45	21.50	21.52	21.51	21.50	16.44	5.05
79.9	29.284	8	4	21.52	21.53	21.55	16.16	16.18	16.16	16.18	16.14	21.53	21.52	21.53	21.53	16.16	5.37
79.9	29.284	8	6	21.59	21.59	21.59	15.52	15.58	15.51	15.48	15.51	21.60	21.60	21.61	21.60	15.51	6.09
79.9	29.284	8	8	21.64	21.65	21.66	14.79	14.80	14.76	14.82	14.84	21.65	21.66	21.66	21.65	14.80	6.85
79.9	29.284	8	10	21.45	21.43	21.43	17.23	17.21	17.21	17.24	17.23	21.45	21.44	21.42	21.42	17.22	4.20
79.9	29.284	8	0	21.43	21.42	21.44	16.84	16.86	16.90	16.87	16.87	21.34	21.34	21.35	21.39	16.87	4.52
81.4	29.270	9	0	21.36	21.35	21.36	16.78	16.79	16.78	16.80	16.80	21.22	21.24	21.25	21.30	16.79	4.51
80.0	29.181	10	0	21.34	21.34	21.33	16.57	16.61	16.62	16.63	16.64	21.37	21.38	21.38	21.36	16.61	4.75
80.0	29.181	11	0	21.37	21.38	21.38	16.47	16.47	16.47	16.46	16.46	21.32	21.31	21.31	21.35	16.47	4.88
80.0	29.181	12	0	21.38	21.36	21.38	16.25	16.25	16.26	16.24	16.25	21.35	21.35	21.34	21.36	16.25	5.11
80.0	29.181	13	0	21.40	21.39	21.42	15.98	15.98	15.97	15.99	15.91	21.42	21.40	21.40	21.41	15.97	5.44
80.0	29.181	15	0	21.35	21.36	21.35	16.21	16.19	16.17	16.15	16.17	21.29	21.34	21.36	21.34	16.18	5.16
80.0	29.181	16	0	21.39	21.45	21.40	15.52	15.54	15.46	15.51	15.46	21.46	21.42	21.41	21.42	15.50	5.32
80.0	29.181	17	0														

TABLE XIIa

Raw Front Lift Data for Model with E = .7

Flap Setting	Angle of Attack	Before-Static Readings			Wind-on Readings					After-Static Readings			Static Average	Wind-on Average	Front Lift Force
0	0	39.87	39.88	39.88	35.20	35.25	35.24	35.18	35.22	40.01	40.05	40.04	39.38	35.22	4.66
0	-6	39.12	39.12	39.13	44.66	44.65	44.69	44.65	44.65	39.17	39.18	39.19	39.15	44.66	-5.51
0	-4	39.38	39.38	39.39	41.62	41.63	41.62	41.64	41.63	39.42	39.44	39.44	39.41	41.63	-2.22
0	-2	39.58	39.60	39.60	38.32	38.36	38.33	38.31	38.33	39.64	39.65	39.65	39.62	38.33	1.29
0	0	39.81	39.81	39.82	35.14	35.15	35.11	35.12	35.15	39.83	39.84	39.83	39.88	35.13	4.75
0	2	40.01	40.01	40.02	31.82	31.82	31.83	31.79	31.83	40.03	40.04	40.03	40.02	31.82	8.20
0	4	40.21	40.22	40.22	28.39	28.41	28.35	28.37	28.35	40.21	40.22	40.22	40.22	28.37	11.35
0	6	40.38	40.38	40.39	25.18	25.24	25.20	25.21	25.18	40.36	40.37	40.37	40.38	25.20	15.19
0	8	40.54	40.54	40.54	21.93	22.01	21.98	21.97	22.00	40.51	40.54	40.55	40.54	21.98	18.56
0	10	40.66	40.67	40.68	19.47	19.56	19.45	19.42	19.60	40.72	40.70	40.73	40.69	19.50	21.19
0	0	39.84	39.86	39.86	35.16	35.16	35.13	35.14	35.13	39.85	39.85	39.86	39.88	35.14	4.74
1	0	39.88	39.87	39.88	33.51	33.55	33.53	33.50	33.50	39.85	39.87	39.87	39.87	33.52	6.35
2	0	39.88	39.90	39.90	31.97	31.95	31.94	31.95	31.91	39.90	39.92	39.92	39.90	31.94	7.96
3	0	39.89	39.90	39.91	30.46	30.40	30.41	30.40	30.40				39.89	30.41	9.48
3	0				30.45	30.42	30.46	30.45	30.49	39.85	39.88	39.90	39.89	30.45	9.44
4	0	39.90	39.90	39.90	29.18	29.15	29.24	29.22	29.33				39.87	29.22	10.65
4	-6	39.15	39.15	39.15	38.78	38.78	38.78	38.78	38.79				39.15	38.78	.37
4	-4	39.44	39.47	39.46	35.47	35.47	35.52	35.46	35.42				39.46	35.48	3.98
4	-2	39.66	39.68	39.69	32.25	32.25	32.23	32.24	32.25				39.68	32.24	7.44
4	0	39.85	39.86	39.86	29.18	29.14	29.11	29.15	29.16				39.87	29.15	10.72
4	2	40.04	40.05	40.06	25.71	25.65	25.70	25.68	25.70				40.05	25.69	14.36
4	4	40.26	40.26	40.27	22.28	22.24	22.16	22.16	22.27				40.26	22.22	18.04
4	6	40.45	40.44	40.44	19.01	19.08	19.14	19.22	19.03				40.44	19.10	21.34
4	8	40.61	40.63	40.64	16.60	16.53	16.67	16.74	16.65				40.63	16.64	23.99
4	10	40.77	40.78	40.79	16.15	16.18	16.17	16.24	16.14				40.78	16.18	24.60
4	0	39.83	39.84	39.84											
4	10				16.20	16.08	15.94	16.16	16.34				40.78	16.14	24.64
4	6				19.24	19.20	19.05	19.09	19.19				40.44	19.15	21.29
4	2				22.30	22.36	22.45	22.42	22.35				40.26	22.38	17.88
4	0				29.00	29.06	29.02	29.05	29.02	39.85	39.89	39.89	39.87	29.03	10.84
5	0	39.87	39.92	39.91	27.52	27.56	27.61	27.55	27.56	39.80	39.88	39.88	39.88	27.56	12.32
4	0	39.84	39.84	39.85	28.93	29.06	28.96	28.94	29.02	39.80	39.82	39.85	39.83	28.98	10.85
6	0	39.90	39.92	39.91	25.84	25.80	25.79	25.84	25.82	39.52	39.65	39.72	39.77	25.82	13.95
7	0	39.90	39.91	39.90	24.63	24.64	24.56	24.65	24.59	39.81	39.85	39.86	39.87	24.61	15.26
8	0	39.89	39.88	39.89	22.92	22.93	22.95	22.96	22.93	39.90	39.93	39.94	39.87	22.94	16.93
8	-6	39.16	39.15	39.16	32.76	32.80	32.78	32.80	32.80	39.16	39.18	39.16	39.16	32.79	6.37
8	-4	39.45	39.46	39.48	29.42	29.48	29.45	29.46	29.43	39.43	39.45	39.43	39.45	29.45	10.00
8	-2	39.65	39.66	39.65	26.14	26.10	26.17	26.16	26.20	39.64	39.63	39.65	39.65	26.15	13.50
8	0	39.85	39.86	39.87	23.30	23.29	23.26	23.28	23.20	39.84	39.85	39.85	39.87	23.27	16.60
8	2	40.05	40.06	40.06	20.28	20.27	20.11	20.19	20.09	40.03	40.08	40.06	40.06	20.19	19.87
8	4	40.25	40.25	40.27	17.17	17.11	16.91	17.17	16.93	40.22	40.25	40.25	40.25	17.06	23.19
8	6	40.42	40.42	40.42	14.79	14.48	14.56	14.50	14.72	40.38	40.39	40.41	40.41	14.61	25.80
8	8	40.64	40.64	40.65	14.28	14.46	14.38	14.76	15.08	40.60	40.64	40.62	40.63	14.69	25.94
8	10	40.77	40.78	40.79	16.43	16.60	16.35	16.42	16.80	40.73	40.75	40.75	40.76	16.52	24.24
8	0	39.83	39.83	39.84	23.40	23.44	23.40	23.35	23.44	39.88	39.88	39.89	39.87	23.41	16.46
9	0	39.91	39.91	39.92	21.70	21.66	21.62	21.62	21.80	39.92	39.97	39.98	39.94	21.68	18.26
10	0	39.91	39.92	39.92	20.45	20.52	20.57	20.58	20.52	39.71	39.81	39.83	39.85	20.53	19.32
11	0	39.94	39.95	39.95	18.84	18.86	18.85	19.08	18.80				39.89	18.89	21.00
11	0				18.82	18.93	18.80	18.91	18.93	39.82	39.83	39.84	39.89	18.88	21.01
12	0	39.92	39.94	39.94	17.75	17.65	17.65	17.55	17.63	39.78	39.82	39.83	39.87	17.65	22.22
13	0	39.91	39.92	39.92	16.38	16.12	16.22	16.25	16.14	39.86	39.89	39.90	39.90	16.23	23.67
15	0	39.96	39.99	39.98	14.00	13.95	14.60	14.12	14.40				39.92	14.21	25.70
15	0				13.52	13.82	13.95	14.09	14.04	39.83	39.85	39.88	39.93	13.90	26.03

TABLE XIIb

Raw Rear Lift Data for Model with E = .7

Flap Setting	Angle of Attack	Before-Static Readings			Wind-on Readings					After-Static Readings			Static Average	Wind-on Average	Rear Lift Force
0	0	19.19	19.19	19.19	19.60	19.61	19.60	19.60	19.61	19.20	19.20	19.19	19.20	19.60	-.40
0	-6	19.95	19.96	19.96	23.20	23.20	23.20	23.19	23.19	19.92	19.93	19.93	19.94	23.20	-3.26
0	-4	19.63	19.62	19.63	22.01	22.01	22.01	22.01	22.02	19.63	19.63	19.63	19.63	22.01	-2.38
0	-2	19.36	19.37	19.37	20.79	20.80	20.79	20.81	20.81	19.37	19.36	19.36	19.37	20.80	-1.43
0	0	19.22	19.22	19.22	19.59	19.59	19.59	19.58	19.61	19.20	19.20	19.19	19.20	19.59	-.39
0	2	18.96	18.96	18.97	18.03	18.03	18.04	18.02	18.03	18.96	18.96	18.96	18.96	18.03	.93
0	4	18.76	18.76	18.77	16.10	16.11	16.09	16.12	16.09	18.79	18.78	18.79	18.78	16.10	2.68
0	6	18.64	18.64	18.64	14.29	14.32	14.28	14.29	14.27	18.62	18.62	18.62	18.63	14.29	4.34
0	8	18.45	18.46	18.46	12.78	12.79	12.81	12.80	12.81	18.46	18.46	18.46	18.46	12.80	5.66
0	10	18.32	18.32	18.32	11.90	11.93	11.90	11.88	11.95	18.30	18.30	18.30	18.31	11.91	6.40
0	0	19.17	19.18	19.18	19.60	19.59	19.59	19.59	19.60	19.19	19.19	19.18	19.20	19.59	-.39
1	0	19.19	19.18	19.19	19.34	19.35	19.35	19.34	19.35	19.16	19.16	19.17	19.18	19.35	-.17
2	0	19.19	19.18	19.19	19.12	19.12	19.12	19.12	19.12	19.17	19.18	19.18	19.18	19.12	.06
3	0	19.17	19.17	19.17	18.86	18.86	18.87	18.86	18.87				19.16	18.86	.30
3	0				18.86	18.86	18.86	18.85	18.87	19.15	19.16	19.16	19.16	18.86	.30
4	0	19.18	19.17	19.18	18.65	18.65	18.66	18.67	18.68				19.17	18.66	.51
4	-6	19.91	19.91	19.92	21.87	21.87	21.87	21.86	21.87				19.91	21.87	-1.96
4	-4	19.60	19.61	19.61	20.72	20.74	20.74	20.74	20.73				19.61	20.73	-1.12
4	-2	19.35	19.35	19.35	19.67	19.67	19.67	19.66	19.67				19.35	19.67	-.32
4	0	19.19	19.17	19.18	18.68	18.69	18.69	18.68	18.69				19.17	18.69	.48
4	2	18.96	18.95	18.95	17.37	17.37	17.41	17.40	17.40				18.95	17.39	1.56
4	4	18.75	18.75	18.76	15.88	15.89	15.88	15.88	15.91				18.75	15.89	2.86
4	6	18.59	18.60	18.60	14.09	14.13	14.13	14.15	14.11				18.60	14.12	4.48
4	8	18.44	18.44	18.44	12.35	12.32	12.36	12.36	12.34				18.44	12.35	6.09
4	10	18.26	18.26	18.26	11.43	11.38	11.40	11.44	11.41				18.26	11.41	6.85
4	0	19.16	19.17	19.17											
4	10				11.45	11.40	11.35	11.42	11.46				18.26	11.42	6.84
4	6				14.16	14.15	14.09	14.09	14.12				18.60	14.12	4.48
4	2				15.88	15.88	15.93	15.91	15.88				18.75	15.90	2.85
4	0				18.66	18.65	18.65	18.65	18.64	19.15	19.15	19.15	19.17	18.65	.52
5	0	19.15	19.15	19.14	18.38	18.39	18.40	18.40	18.39	19.12	19.14	19.13	19.14	18.39	.75
4	0	19.15	19.14	19.16	18.60	18.62	18.62	18.64	18.62	19.13	19.14	19.15	19.15	18.62	.53
6	0	19.18	19.18	19.17	18.11	18.11	18.11	18.11	18.11	19.06	19.12	19.14	19.14	18.11	1.03
7	0	19.18	19.18	19.18	17.88	17.88	17.87	17.87	17.87	19.12	19.15	19.15	19.16	17.87	1.29
8	0	19.17	19.17	19.17	17.55	17.55	17.56	17.56	17.57	19.12	19.12	19.12	19.17	17.56	1.61
8	-6	19.96	19.95	19.95	20.58	20.58	20.57	20.58	20.57	19.92	19.92	19.93	19.94	20.58	-.64
8	-4	19.61	19.59	19.60	19.50	19.51	19.51	19.50	19.50	19.62	19.59	19.61	19.60	19.50	.10
8	-2	19.36	19.36	19.36	18.46	19.45	18.45	18.45	18.46	19.34	19.34	19.35	19.35	18.45	.90
8	0	19.19	19.19	19.19	17.62	17.63	17.62	17.62	17.61	19.18	19.19	19.19	19.17	17.62	1.55
8	2	18.93	18.94	18.94	16.60	16.60	16.58	16.58	16.56	18.95	18.94	18.93	18.94	16.58	2.36
8	4	18.75	18.74	18.75	15.39	15.47	15.44	15.48	15.41	18.75	18.75	18.76	18.75	15.44	3.31
8	6	18.58	18.58	18.58	14.19	14.09	14.11	14.10	14.17	18.59	18.59	18.59	18.59	14.13	4.46
8	8	18.40	18.40	18.40	12.34	12.26	12.24	12.31	12.42	18.40	18.40	18.40	18.40	12.31	6.09
8	10	18.24	18.24	18.24	11.06	11.08	11.04	11.07	11.15	18.24	8.24	18.25	18.24	11.08	7.16
8	0	19.16	19.18	19.17	17.62	17.62	17.60	17.60	17.60	19.16	19.17	19.18	19.17	17.61	1.56
9	0	19.17	19.17	19.17	17.33	17.33	17.32	17.33	17.35	19.09	19.13	19.13	19.15	17.33	1.82
10	0	19.13	19.14	19.14	17.08	17.11	17.11	17.11	17.09	19.07	19.12	19.12	19.12	17.10	2.02
11	0	19.13	19.13	19.13	16.21	16.28	16.38	16.25	16.20				19.12	16.26	2.86
11	0				16.25	16.18	16.15	16.31	16.24	19.09	19.11	19.11	19.12	16.23	2.89
12	0	19.16	19.12	19.14	16.01	15.62	15.94	15.95	16.02	19.05	19.08	19.09	19.11	15.91	3.22
13	0	19.15	19.14	19.14	15.48	15.36	15.44	15.48	15.45	19.06	19.10	19.10	19.12	15.44	3.68
15	0	19.10	19.10	19.11	14.91	15.20	14.92	14.85	15.31				19.08	15.04	4.04
15	0				14.83	14.92	14.38	14.94	14.97	19.03	19.05	19.06	19.08	14.91	4.17

TABLE XIIc

Raw Drag Data for Model with E = .7

Avg. Temp.	Avg. Press.	n	α	Before-Static Readings			Wind-on Readings					After-Static Readings			Static Average	Wind-on Average	Drag Force
74.1	29.272	0	0	21.47	21.46	21.46	17.90	17.92	17.92	17.91	17.92	21.58	21.56	21.55	21.50	17.91	3.59
74.1	29.272	0	-6	21.09	21.12	21.12	17.59	17.60	17.60	17.60	17.60	21.31	21.27	21.26	21.20	17.60	3.60
74.1	29.272	0	-4	21.19	21.21	21.22	17.75	17.75	17.77	17.76	17.77	21.32	21.32	21.32	21.26	17.76	3.50
74.1	29.272	0	-2	21.26	21.27	21.26	17.83	17.84	17.83	17.83	17.83	21.37	21.38	21.38	21.32	17.34	3.98
74.1	29.272	0	0	21.43	21.40	21.39	17.38	17.89	17.89	17.89	17.89	21.42	21.43	21.42	21.50	17.89	3.61
74.1	29.272	0	2	21.45	21.46	21.46	17.89	17.90	17.90	17.90	17.91	21.48	21.48	21.48	21.47	17.90	3.57
74.1	29.272	0	4	21.52	21.55	21.54	17.76	17.78	17.79	17.78	17.78	21.54	21.55	21.56	21.54	17.78	3.76
74.1	29.272	0	6	21.63	21.62	21.61	17.57	17.57	17.58	17.58	17.58	21.59	21.59	21.60	21.61	17.58	4.03
74.1	29.272	0	8	21.66	21.66	21.66	17.28	17.30	17.30	17.29	17.31	21.64	21.65	21.66	21.66	17.30	4.36
74.1	29.272	0	10	21.70	21.71	21.70	16.98	16.99	17.00	16.99	17.01	21.21	21.23	21.23	21.21	16.99	4.22
74.1	29.272	0	0	21.49	21.45	21.45	18.09	18.04	18.04	18.03	18.03	21.49	21.48	21.47	21.50	18.05	3.45
77.0	29.269	1	0	21.37	21.36	21.36	17.71	17.74	17.76	17.76	17.76	21.51	21.49	21.49	21.43	17.75	3.68
77.0	29.269	2	0	21.55	21.50	21.49	17.74	17.76	17.75	17.74	17.73	21.52	21.50	21.49	21.51	17.74	3.77
77.0	29.269	3	0	21.43	21.43	21.43	17.66	17.67	17.66	17.68	17.67				21.48	17.67	3.81
77.0	29.269	3	0				17.63	17.64	17.65	17.65	17.66	21.54	21.51	21.53	21.48	17.65	3.83
77.0	29.269	4	0	21.38	21.39	21.40	17.60	17.61	17.63	17.62	17.63				21.44	17.62	3.82
77.0	29.269	4	-6	21.14	21.17	21.15	17.63	17.64	17.65	17.64	17.64				21.15	17.64	3.51
77.0	29.269	4	-4	21.28	21.18	21.23	17.73	17.72		17.73	17.72				21.23	17.72	3.51
77.0	29.269	4	-2	21.41	21.38	21.35	17.79	17.78	17.78	17.77	17.77				21.38	17.78	3.60
77.0	29.269	4	0	21.44	21.44	21.41	17.65	17.65	17.63	17.64	17.65				21.44	17.64	3.80
77.0	29.269	4	2	21.46	21.46	21.46	17.49	17.45		17.47	17.49				21.46	17.48	3.98
77.0	29.269	4	4	21.54	21.55	21.56	17.32	17.31	17.32	17.32	17.31				21.55	17.32	4.23
77.0	29.269	4	6	21.52	21.52	21.55	16.99	17.02	17.03	17.05	17.02				21.53	17.02	4.51
77.0	29.269	4	8	21.82	21.79	21.77	16.70	16.69	16.72	16.72	16.71				21.79	16.71	5.08
77.0	29.269	4	10	21.76	21.76	21.76	16.44	16.48	16.41	16.44	16.43				21.76	16.44	5.32
77.0	29.269	4	0	21.51	21.50	21.49											
77.0	29.269	4	10				16.43	16.41	16.38	16.44	16.44				21.76	16.42	5.32
77.0	29.269	4	6				17.06	17.06		17.06	17.06				21.53	17.06	4.47
77.0	29.269	4	2				17.43	17.44	17.45	17.43	17.42				21.46	17.43	4.03
77.0	29.269	4	0				17.72	17.70	17.70	17.70	17.70				21.44	17.70	3.74
77.0	29.269	5	0	21.47	21.43	21.40	17.49	17.49	17.50	17.50	17.49	21.53	21.50	21.46	21.47	17.49	3.98
77.0	29.269	4	0	21.37	21.36	21.42	17.57	17.58	17.59	17.59	17.58	21.52	21.50	21.50	21.45	17.58	3.87
75.0	29.239	6	0	21.42	21.42	21.42	17.34	17.35	17.35	17.35	17.36	21.37	21.39	21.41	21.41	17.35	4.06
75.0	29.239	7	0	21.54	21.52	21.52	17.31	17.31	17.29	17.31	17.29	21.51	21.49	21.47	21.51	17.30	4.21
75.0	29.239	8	0	21.47	21.46	21.45	17.13	17.16	17.16	17.16	17.15	21.56	21.54	21.52	21.50	17.15	4.35
75.0	29.239	8	-6	21.27	21.27	21.25	17.59	17.57	17.55	17.55	17.54	21.31	21.28	21.27	21.28	17.56	3.72
75.0	29.239	8	-4	21.31	21.34	21.34	17.55	17.56	17.54	17.55	17.54	21.33	21.34	21.35	21.34	17.55	3.79
75.0	29.239	8	-2	21.35	21.35	21.35	17.45	17.45	17.46	17.46	17.46	21.37	21.38	21.38	21.36	17.46	3.90
75.0	29.239	8	0	21.40	21.43	21.40	17.23	17.25	17.23	17.24	17.24	21.43	21.44	21.42	21.42	17.24	4.18
75.0	29.239	8	2	21.47	21.52	21.49	17.08	17.08	17.07	17.09	17.08	21.49	21.43	21.47	21.48	17.08	4.40
75.0	29.239	8	4	21.54	21.55	21.55	16.84	16.80	16.84	16.81	16.79	21.55	21.52	21.53	21.54	16.82	4.72
75.0	29.239	8	6	21.59	21.59	21.60	16.45	16.42	16.43	16.42	16.45	21.58	21.58	21.59	21.59	16.43	5.16
75.0	29.239	8	8	21.84	21.82	21.78	15.89	15.87	15.85	15.87	15.93	21.66	21.62	21.63	21.73	15.88	5.85
75.0	29.239	8	10	21.81	21.82	21.81	15.08	15.09	15.05	15.07	15.12	21.71	21.71	21.71	21.76	15.08	6.63
75.0	29.239	8	0	21.39	21.45	21.42	17.40	17.39	17.39	17.39	17.39	21.50	21.50	21.48	21.46	17.39	4.07
79.0	29.217	9	0	21.52	21.52	21.55	17.20	17.18	17.17	17.18	17.20	21.51	21.51	21.52	21.52	17.19	4.33
79.0	29.217	10	0	21.47	21.41	21.45	17.00	17.00	17.01	17.02	17.02	21.51	21.48	21.48	21.47	17.01	4.46
79.0	29.217	11	0	21.47	21.47	21.48	16.62	16.63	16.65	16.66	16.64				21.46	16.64	4.82
79.0	29.217	11	0				16.69	16.70	16.67	16.71	16.70	21.45	21.44	21.44	21.46	16.69	4.77
79.0	29.217	12	0	21.57	21.53	21.52	16.48	16.42	16.51	16.50	16.51	21.47	21.46		21.51	16.48	5.03
79.0	29.217	13	0	21.43	21.44	21.40	16.32	16.24	16.26	16.29	16.27	21.50	21.50	21.51	21.46	16.28	5.18
79.0	29.217	15	0	21.55	21.52	21.50	15.91	15.95	15.96	15.89	16.03				21.49	15.95	5.54
79.0	29.217	15	0				15.78	15.83	15.34	15.87	15.89	21.49	21.45	21.45	21.49	15.34	5.65

TABLE XIIIa

Raw Front Lift Data for Model with E = .8

Flap Setting	Angle of Attack	Before-Static Readings			Wind-on Readings					After-Static Readings			Static Average	Wind-on Average	Front Lift Force
0	0	39.64	39.63	39.63	35.15	35.17	35.15	35.10	35.11	39.68	39.70	39.70	39.67	35.14	4.23
0	-6	38.95	38.95	38.95	44.48	44.50	44.51	44.52	44.50	38.90	38.90	38.90	38.93	44.50	-5.27
0	-4	39.26	39.27	39.27	41.44	41.53	41.55	41.54	41.57	39.25	39.25	39.25	39.26	41.53	-2.27
0	-2	39.50	39.50	39.51	38.35	38.35	38.36	38.28	38.30	39.50	39.52	39.50	39.51	38.33	1.13
0	0	39.70	39.71	39.72	35.30	35.35	35.31	35.30	35.34	39.71	39.71	39.71	39.67	35.32	4.35
0	2	39.90	39.91	39.91	31.20	31.20	31.25	31.22	31.21	39.93	39.95	39.95	39.93	31.72	8.21
0	4	40.09	40.10	40.09	28.55	28.55	28.50	28.55	28.59	40.10	40.12	40.11	40.10	28.55	11.55
0	6	40.23	40.24	40.24	25.11	25.10	25.07	25.10	25.07	40.25	40.25	40.25	40.24	25.09	15.15
0	8	40.48	40.49	40.50	21.91	21.91	21.94	21.94	21.90	40.39	40.39	40.40	40.44	21.92	18.52
0	10	40.62	40.63	40.63	19.19	19.23	19.12	19.08	19.15	40.52	40.53	40.53	40.58	19.15	21.43
0	0	39.66	39.67	39.67	35.20	35.21	35.20	35.21	35.20	39.59	39.60	39.59	39.67	35.20	4.47
1	0	39.66	39.68	39.68	33.43	33.45	33.43	33.40	33.41	39.64	39.65	39.67	39.66	33.42	6.24
2	0	39.66	39.66	39.66	31.70	31.69	31.66	31.68	31.70	39.58	39.62	39.64	39.64	31.69	7.95
3	0	39.70	39.70	39.70	30.30	30.27	30.30	30.32	30.28				39.62	30.29	9.33
3	0				30.30	30.32	30.34	30.30	30.32	39.52	39.55	39.56	39.62	30.32	9.30
4	0	39.68	39.69	39.69	28.40	28.35	28.55	28.53	28.55				39.70	28.48	11.22
4	-6	38.90	38.90	38.90	38.40	38.39	38.34	38.34	38.34				38.90	38.36	.54
4	-4	39.23	39.26	39.25	35.06	35.09	35.06	35.05	35.05				39.25	35.06	4.19
4	-2	39.51	39.52	39.52	31.79	31.76	31.78	31.78	31.77				39.52	31.78	7.74
4	0	39.76	39.77	39.79	28.82	28.81	28.78	28.84	28.85				39.70	28.82	10.98
4	2	40.06	40.07	40.07	25.26	25.35	25.34	25.38	25.35				40.07	25.34	14.73
4	4	40.24	40.25	40.25	22.17	22.18	22.10	22.10	22.11				40.25	22.13	18.12
4	6	40.40	40.41	40.42	18.79	18.81	18.79	18.86	18.84				40.41	18.82	21.59
4	8	40.55	40.55	40.56	16.20	16.20	16.29	16.30	16.28				40.55	16.25	24.30
4	10	40.66	40.67	40.68	15.52	15.51	15.51	15.60	15.62				40.67	15.55	25.12
4	10				15.51	15.46	15.65	15.79	15.63				40.67	15.61	25.06
4	6				18.99	19.00	19.04	19.10	19.08				40.41	19.04	21.37
4	2				25.43	25.38	25.37	25.40	25.37				40.07	25.39	14.68
4	0	39.62	39.63	39.63	28.27	28.80	28.80	28.80	28.80	39.70	39.73	39.73	39.70	28.79	10.91
5	0	39.73	39.73	39.73	26.76	26.80	26.80	26.87	26.83	39.68	39.70	39.70	39.71	26.81	12.90
6	0	39.65	39.68	39.65	25.52	25.51	25.49	25.51	25.55	39.45	39.53	39.50	39.58	25.52	14.06
7	0	39.65	39.68	39.66	23.90	23.84	23.82	23.93	24.00				39.65	23.90	15.25
7	0				24.09	23.96	23.99	24.07	24.00	39.61	39.65	39.65	39.65	24.02	15.63
8	0	39.70	39.71	39.70	22.20	22.20	22.17	22.15	22.16				39.71	22.18	17.53
8	-6	38.89	38.90	38.89	31.70	31.68	31.62	31.68	31.70				38.89	31.68	7.21
8	-4	39.25	39.24	39.24	28.47	28.51	28.50	28.48	28.48				39.24	28.49	10.75
8	-2	39.55	39.55	39.55	25.50	25.45	25.51	25.35	25.40				39.55	25.44	14.11
8	0	39.76	39.78	39.78	22.40	22.40	22.42	22.42	22.40				39.71	22.41	17.30
8	2	40.00	40.01	40.01	19.45	19.40	19.40	19.37	19.49				40.01	19.42	20.59
8	4	40.18	40.18	40.20	16.45	16.35	16.25	16.30	16.30				40.19	16.33	23.86
8	6	40.30	40.31	40.30	13.86	14.02	13.95	13.97	13.99				40.30	13.96	26.34
8	8	40.43	40.45	40.44	14.18	14.21	14.23	14.17					40.44	14.20	25.24
8	10				13.45	13.42	13.28	13.72	13.46				40.44	13.47	26.97
8	4				16.23	16.15	16.11	16.23	16.05				40.19	16.15	24.04
8	0	39.65	39.65	39.67	22.38	22.40	22.36	22.41		39.66	39.72	39.72	39.71	22.39	17.32
9	0	39.72	39.72	39.72	20.27	20.80	20.86	20.84	20.87				39.72	20.83	18.39
10	0	39.75	39.75	39.75	19.45	19.46	19.45	19.46	19.36				39.75	19.44	20.31
11	0	39.75	39.75	39.77	12.95	12.85	12.85	12.76	12.86				39.76	17.85	21.91
12	0	39.78	39.78	39.78	16.65	16.60	16.57	16.56	16.62				39.78	16.60	23.18
13	0	39.70	39.70	39.70	15.21	15.10	15.02	14.95	14.96				39.70	15.05	24.65
13	0				15.42	15.64	15.57	15.45	15.37				39.70	15.49	24.21
15	0	39.74	39.75	39.74	12.98	12.98	12.99	12.87	12.87				39.74	12.94	26.80
16	0	39.78	39.77	39.79	12.02	12.05	12.10	12.15	12.05				39.78	12.[illegible]	27.71

TABLE XIIIb

Raw Rear Lift Data for Model with E = .8

Flap Setting	Angle of Attack	Before-Static Readings			Wind-on Readings					After-Static Readings			Static Average	Wind-on Average	Rear Lift Force
0	0	19.16	19.16	19.16	19.65	19.67	19.65	19.64	19.64	19.16	19.16	19.16	19.15	19.65	-.50
0	-6	19.93	19.93	19.94	23.15	23.15	23.16	23.16	23.14	19.98	19.98	19.98	19.96	23.15	-3.19
0	-4	19.56	19.56	19.56	21.96	21.98	22.00	21.99	22.00	19.59	19.59	19.59	19.58	21.99	-2.41
0	-2	19.28	19.27	19.27	20.73	20.74	20.75	20.75	20.75	19.29	19.28	19.29	19.28	20.74	-1.46
0	0	19.08	19.08	19.08	19.57	19.57	19.54	19.54	19.56	19.09	19.08	19.08	19.15	19.56	-.41
0	2	18.83	18.83	18.83	17.75	17.76	17.79	17.78	17.79	18.81	18.80	18.80	18.82	17.77	1.05
0	4	18.66	18.66	18.65	15.87	15.86	15.86	15.88	15.89	18.63	18.63	18.63	18.64	15.87	2.77
0	6	18.52	18.52	18.52	14.00	14.02	13.99	13.98	14.00	18.50	18.50	18.50	18.51	14.00	4.51
0	8	18.34	18.34	18.34	12.67	12.67	12.67	12.66	12.65	18.33	18.34	18.33	18.34	12.66	5.68
0	10	18.18	18.18	18.18	11.69	11.76	11.69	11.67	11.70	18.18	18.18	18.18	18.18	11.70	6.48
0	0	19.21	19.22	19.22	19.55	19.54	19.52	19.55	19.53	19.20	19.21	19.21	19.15	19.54	-.39
1	0	19.21	19.22	19.21	19.44	19.44	19.44	19.41	19.43	19.19	19.20	19.21	19.21	19.43	-.22
2	0	19.22	19.22	19.22	19.25	19.24	19.23	19.23	19.24	19.15	19.18	19.18	19.20	19.24	-.04
3	0	19.22	19.19	19.20	19.08	19.06	19.08	19.06	19.06				19.19	19.07	.12
5	0				19.06	19.06	19.07	19.07	19.07	19.16	19.18	19.19	19.19	19.07	.12
4	0	19.21	19.20	19.21	18.84	18.32	18.84	18.82	18.82				19.16	18.33	.83
4	-6	19.98	19.98	19.98	21.94	21.92	21.93	21.93	21.94				19.98	21.93	-1.95
4	-4	19.62	19.62	19.62	20.75	20.76	20.76	20.76	20.75				19.62	20.76	-1.14
4	-2	19.30	19.30	19.31	19.64	19.65	19.65	19.64	19.64				19.30	19.64	-.34
4	0	19.09	19.09	19.09	18.56	18.56	18.58	18.58	18.59				19.16	18.57	.59
4	2	18.81	18.81	18.80	17.28	17.30	17.29	17.33	17.31				18.81	17.30	1.51
4	4	18.61	18.61	18.61	15.80	15.79	15.77	15.76	15.80				18.61	15.78	2.83
4	6	18.45	18.45	18.45	13.96	13.98	13.95	13.99	13.97				18.45	13.97	4.48
4	8	18.29	18.29	18.30	12.23	12.22	12.25	12.25	12.24				18.29	12.24	6.05
4	10	18.15	18.16	18.16	11.22	11.28	11.22	11.31	11.27				18.16	11.26	6.90
4	10				11.22	11.22	11.30	11.34	11.28				18.16	11.27	6.89
4	6				14.07	14.07	14.05	14.06	14.05				18.45	14.06	4.39
4	2				17.37	17.29	17.31	17.32	17.32				18.81	17.32	1.49
4	0	19.22	19.21	19.22	18.69	18.69	18.70	18.70	18.70	19.12	19.13	19.13	19.16	18.70	.46
5	0	19.17	19.17	19.16	18.53	18.52	18.50	18.51	18.51	19.14	19.15	19.14	19.16	18.51	.65
6	0	19.20	19.19	19.19	18.35	18.36	18.36	18.35	18.34	19.13	19.14	19.15	19.17	18.35	.82
7	0	19.19	19.17	19.19	18.15	18.14	18.12	18.14	18.15				19.16	18.14	1.02
7	0				18.05	18.04	18.05	18.07	18.05	19.12	19.13	19.13	19.16	18.05	1.11
8	0	19.17	19.16	19.17	17.85	17.84	17.83	17.82	17.84				19.12	17.84	1.28
8	-6	19.96	19.95	19.95	20.84	20.85	20.85	20.86	20.85				19.95	20.85	-.90
8	-4	19.61	19.61	19.60	19.54	19.54	19.54	19.54	19.54				19.61	19.54	.07
8	-2	19.28	19.26	19.27	18.57	18.56	18.59	18.56	18.57				19.27	18.57	.70
8	0	19.05	19.05	19.05	17.65	17.65	17.66	17.65	17.65				19.12	17.65	1.47
8	2	18.79	18.79	18.77	16.66	16.64	16.64	16.64	16.67				18.78	16.65	2.13
8	4	18.61	18.61	18.62	15.50	15.47	15.40	15.48	15.48				18.63	15.47	3.16
8	6	18.44	18.44	18.44	14.02	14.04	14.01	14.03	14.06				18.44	14.03	4.41
8	8	18.28	18.28	18.28	12.16	12.23	12.19	12.18					18.28	12.19	6.09
8	10				12.09	12.00	12.03	12.08	12.06				18.28	12.05	6.23
8	4				15.64	15.60	15.60	15.64	15.52				18.63	15.61	3.02
8	0	19.16	19.16	19.17	17.73	17.74	17.74	17.76		19.08	19.10	19.10	19.12	17.74	1.38
9	0	19.10	19.10	19.10	12.55	17.55	17.55	17.56	17.56				19.10	17.55	1.55
10	0	19.12	19.11	19.11	17.33	17.33	17.32	17.33	17.31				19.11	17.32	1.79
11	0	19.08	19.08	19.09	16.66	16.61	16.61	16.63	16.64				19.08	16.63	2.45
12	0	19.06	19.07	19.07	16.40	16.32	16.38	16.37	16.32				19.06	16.36	2.70
13	0	19.08	19.09	19.08	16.17	16.12	16.09	16.08	16.07				19.08	16.11	2.97
13	0				16.08	16.13	16.09	16.06	16.10				19.08	16.09	2.99
15	0	19.07	19.07	19.07	15.62	15.27	15.35	15.48	15.30				19.07	15.40	3.67
16	0	19.06	19.06	19.06	15.03	15.42	15.53	15.11	15.09				19.06	15.24	3.66

TABLE XIIIc

Raw Drag Data for Model with E = .8

Avg. Temp.	Avg. Press.	n	α	Before-Static Readings			Wind-on Readings					After-Static Readings			Static Average	Wind-on Average	Drag Force
72.2	29.311	0	0	21.23	21.24	21.24	17.62	17.63	17.62	17.62	17.63	21.43	21.40	21.40	21.30	17.62	[illegible]
72.2	29.311	0	-6	20.94	20.98	20.99	17.39	17.40	17.38	17.38	17.39	21.12	21.13	21.14	21.05	17.39	[illegible]
72.2	29.311	0	-4	21.06	21.07	21.07	17.46	17.48	17.47	17.48	17.48	21.20	21.20	21.21	21.14	17.47	3.67
72.2	29.311	0	-2	21.11	21.13	21.13	17.52	17.54	17.54	17.55	17.56	21.24	21.26	21.25	21.19	17.54	3.65
72.2	29.311	0	0	21.19	21.19	21.19	17.60	17.60	17.62	17.62	17.60	21.28	21.28	21.29	21.30	17.61	[illegible]
72.2	29.311	0	2	21.25	21.27	21.27	17.55	17.57	17.57	17.57	17.58	21.36	21.37	21.37	21.32	17.57	3.75
72.2	29.311	0	4	21.33	21.33	21.34	17.48	17.49	17.48	17.49	17.49	21.41	21.42	21.42	21.38	17.49	[illegible]
72.2	29.311	0	6	21.36	21.36	21.36	17.27	17.25	17.25	17.25	17.26	21.45	21.46	21.47	21.41	17.26	4.15
72.2	29.311	0	8	21.60	21.57	21.57	16.90	16.90	16.92	16.91	16.91	21.52	21.53	21.53	21.55	16.91	4.64
72.2	29.311	0	10	21.62	21.61	21.61	16.58	16.51	16.57	16.57	16.57	21.57	21.59	21.58	21.60	16.58	5.02
72.2	29.311	0	0	21.38	21.35	21.33	17.88	17.85	17.84	17.83	17.83	21.37	21.34	21.34	21.30	17.85	3.45
75.5	29.316	1	0	21.40	21.36	21.38	17.57	17.59	17.59	17.59	17.59	21.43	21.40	21.40	21.40	17.59	3.81
75.5	29.316	2	0	21.35	21.36	21.35	17.44	17.45	17.47	17.42	17.48	21.37	21.35	21.36	21.36	17.46	3.90
75.5	29.316	3	0	21.45	21.41	21.41	17.41	17.43	17.43	17.42	17.43				21.40	17.42	3.98
75.5	29.316	3	0				17.40	17.41	17.42	17.42	17.43	21.39	21.37	21.36	21.40	17.42	3.98
75.5	29.316	4	0	21.45	21.43	21.41	17.29	17.29	17.32	17.32	17.32				21.36	17.31	4.05
75.5	29.316	4	-6	21.06	21.07	21.09	17.53	17.52	17.52	17.52	17.51				21.07	17.52	3.55
75.5	29.316	4	-4	21.12	21.14	21.15	17.52	17.52	17.53	17.53	17.52				21.14	17.52	3.62
75.5	29.316	4	-2	21.18	21.21	21.21	17.39	17.39	17.39	17.41	17.42				21.20	17.40	3.80
75.5	29.316	4	0	21.21	21.23	21.25	17.45	17.45	17.44	17.44	17.44				21.36	17.44	3.92
75.5	29.316	4	2	21.33	21.35	21.36	17.24	17.25	17.25	17.26	17.26				21.35	17.25	4.10
75.5	29.316	4	4	21.39	21.40	21.41	17.06	17.06	17.06	17.07	17.07				21.40	17.06	4.34
75.5	29.316	4	6	21.56	21.54	21.52	16.64	16.67	16.64	16.67	16.67				21.54	16.66	4.88
75.5	29.316	4	8	21.56	21.57	21.55	16.29	16.28	16.31	16.29	16.28				21.56	16.29	5.27
75.5	29.316	4	10	21.60	21.60	21.60	15.64	15.70	15.67	15.71	15.71				21.60	15.69	5.91
75.5	29.316	4	10				15.63	15.62	15.69	15.68	15.69				21.60	15.66	5.94
75.5	29.316	4	6				16.95	16.92	16.94	16.93	16.91				21.54	16.93	4.61
75.5	29.316	4	2				17.41	17.42	17.41	17.41	17.42				21.35	17.41	3.94
75.5	29.316	4	0	21.34	21.33	21.35	17.49	17.49	17.51	17.50	17.51	21.43	21.42	21.42	21.36	17.50	3.86
79.0	29.271	5	0	21.31	21.31	21.31	17.13	17.16	17.16	17.18	17.18	21.43	21.40	21.39	21.36	17.16	4.20
79.0	29.271	6	0	21.30	21.27	21.27	17.12	17.13	17.14	17.13	17.14	21.36	21.30	21.32	21.30	17.13	4.17
79.0	29.271	7	0	21.43	21.42	21.42	16.97	16.98	16.98	16.98	16.99				21.42	16.98	4.44
79.0	29.271	7	0				17.05	17.05	17.04	17.06	17.05	21.44	21.41	21.41	21.42	17.05	4.32
79.0	29.271	8	0	21.41	21.38	21.40	16.82	16.84	16.85	16.84	16.84				21.39	16.84	4.55
79.0	29.271	8	-6	21.18	21.17	21.14	17.08	17.08	17.07	17.07	17.08				21.16	17.08	4.08
79.0	29.271	8	-4	21.16	21.15	21.12	17.37	17.37	17.36	17.36	17.38				21.14	17.37	3.77
79.0	29.271	8	-2	21.22	21.23	21.24	17.07	17.07	17.08	17.07	17.08				21.23	17.07	4.16
79.0	29.271	8	0	21.40	21.37	21.38	16.97	16.95	16.97	16.97	16.95				21.39	16.96	4.43
79.0	29.271	8	2	21.39	21.41	21.39	16.75	16.74	16.75	16.76	16.78				21.40	16.76	4.64
79.0	29.271	8	4	21.47	21.46	21.45	16.44	16.41	16.41	16.44	16.44				21.46	16.43	5.03
79.0	29.271	8	6	21.46	21.48	21.48	16.00	16.04	16.00	16.02	16.03				21.47	16.02	5.45
79.0	29.271	8	8	21.57	21.54	21.56	15.03	15.05	15.05	15.00					21.56	15.03	6.53
79.0	29.271	8	10				14.98	14.92	14.92	14.93	14.90				21.56	14.93	6.63
79.0	29.271	8	4				16.65	16.61	16.59	16.64	16.56	21.51	21.46	21.45	21.46	16.61	4.85
79.0	29.271	8	0	21.28	21.28	21.30	17.21	17.19	17.19	17.19					21.39	17.20	4.19
77.0	29.201	9	0	21.38	21.37	21.37	16.70	16.73	16.73	16.74	16.74				21.37	16.73	4.54
77.0	29.201	10	0	21.49	21.47	21.44	16.59	16.62	16.64	16.64	16.63				21.46	16.62	4.84
77.0	29.201	11	0	21.49	21.49	21.46	16.40	16.40	16.40	16.41	16.42				21.48	16.41	5.07
77.0	29.201	12	0	21.47	21.47	21.46	16.18	16.16	16.19	16.18	16.18				21.47	16.18	5.29
77.0	29.201	13	0	21.43	21.44	21.45	16.03	16.02	16.01	16.01	16.02				21.44	16.02	5.42
77.0	29.201	13	0				16.17	16.20	16.20	16.18	16.18				21.44	16.19	5.25
77.0	29.201	15	0	21.38	21.38	21.38	15.80	15.72	15.73	15.76	15.72				21.38	15.75	5.63
77.0	29.201	16	0	21.51	21.50	21.48	15.43	15.50	15.36	15.48	15.48				21.50	15.49	[illegible]

Appendix G

Data Reduction Calculations

This appendix explains in detail and by example how the experimental data in Appendix F was reduced to obtain the experimental points for the plots of experiment versus theory for the change in zero-lift angle of attack divided by flap deflection ($\Delta\alpha_{LO}/\eta$) versus flap-chord ratio (E) and the change in moment coefficient about the aerodynamic center divided by flap deflection ($\Delta C_{mac}/\eta$) versus E, Figs. 22 thru 28 in Appendix H. The model used as the example is E = .7. The reduction process for the $\Delta\alpha_{LO}/\eta$ versus E experimental points will be described first.

The total lift generated by the model at a particular angle of attack and flap setting was obtained by adding the lift force from the raw front lift data to the lift force from the raw rear lift data. The lift was then divided by the dynamic pressure times the wing span times the chord length (qbc) to produce the lift coefficient, C_ℓ. The dynamic pressure was converted from 3 inches of water to lbs/ft^2 by finding the weight of one cubic foot of water at the testing temp, dividing by 12 to give the weight of one inch of water on one square foot, and then multiplying by 3 to give the pressure of 3 inches of water in lbs/ft^2. At this point, C_ℓ should have been corrected for any errors induced by the wind tunnel. However, the corrections from Pope (Ref 6:305-318)

for the two dimensional wind tunnel were so small that they were considered negligible for these models. C_ℓ was then plotted versus its angle of attack for a particular flap deflection. This process was accomplished for the three flap settings of 0°, 4°, and 8° at angles of attack -6°, -4°, -2°, 0°, 2°, 4°, 6°, 8°, and 10°. This gave three plots for C_ℓ versus α for a model with a particular E. Each plot had an angle of zero-lift and by subtracting them appropriately the changes in the angle of zero-lift ($\Delta\alpha_{LO}$) were found. Dividing the $\Delta\alpha_{LO}$s by the appropriate change in flap deflection then gave three $\Delta\alpha_{LO}/\eta$ experimental points for a model with a particular E. Table XIV gives the numerical values for L, qbc, and C_ℓ for the model with E = .7. Figures 22a through 28b give the values for α_{LO} for all seven models.

$\Delta C_{mac}/\eta$ versus E experimental points were obtained in a manner similar to $\Delta\alpha_{LO}/\eta$ versus E points. The calculations about to be presented were initially done with an assumed aerodynamic center of .25c. This resulted in a positive result for $\Delta C_{mac}/\eta$ for E = .7 and was the first indication that the data was biased in some manner. Calculations for the aerodynamic center from the data at 0° flap deflection gave an x_{ac} location of approximately 4 inches which was not possible for the 9 inch 4412 airfoil. In fact, for the low Reynolds number of the airfoil in this experiment, it was more likely that the aerodynamic center was in front of the quarter chord. Since no reliable data for the Reynolds number of approx $5x10^5$ could be found, an assumed location of .245c was

TABLE XIV

Calculations for Model with E = .7

Flap Setting (η)	Angle of Attack (α)	Total Lift L (lbs)	qbc (lbs)	C_L $\left(\frac{L}{qbc}\right)$	Moment From Front Lift (1) (lbs in)	Moment From Rear Lift (2) (lbs in)	Total Moment Mac (1+2) (lbs in)	qbc^2 (lbs in)	C_{mac} $\left(\frac{Mac}{qbc^2}\right)$
0	0	4.26	22.925	.186	11.536	5.424	16.96	203.574	.083
0	-6	-8.77	22.925	.383				203.574	
0	-4	-4.60	22.925	.201				203.574	
0	-2	-.14	22.925	.006					
0	0	4.36	22.925	.190	11.744	5.265	17.009		.084
0	2	9.13	22.925	.398					
0	4	14.53	22.925	.634					
0	6	19.52	22.925	.851					
0	8	24.22	22.925	1.056					
0	10	27.59	22.925	1.203					
0	0	4.35	22.925	.190	11.719	5.291	17.01	203.574	.084
1	0	6.18	22.915	.270	15.728	2.268	17.996	203.485	.088
2	0	8.02	22.915	.350	19.706	-.822	18.884	203.485	.093
3	0	9.78	22.915	.427	23.46	-3.978	19.488	203.485	.096
3	0	9.74	22.915	.425	23.36	-4.031	19.329	203.485	.095
4	0	11.16	22.915	.487	26.357	-6.71	19.647	203.485	.097
4	-6	-1.59	22.915	-.069					
4	-4	2.86	22.915	.125					
4	-2	7.12	22.915	.311					
4	0	11.20	22.915	.489	26.545	-6.392	20.153		.099
4	2	15.92	22.915	.695					
4	4	20.90	22.915	.912					
4	6	25.82	22.915	1.127					
4	8	30.08	22.915	1.313					
4	10	31.45	22.915	1.372					
4	10	31.48	22.915	1.374					
4	6	25.77	22.915	1.125					
4	4	20.73	22.915	.905					
4	0	11.36	22.915	.496	26.837	-6.869	19.968	203.485	.098
5	0	13.07	22.921	.57	30.497	-9.906	20.591	203.538	.101
4	0	11.38	22.921	.497	26.49	-6.962	19.528	203.538	.096
6	0	14.98	22.921	.654	34.545	-13.685	20.86	203.538	.102
7	0	16.55	22.921	.722	37.279	-17.054	20.725	203.538	.102
8	0	18.54	22.921	.809	41.929	-21.35	20.579	203.538	.101
8	-6	5.73	22.921	.25					
8	-4	10.10	22.921	.441					
8	-2	14.40	22.921	.628					
8	0	18.15	22.921	.792	41.116	-20.528	20.588	203.538	.101
8	2	22.23	22.921	.970					
8	4	26.50	22.921	1.156					
8	6	30.26	22.921	1.320					
8	8	32.03	22.921	1.397					
8	10	31.40	22.921	1.370					
8	0	18.02	22.921	.786	40.77	-20.687	20.083	203.538	.099
9	0	20.08	22.915	.876	45.2	-24.042	21.158	203.485	.104
10	0	21.34	22.915	.931	47.84	-26.787	21.053	203.485	.103
11	0	23.86	22.915	1.04	52.003	-37.834	14.169	203.485	.07
11	0	23.90	22.915	1.043	52.023	-38.338	13.685	203.485	.067
12	0	25.42	22.915	1.109	55.032	-42.422	12.61	203.485	.062
13	0	27.35	22.915	1.194	58.602	-48.708	9.894	203.485	.049

made from trends of the aerodynamic center location in Abbott and Doenhoff (Ref 5:489). The calculations were then repeated with .245c. The forces for the moment were the rear lift and front lift with the front lift producing a positive moment and the rear lift producing a negative moment when the rear lift was positive. The moment arm for the front lift was found by taking .245c of the chord length plus the distance from the trunnion screw to the model, 2.476 inches for E = .7. The rear moment arm was found by subtracting the front lift moment arm from the horizontal distance e as given in Table III, thus the rear lift moment arm for the E = .7 model was 13.261 inches. After finding the moment for a particular flap setting at 0° angle of attack, it was then divided by qbc^2 to give C_{mac}. Table XIV gives the calculations for C_{mac} with E = .7. This value of C_{mac} was then plotted against the value of the flap deflection it was computed for. By doing this for flap deflections from 0° to 13° at an angle of attack of 0°, the C_{mac} versus η figures in Appendix H were obtained. The experimental $\Delta C_{mac}/\eta$ points for a particular E was then found by measuring the slope of the corresponding C_{mac} versus η figure.

Appendix H

Experimental Data Plots

This Appendix contains the experimental plots of the lift coefficient versus angle of attack and the moment coefficient about the aerodynamic center versus flap deflection for all seven models. The plots were used to determine the change in zero-lift angle of attack divided by flap deflection versus flap-chord ratio and the change in the moment coefficient about the aerodynamic center divided by flap deflection versus flap-chord ratio. The points for the plots came from reducing the experimental data in Appendix F with the method of reduction described in Appendix G.

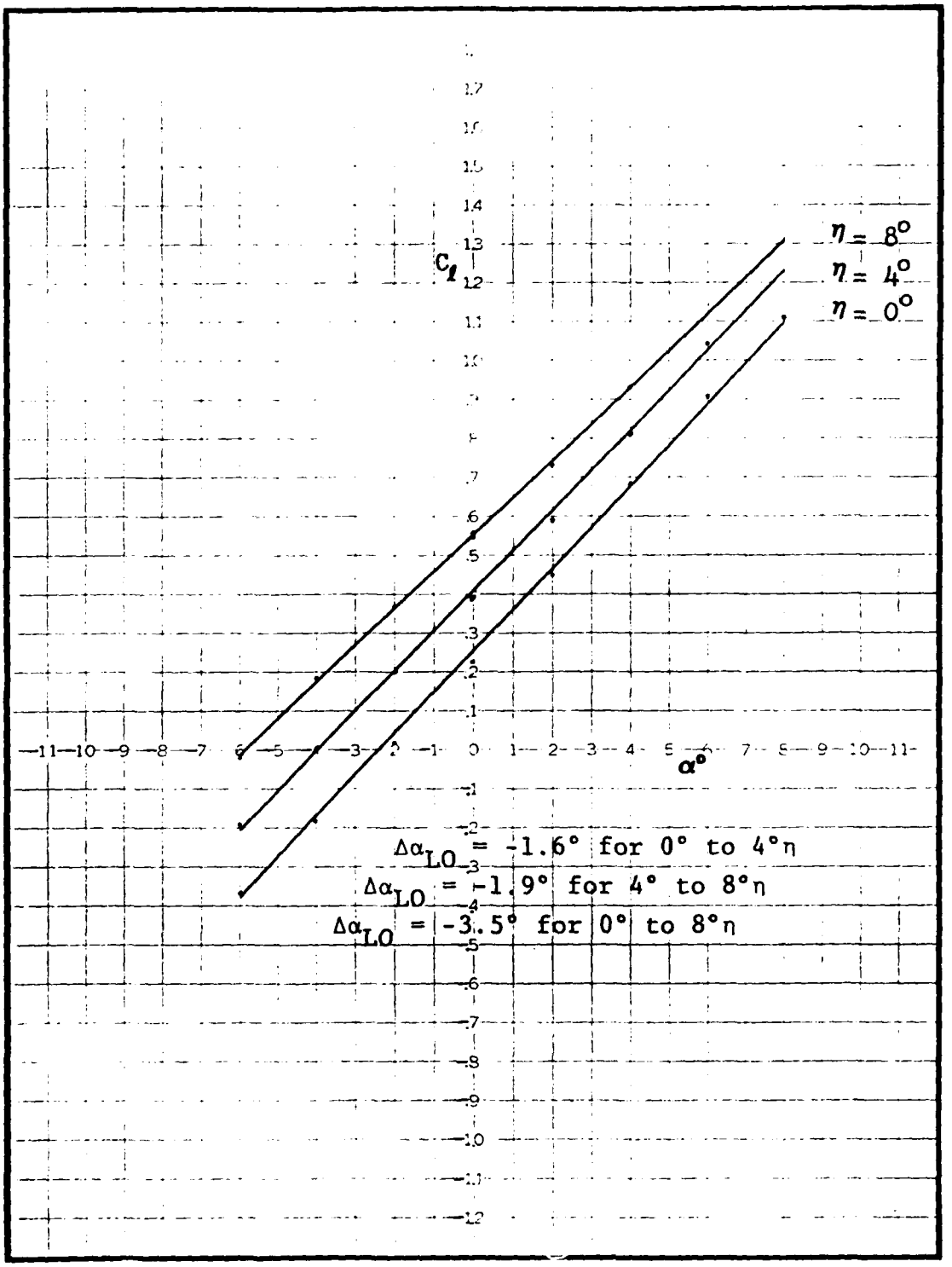

Fig. 22a Experimental C_ℓ versus α plots used to find $\Delta\alpha_{LO}/\eta$ for E = .2

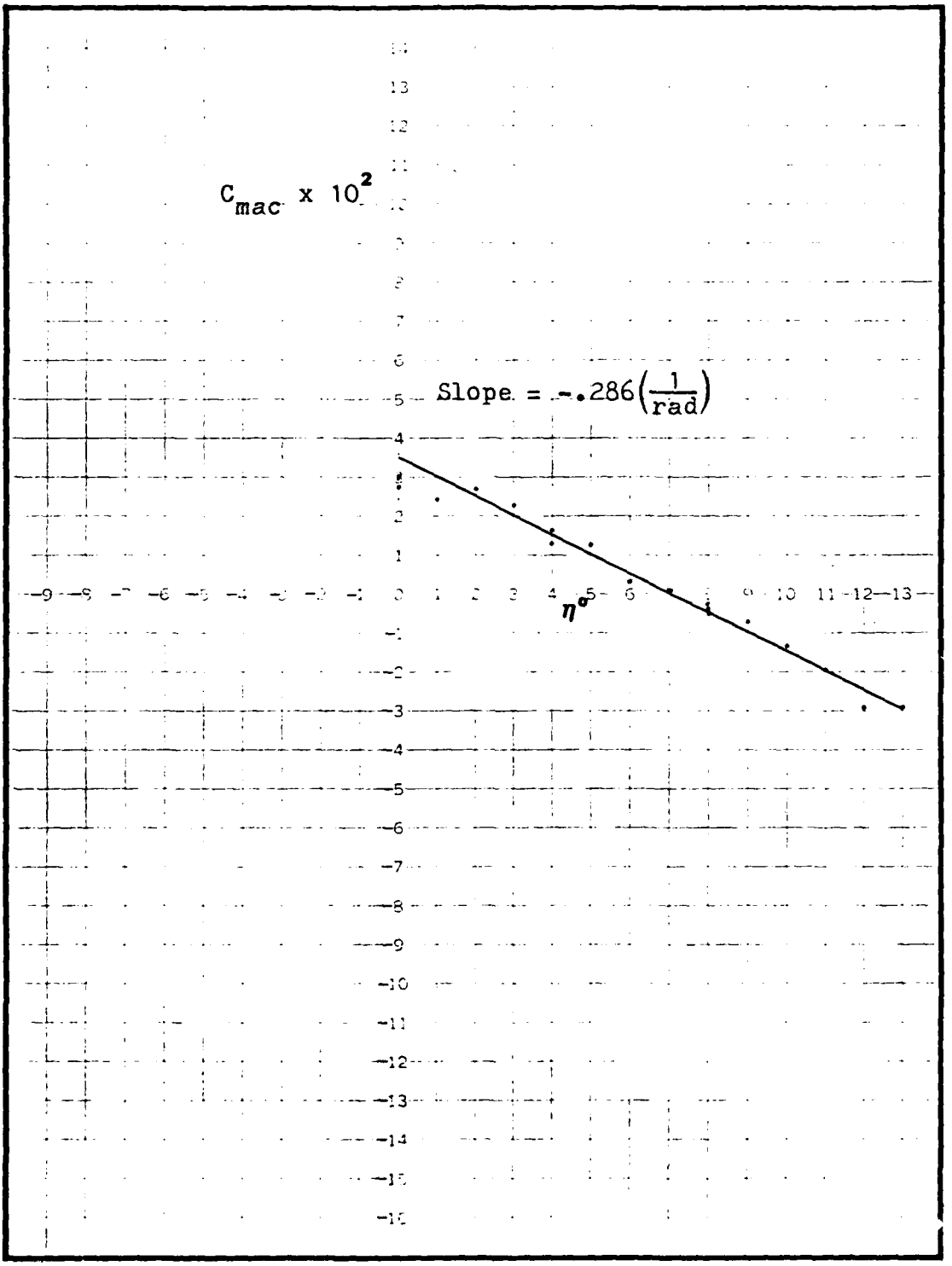

Fig. 22b Experimental C_{mac} versus η plots used to find $\Delta C_{mac}/\eta$ for E = .2

AD-A124 703 WIND TUNNEL INVESTIGATION OF VARYING-HINGED FLAPS(U) AIR FORCE INST OF TECH WRIGHT-PATTERSON AFB OH SCHOOL OF ENGINEERING H J PRICE DEC 82 AFIT/GAE/AA/82D-23 2/2

UNCLASSIFIED F/G 14/2 NL

END
DATE FILMED
DTIC

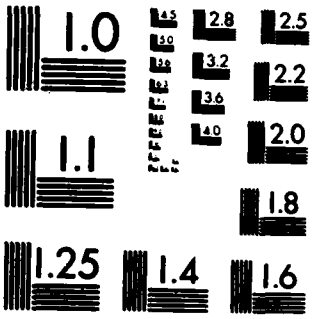

MICROCOPY RESOLUTION TEST CHART
NATIONAL BUREAU OF STANDARDS-1963-A

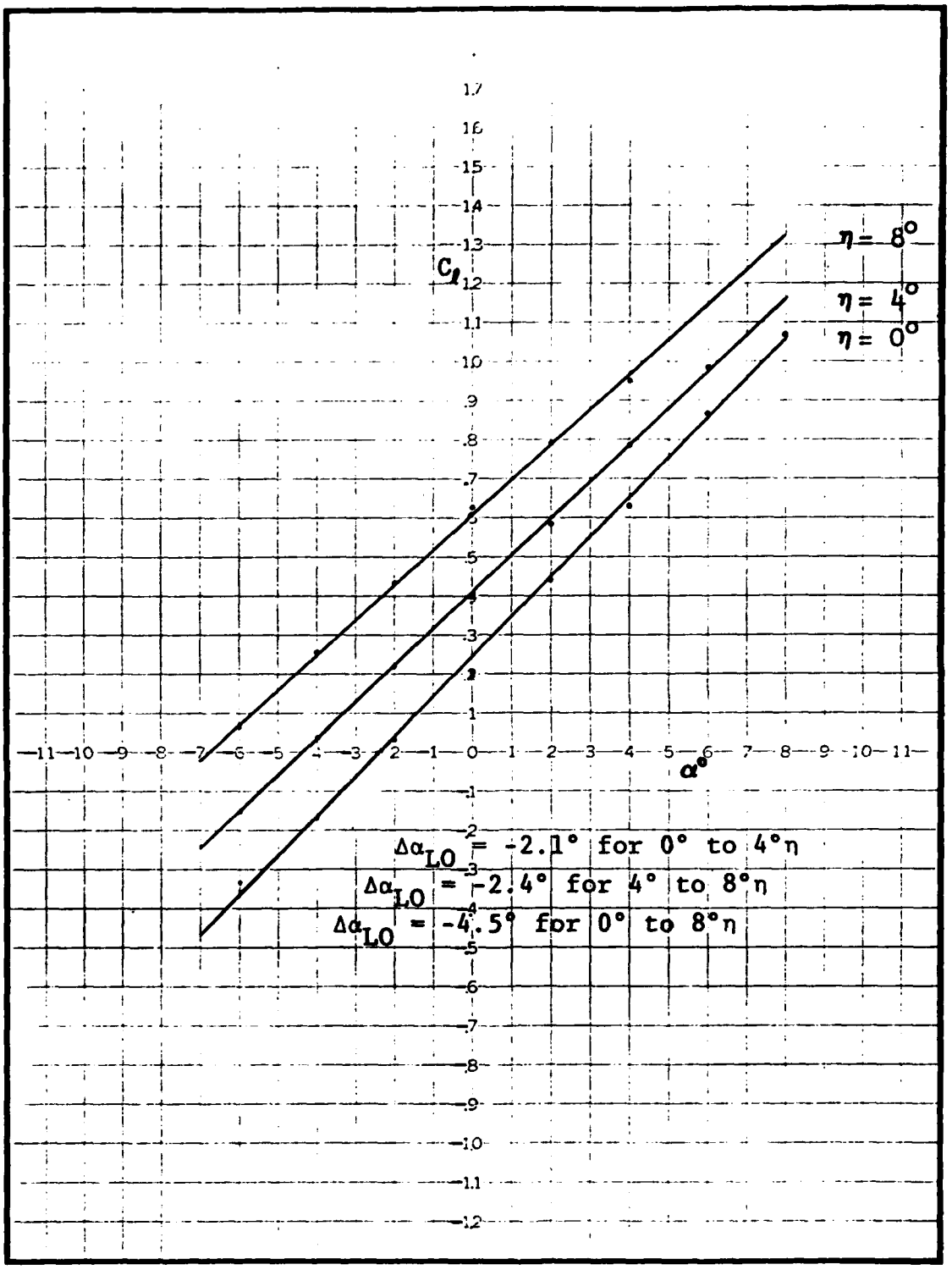

Fig. 23a Experimental C_ℓ versus α plots used to find $\Delta\alpha_{LO}/\eta$ for E = .3

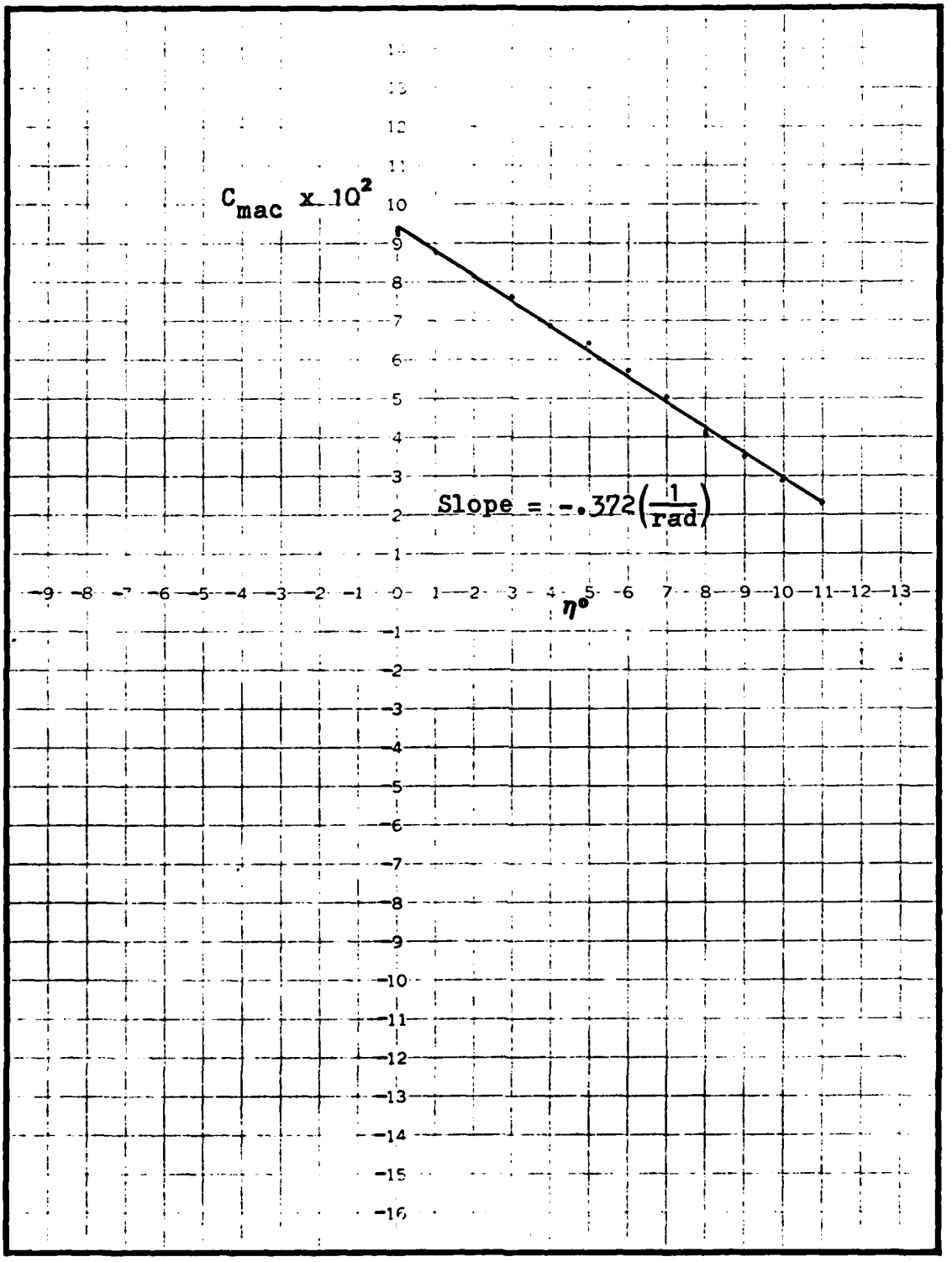

Fig. 23b Experimental C_{mac} versus η plots used to find $\Delta C_{mac}/\eta$ for E = .3

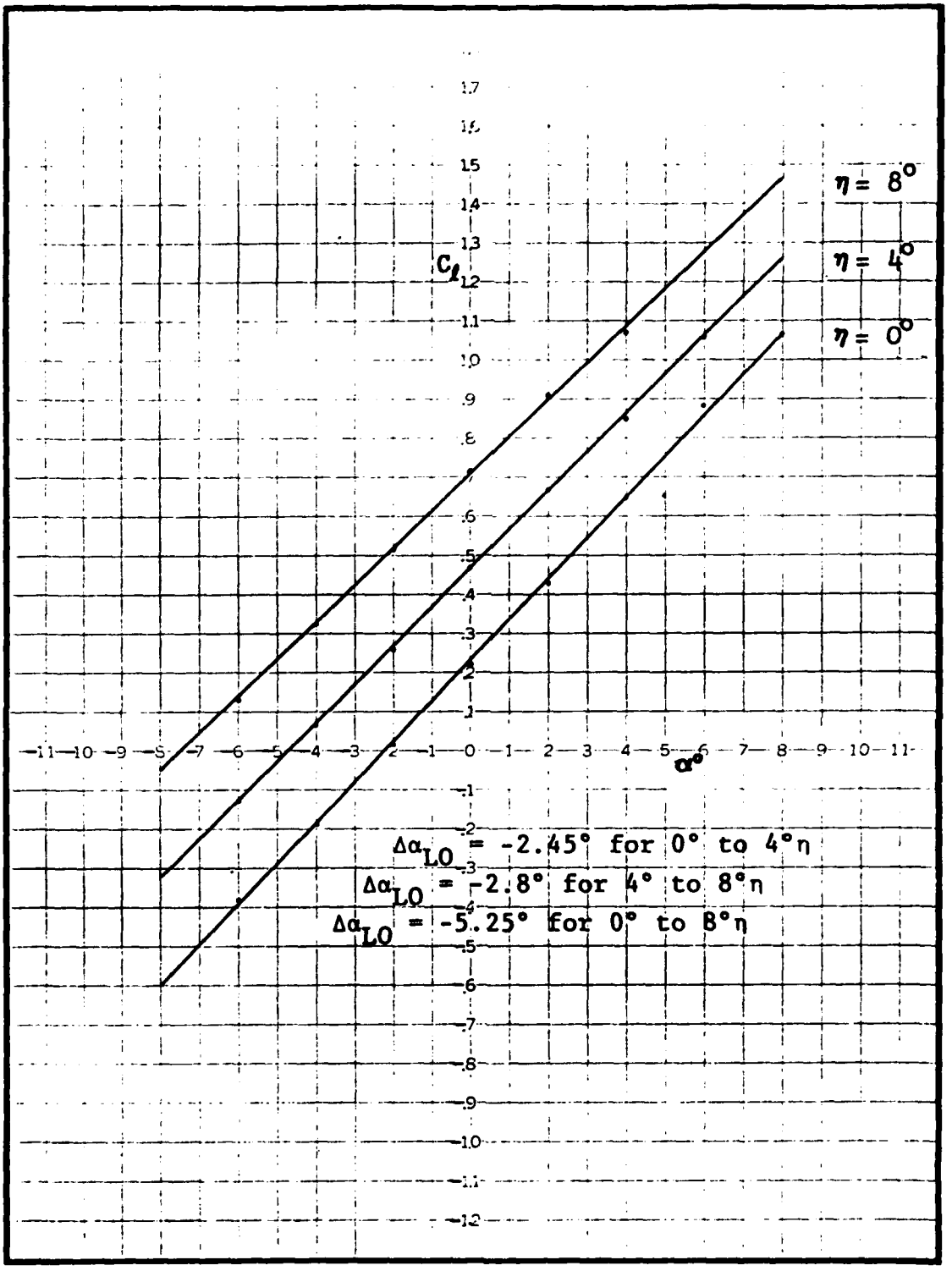

Fig. 24a Experimental C_ℓ versus α plots used to find $\Delta\alpha_{LO}/\eta$ for E = .4

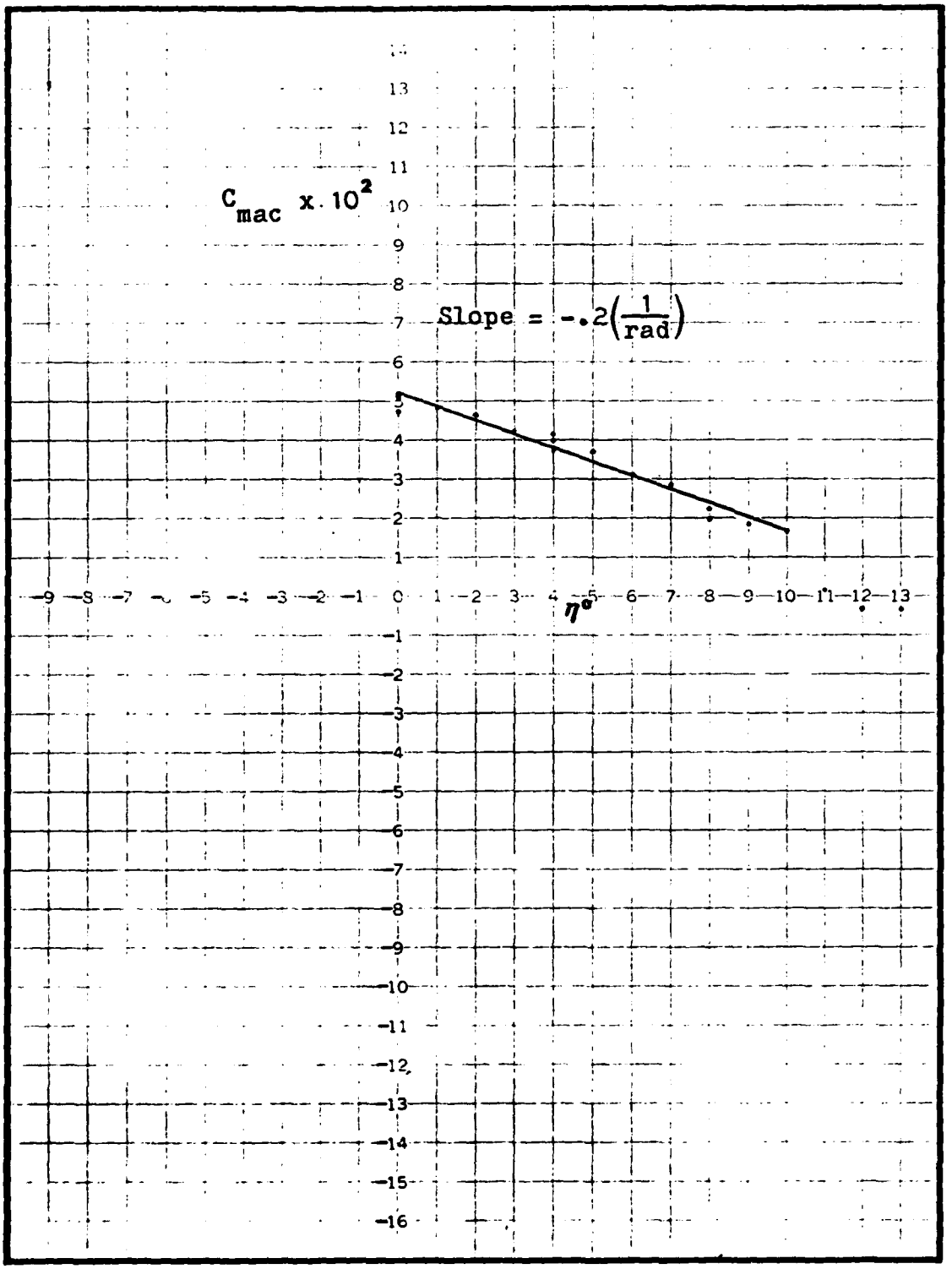

Fig. 24b Experimental C_{mac} versus η plots used to find $\Delta C_{mac}/\eta$ for E = .4

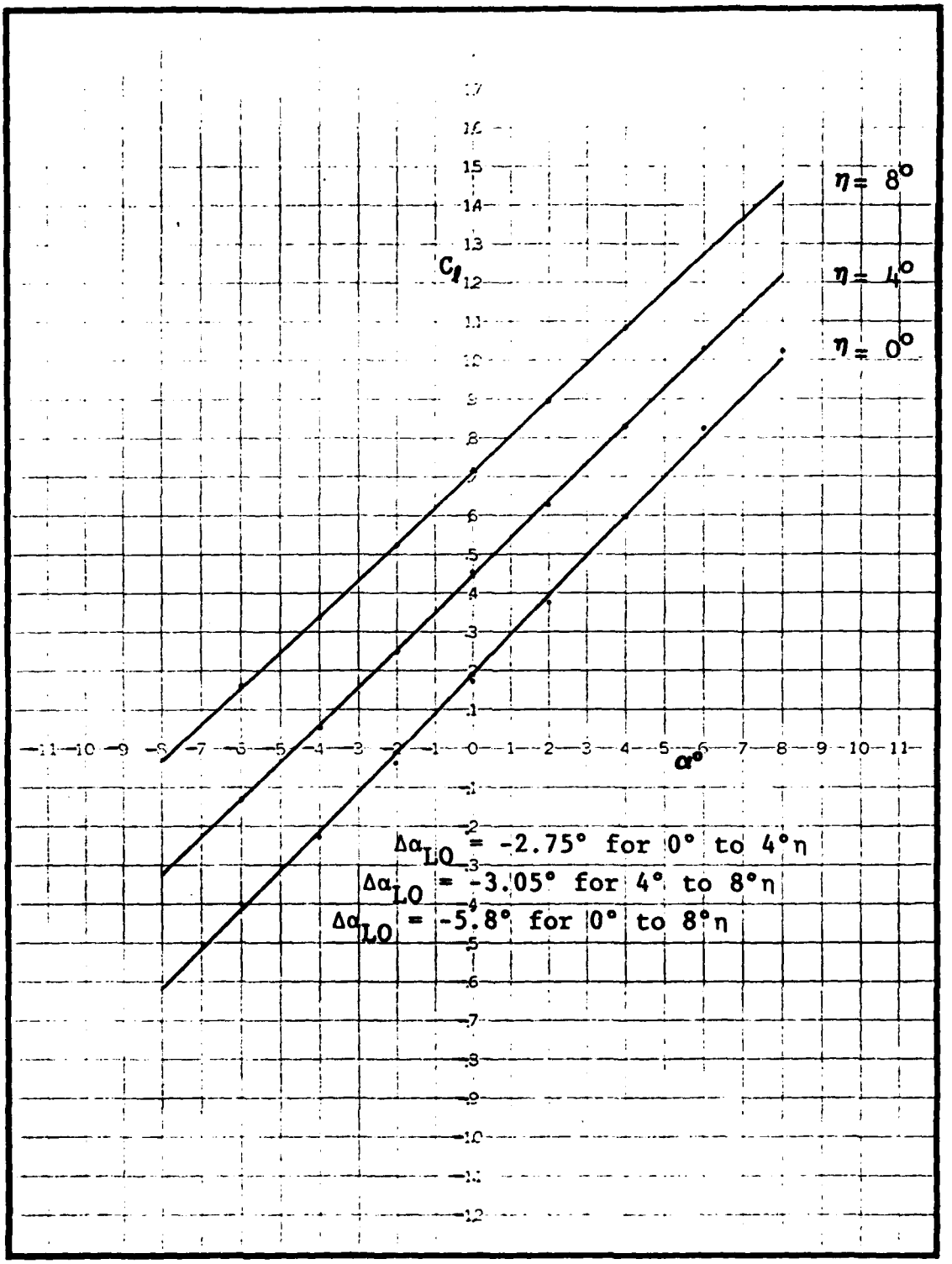

Fig. 25a Experimental C_ℓ versus α plots used to find $\Delta\alpha_{LO}/\eta$ for E = .5

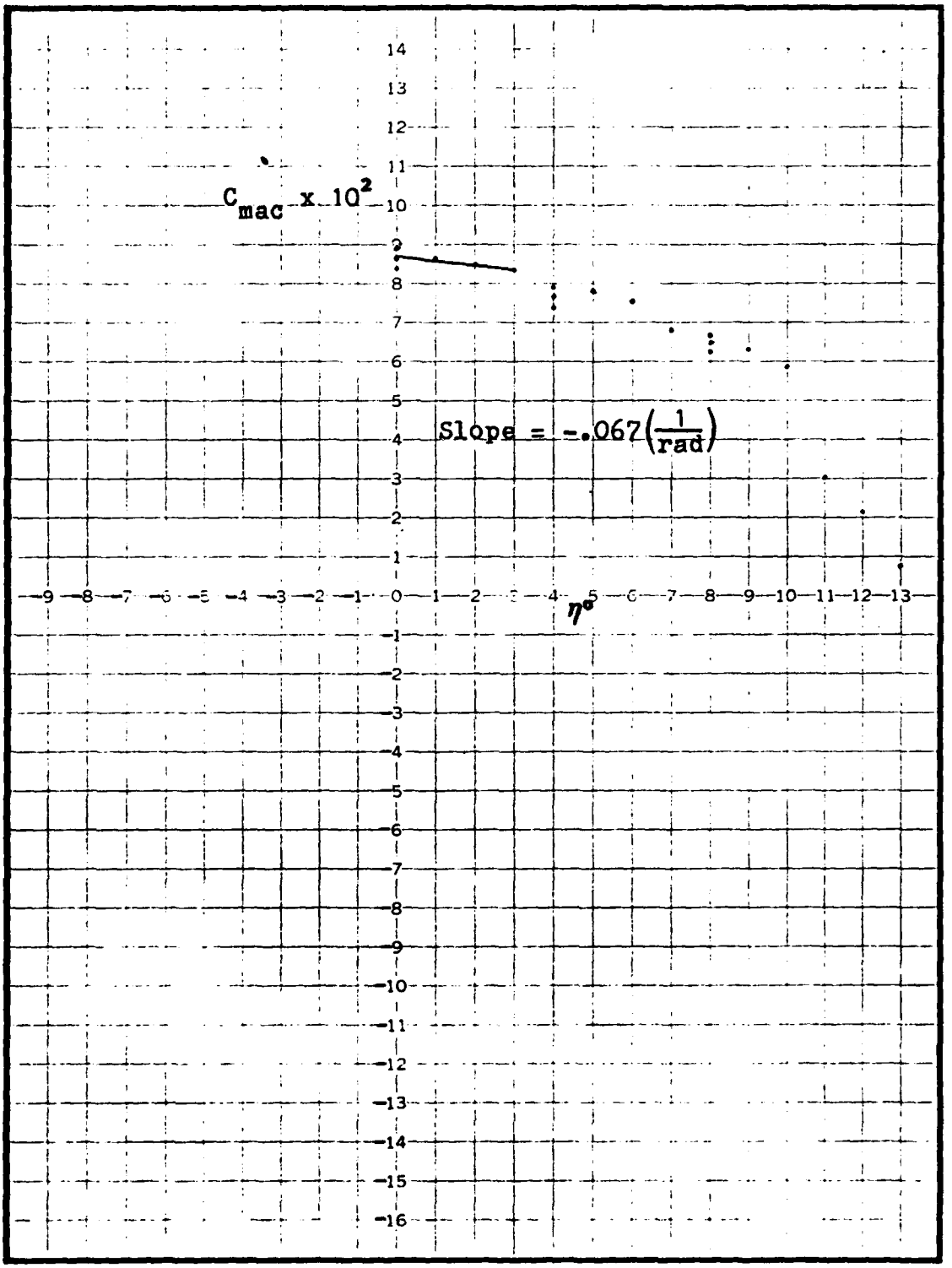

Fig. 25b Experimental C_{mac} versus η plots used to find $\Delta C_{mac}/\eta$ for E = .5

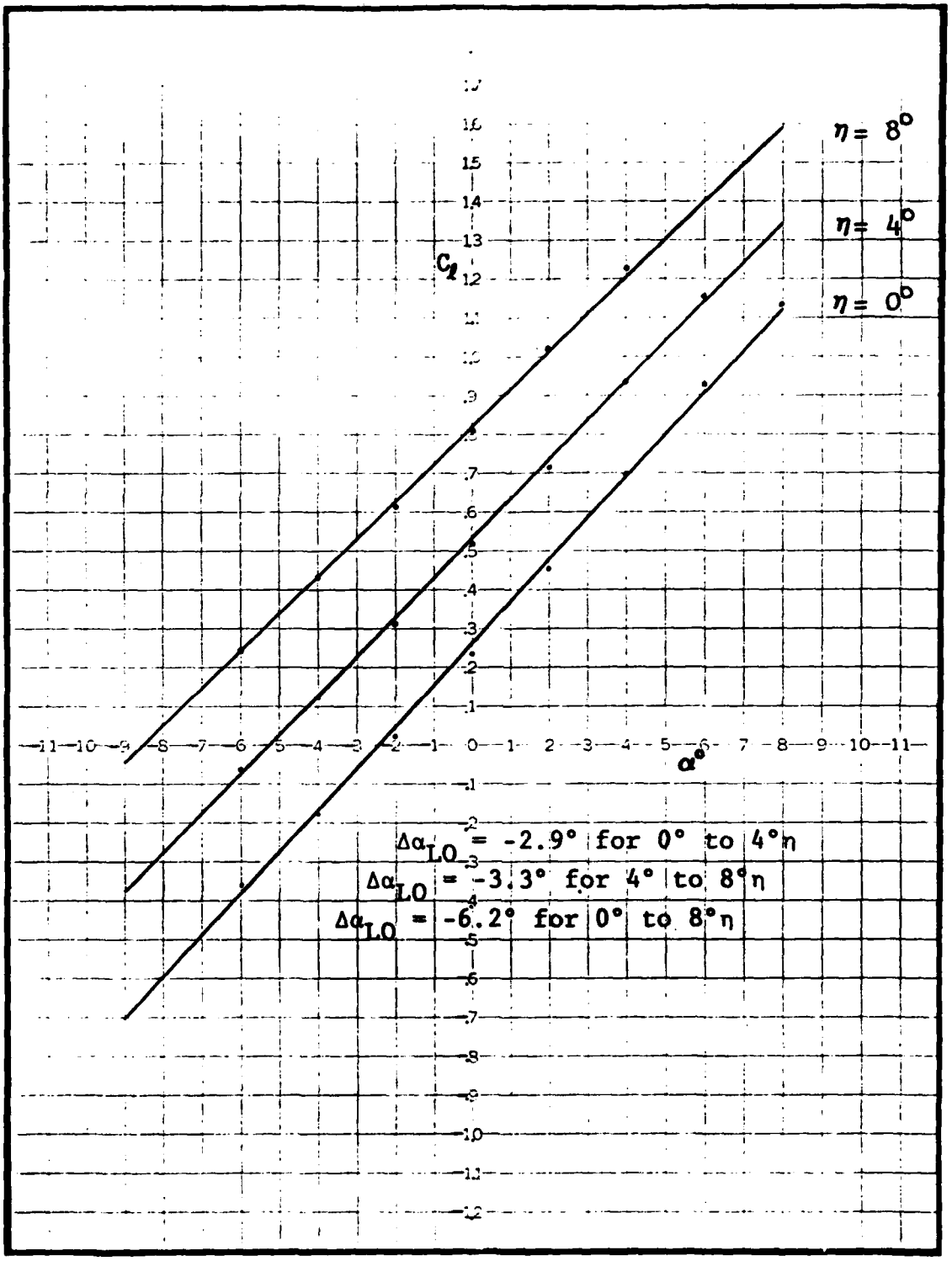

Fig. 26a Experimental C_ℓ versus α plots used to find $\Delta\alpha_{LO}/\eta$ for E = .6

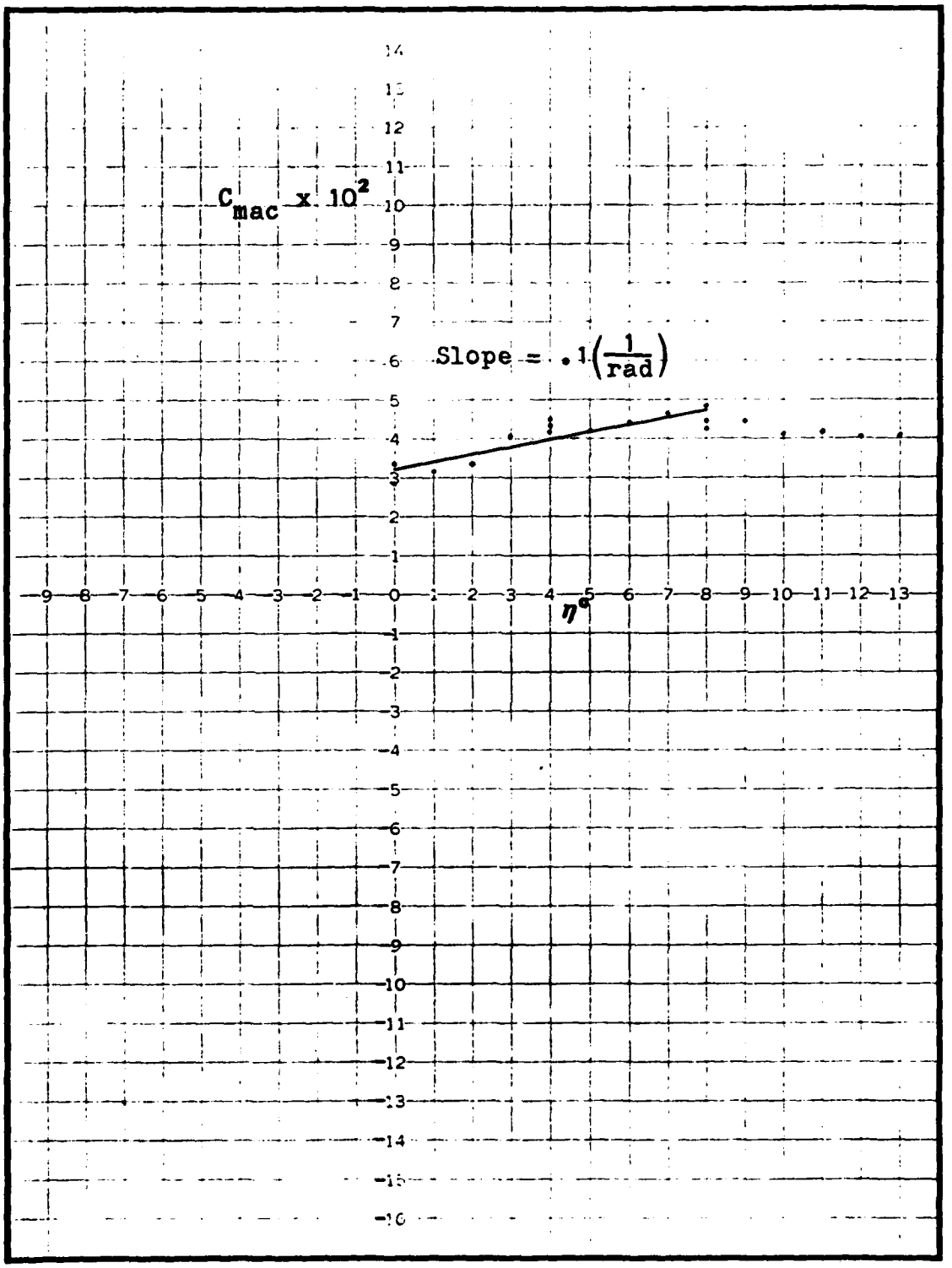

Fig. 26b Experimental C_{mac} versus η plots used to find $\Delta C_{mac}/\eta$ for E = .6

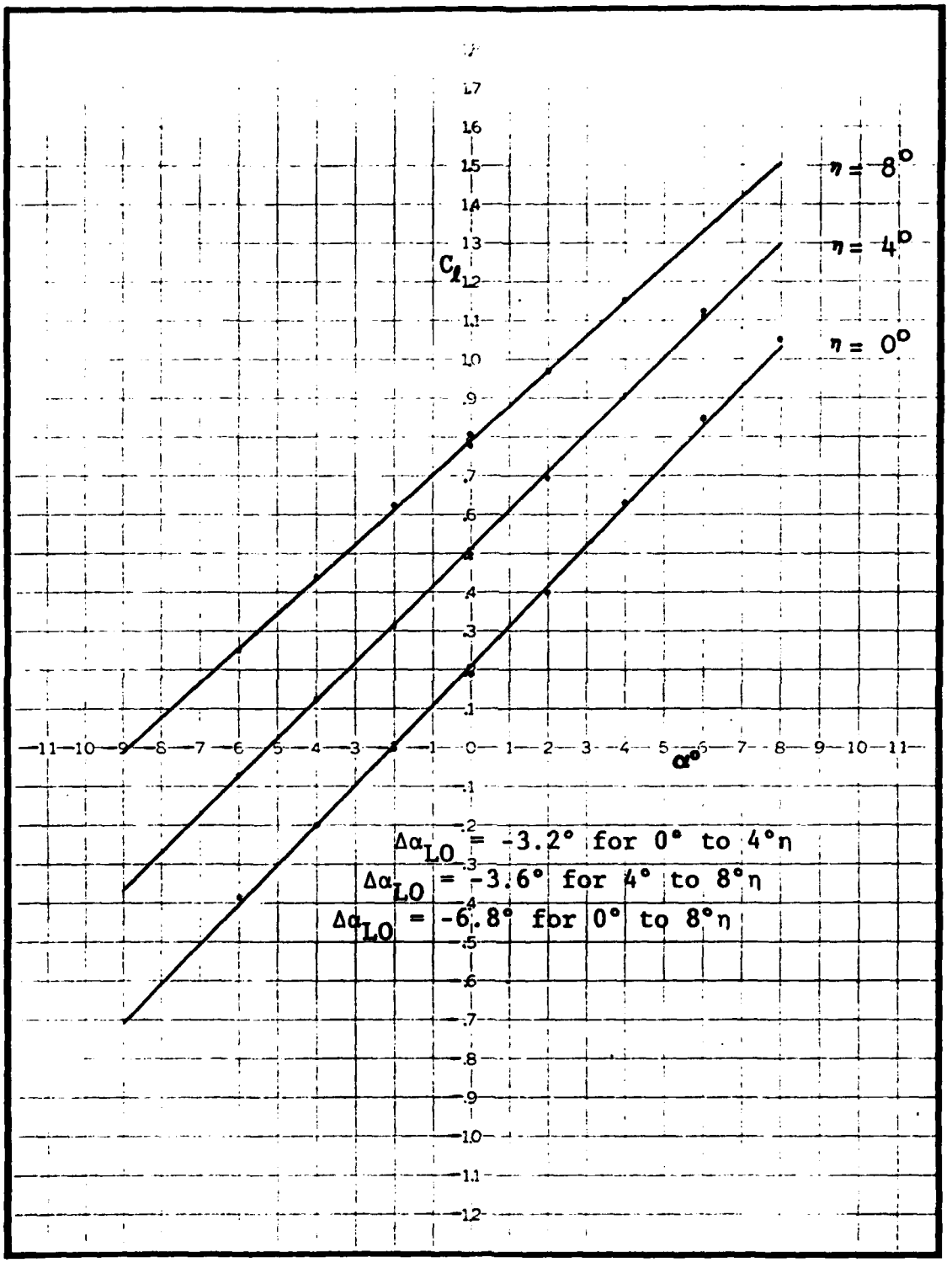

Fig. 27a Experimental C_ℓ versus α plots used to find $\Delta\alpha_{LO}/\eta$ for E = .7

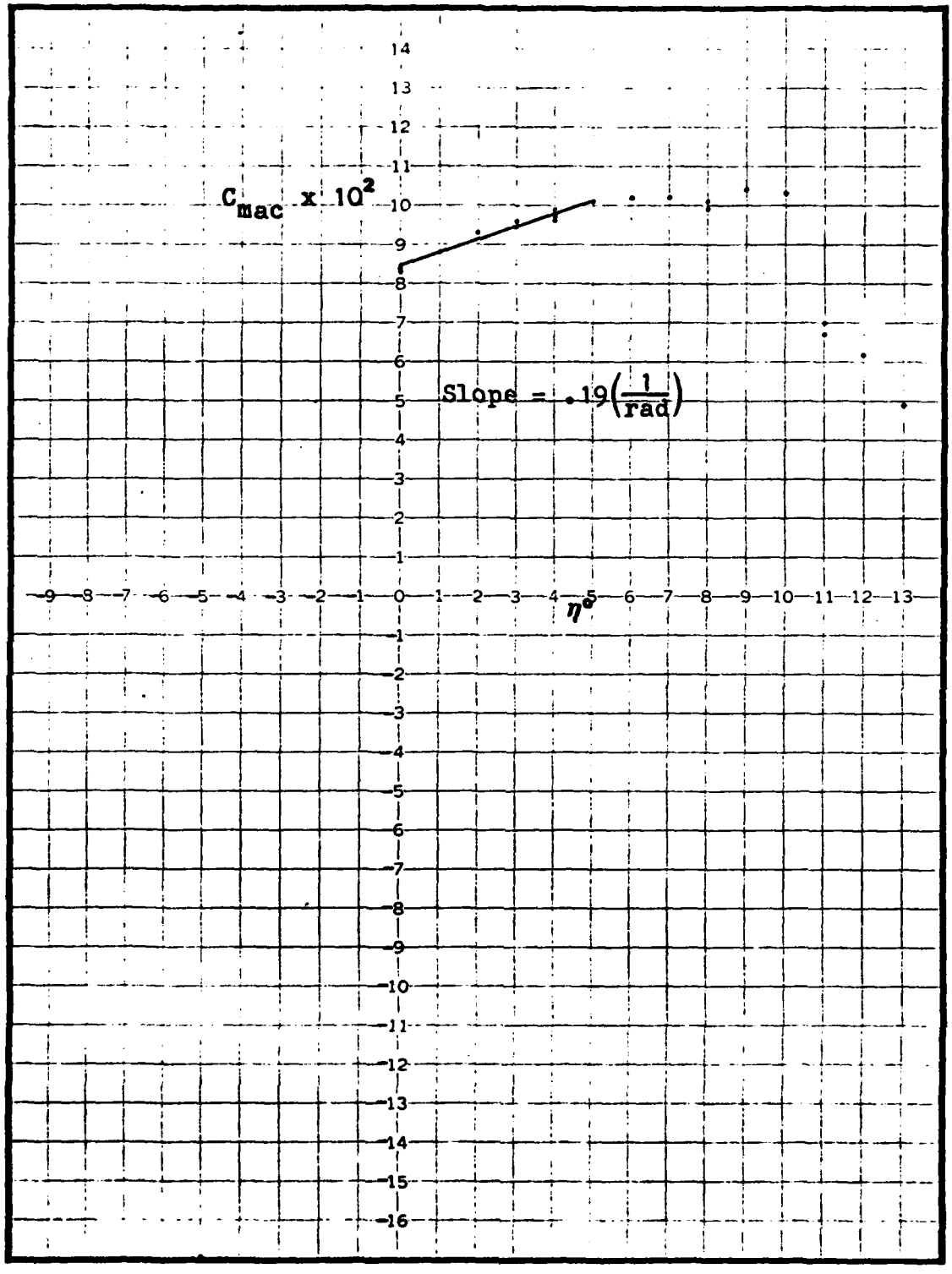

Fig. 27b Experimental C_{mac} versus η plots used to find $\Delta C_{mac}/\eta$ for E = .7

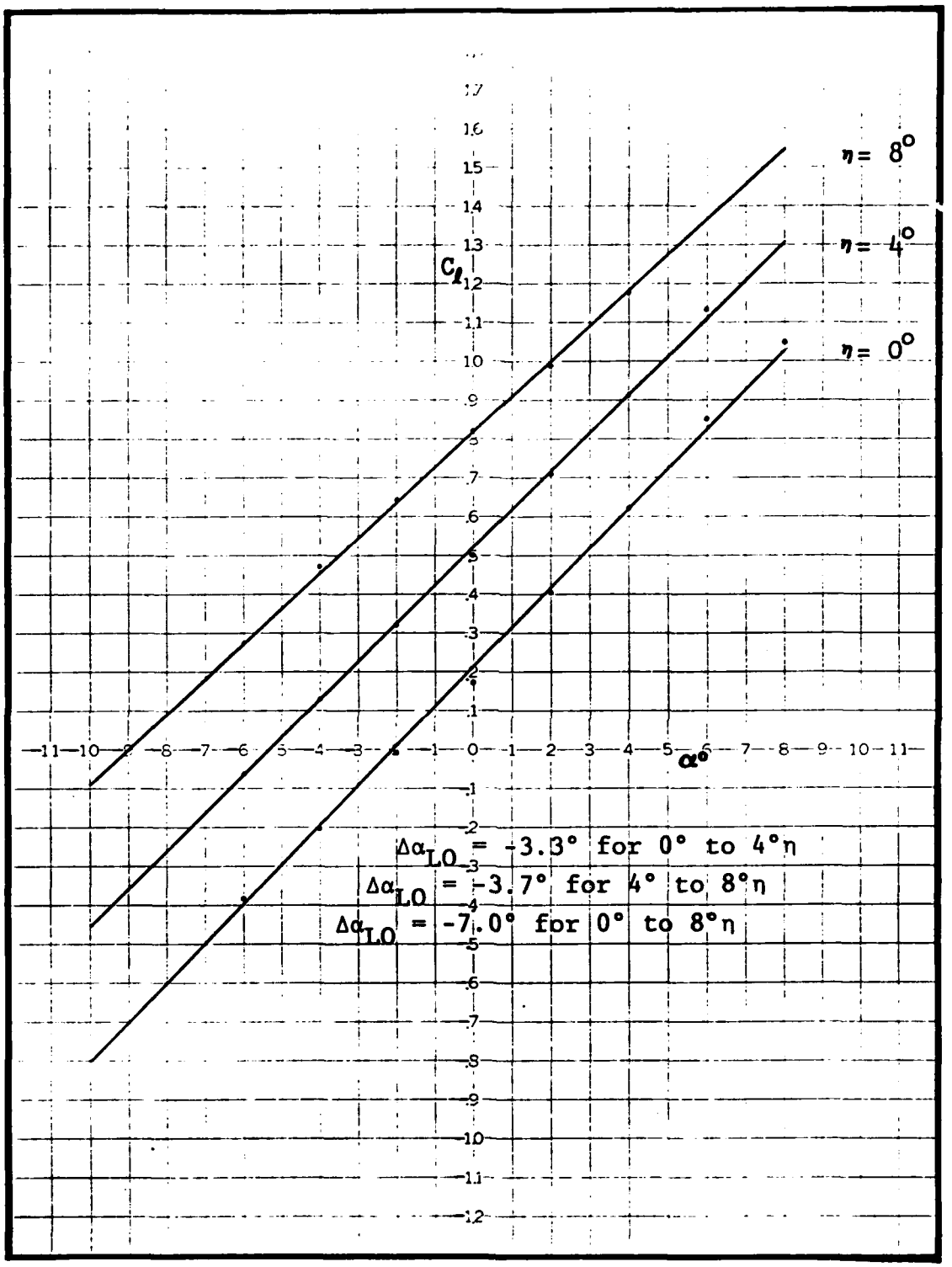

Fig. 28a Experimental C_ℓ versus α plots used to find $\Delta\alpha_{LO}/\eta$ for E = .8

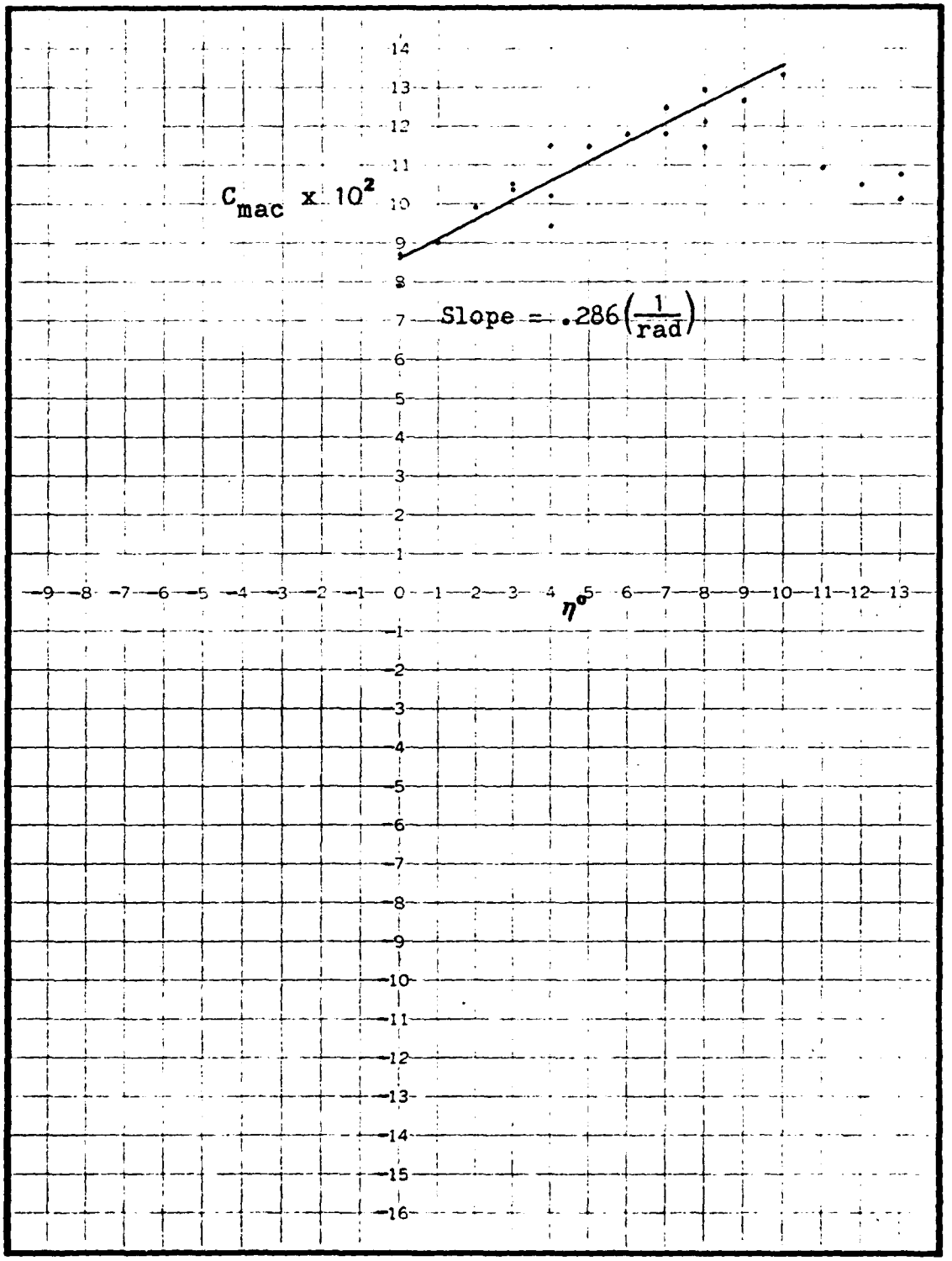

Fig. 28b Experimental C_{mac} versus η plots used to find $\Delta C_{mac}/\eta$ for E = .8

VITA

Howard J. Price, Jr. was born on 25 Jan 1949 in Benham, Kentucky. He graduated from high school in Richmond, Indiana in 1966 and then attended Purdue University to receive the degree of Bachelor of Science in Aeronautical and Astronautical Engineering in Jun 1970. He received his commission in the USAF through the Officer Training School program in Aug 1971. He completed Undergraduate Pilot Training to earn the aeronautical rating of pilot in Sep 1972. His first flying assignment was to Fairchild AFB, Washington to fly B-52s with the 325th Bombardment Squadron from Sept 1972 to Oct 1976. He then flew T-37s with the 35th Flying Training Squadron at Reese AFB, Texas until entering the School of Engineering at the Air Force Institute of Technology in Jun 1981.

Permanent Address: 1104 S 24th St
Richmond, Indiana
47374

UNCLASSIFIED

SECURITY CLASSIFICATION OF THIS PAGE (When Data Entered)

REPORT DOCUMENTATION PAGE		READ INSTRUCTIONS BEFORE COMPLETING FORM
1. REPORT NUMBER AFIT/GAE/AA/82D-23	2. GOVT ACCESSION NO. AD-A124703	3. RECIPIENT'S CATALOG NUMBER
4. TITLE (and Subtitle) WIND TUNNEL INVESTIGATION OF VARYING HINGED FLAPS		5. TYPE OF REPORT & PERIOD COVERED MS Thesis 6. PERFORMING ORG. REPORT NUMBER
7. AUTHOR(s) Howard J. Price, Jr. Capt.		8. CONTRACT OR GRANT NUMBER(s)
9. PERFORMING ORGANIZATION NAME AND ADDRESS Air Force Institute of Technology(AFIT-EN) Wright-Patterson AFB, Ohio 45433		10. PROGRAM ELEMENT, PROJECT, TASK AREA & WORK UNIT NUMBERS
11. CONTROLLING OFFICE NAME AND ADDRESS		12. REPORT DATE December 1982 13. NUMBER OF PAGES 110
14. MONITORING AGENCY NAME & ADDRESS(if different from Controlling Office)		15. SECURITY CLASS. (of this report) Unclassified 15a. DECLASSIFICATION/DOWNGRADING SCHEDULE

16. DISTRIBUTION STATEMENT (of this Report)

Approved for public release; distribution unlimited

17. DISTRIBUTION STATEMENT (of the abstract entered in Block 20, if different from Report)

18. SUPPLEMENTARY NOTES

Approved for public release IAW AFR 190-17.

LYNN E. WOLAVER
Dean for Research and Professional Development
Air Force Institute of Technology (ATC)
Wright-Patterson AFB OH 45433

19 JAN 1983

19. KEY WORDS (Continue on reverse side if necessary and identify by block number)

Wind Tunnel Investigation
Hinged or Plain Flaps
NACA 4412 Airfoil
Zero-lift Angle of Attack
Moment Coefficient about Aerodynamic Center
Changes due to Flap Deflection

20. ABSTRACT (Continue on reverse side if necessary and identify by block number)

This investigation compared thin-airfoil theory predictions of change in zero-lift angle of attack divided by flap deflection ($\Delta\alpha_{LO}/\eta$) versus flap-hinge location (E) and change in moment coefficient about the aerodynamic center divided by flap deflection ($\Delta C_{mac}/\eta$) versus E to wind tunnel studies of the same effect for a cambered airfoil. This comparison for cambered airfoils has not been previously reported. The NACA 4412 air-

DD FORM 1 JAN 73 1473 EDITION OF 1 NOV 65 IS OBSOLETE

UNCLASSIFED

SECURITY CLASSIFICATION OF THIS PAGE (When Data Entered)

foil was chosen for this study. Results of this study show that thin-airfoil theory does predict the trend of the data. The $\Delta\alpha_{LO}/\eta$ versus E prediction favorably matched the data. The $\Delta C_{mac}/\eta$ versus E data differed from the predictions in a similar way to that reported for uncambered airfoils; however, the data in this investigation showed less favorable agreement to thin-airfoil theory than the previously reported results. This difference might be explained in part by the experimental setup used in this study.

END

DATE
FILMED

3—83

DTIC